BRL CR 9

BRL

AD

CONTRACT REPORT NO. 9

ON THE INTERACTION BETWEEN CHEMICAL KINETICS AND GASDYNAMICS IN THE FLOW BEHIND A CYLINDRICAL DETONATION FRONT

Prepared by

Department of Aeronautical
and Astronautical Engineering
University of Illinois
Urbana, Illinois

March 1970

U.S. ARMY ABERDEEN RESEARCH AND DEVELOPMENT CENTER
BALLISTIC RESEARCH LABORATORIES
ABERDEEN PROVING GROUND, MARYLAND

Destroy this report when it is no longer needed.
Do not return it to the originator.

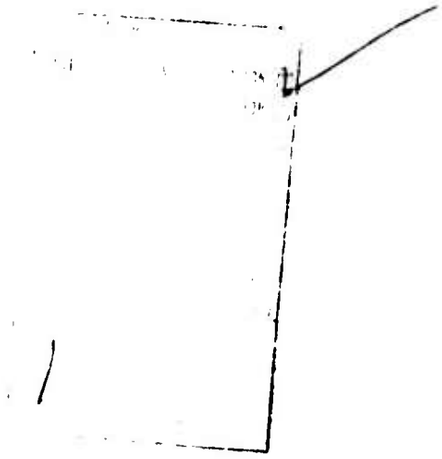

The findings in this report are not to be construed as an official Department of the Army position, unless so designated by other authorized documents.

B A L L I S T I C R E S E A R C H L A B O R A T O R I E S

CONTRACT REPORT NO. 9

MARCH 1970

ON THE INTERACTION BETWEEN CHEMICAL KINETICS AND GASDYNAMICS IN THE FLOW BEHIND A CYLINDRICAL DETONATION FRONT

Prepared by

Suryanarayaniah Rajan, Ph.D.
Department of Aeronautical
and Astronautical Engineering
University of Illinois, 1970

Contract No. DA-18-001-AMC-1016(X)

A B E R D E E N P R O V I N G G R O U N D, M A R Y L A N D

ON THE INTERACTION BETWEEN CHEMICAL KINETICS AND GASDYNAMICS IN THE FLOW BEHIND A CYLINDRICAL DETONATION FRONT

Suryanarayaniah Rajan, Ph.D.
Department of Aeronautical
and Astronautical Engineering
University of Illinois, 1970

What appears to be a plane detonation propagating in a steady manner is actually a complex multifront detonation which is highly non-steady within the period of one cell length. The lead shock of the detonation attenuates from the beginning to the end of the cell. The collision of transverse waves at the end of the cell discontinuously increases the strength of the lead shock to its value at the beginning of the cell. The reactive gas mixture through which the detonation propagates, is instantaneously processed by the lead shock according to definite kinetic rate laws. The gasdynamics of the unsteady flow field interacts with the heat release effects of the chemical reactions to influence the properties of the flow and the strength of the lead shock at later times. This in turn influences the strength and character of the transverse wave collision mechanism at the end of the cell.

To study this coupling between the chemical kinetics and the gasdynamics, the lead shock has been modeled as a cylindrical blast wave propagating into a reactive hydrogen-oxygen mixture diluted with argon. The unsteady reactive flow field is computed using a method of characteristics analysis in cylindrical co-ordinates. The chemical composition of the hydrogen-oxygen system in the reactive region following the induction period is obtained by using the Partial Equilibrium hypothesis. A piston velocity calculated from blast wave theory is used as an input parameter controlling the rate of lead shock decay.

The results of the calculation show that the interaction of the chemical kinetics and the gasdynamics during the unsteady gas expansion behind a pure cylindrical detonation wave does indeed affect the flow properties downstream of the lead shock. Heat addition effects cause a faster decrease of the flow velocity and increase the rate of lead shock decay as compared with the non-reactive case. The temperature rises in the reactive region following the induction period due to the exothermic recombination reactions of the hydrogen-oxygen system.

The rate and extent of lead shock decay is strongly influenced by the rate and extent of chemical reaction, which is itself dependent on the initial pressure and mixture composition. The strength and character of the transverse wave collision-mechanism is coupled with the strength and decay rate of the lead shock. The results show that a decoupling of the shock and reaction fronts occurs at some point in the shock trajectory, after which the lead shock decay rate is analogous to the decay rate of the shock in the frozen composition gas. It is concluded from this study that the lead shock spontaneously chooses the optimum strength and decay rate, consistent with the initial composition, initial pressure and the rate and extent of chemical reaction, such that the related strength of the transverse wave mechanism, operating within the limits of explosion, regenerates the lead shock to its strength at the beginning of the cell. A detonation fails when the strengths of the lead shock and transverse waves and the properties of the gas at the end of the cell are such that the collision of the transverse waves is unable to cause spontaneous explosion of the gas.

ACKNOWLEDGMENT

Sincere appreciation is expressed to Dr. Roger A. Strehlow for his continued guidance, support and encouragement during the entire course of this investigation.

This work was supported by the Department of the Army through Ballistic Research Laboratories under contract No. DA-18-001-AMC-1016(X).

TABLE OF CONTENTS

Page

LIST OF SYMBOLS

a_f	Frozen composition sound velocity
b	Distance between the origin of co-ordinates
A,B,D	Chemical species in a recombination reaction
C	Third body in chemical reaction
c_i	Rate of bi-molecular chemical reactions
C_{pf}	Frozen composition specific heat at constant pressure
f_o, f_1	Coefficients in blast wave theory expansion for flow velocity
h	Enthalpy per unit mass
J_o	Constant in blast wave theory expression for flow velocity
k_{jf}	Forward recombination rate for reaction j
k_{jr}	Reverse rate for reaction j
k_{pj}	Equilibrium constant for reaction j
M	Mach number
M_w	Molecular weight
N	Number of moles
p	Pressure
r	Space co-ordinate
R	Gas constant
R_o	Blast wave decay parameter
R_s	Shock radius
s	Entropy
S	Total number of recombination reactions
t	Time co-ordinate
T	Temperature

u	Flow velocity
U	Shock velocity
W_c	Quantity describing the effect of chemical reaction
x	Space co-ordinate in arbitrary co-ordinate system
X_j	Mole fraction of species j
γ	Specific heat ratio
Δ	Incremental value
$\Delta\phi$	Fraction of delay time used in calculations
ϕ	Stoichiometry on fuel/air basis
τ_i	Fractional induction time
ρ	Density gm/cm^3
ν	Dimensionless parameter indicating the extent of recombination of the H_2-O_2 system
ω_i	Rate of change of species i defined by equation (4)

OPERATORS

$[\ ]$	Concentration, moles/liter
$\frac{\partial(\ )}{\partial[\ ]}$	Partial derivative of ( ) w.r.t. [ ]
$\frac{D(\ )}{D[\ ]}$	Total derivative of ( ) w.r.t. [ ]
$\frac{\delta^+}{\delta t}(\ )$	Directional derivative of ( ) in the direction $\frac{dr}{dt} = (u+a)$
$\frac{\delta^-}{\delta t}(\ )$	Directional derivative of ( ) in the direction $\frac{dr}{dt} = (u-a)$

1. INTRODUCTION

A detonation is generally defined as a shock wave followed by a region of exothermic chemical reaction. A shock wave passing through a gas capable of reacting, first raises its temperature and pressure. In some systems, such as the hydrogen-oxygen system the gas subsequently suffers an induction period. At the end of the induction period, the gas reacts converting chemical energy into thermal energy. During this process the temperature of the gas increases while its pressure and density decrease. The composition of the gas changes during the entire reaction period until finally it stabilizes at some equilibrium value consistent with the prevailing thermodynamic and hydrodynamic constraints. The region of chemical reaction that lies in the wake of the shock is usually termed the reaction wave. In the simplest plane, steady case this reaction wave travels at the same speed as the shock wave, so that the whole travels as one complex.

A detonation may be initiated when a flame accelerates causing disturbances to propagate ahead of it to form a shock wave[1,5]. After the preliminary initiating process, the detonation propagates in a steady manner for all macroscopic purposes. On the other hand it is possible for a detonation wave to attenuate and decay causing the reaction wave to move farther and farther away from the shock front, until finally the detonation ceases to propagate any further.

Since the discovery of detonative combustion in 1881 a considerable amount of effort has been expended in attempting to understand its method of propagation, as well as the specific nature of the coupling between the shock and the chemical reaction occurring behind it. Led by the fact that a detonation is essentially a shock transition followed by a region of heat release through chemical reaction, early investigators applied the equations

of Rankine[2] and Hugoniot[3] for the conservation of mass, momentum and energy across the shock discontinuity. The heat liberated through chemical reaction was taken into account by an additional term in the energy equation. Since for a given set of initial conditions and a prescribed value for the heat release, a large number of final states satisfy the Rankine-Hugoniot equations, it was left for Chapman and Jouguet[5] to postulate relevant criteria establishing the unique final state which would yield the required solution. The Chapman-Jouguet condition states that for a given set of initial conditions such as temperature, pressure and composition of the unshocked gas, the detonation wave propagates such that the velocity of the burnt products relative to the shock, is equal to the velocity of sound in the burnt gas. This furnishes the tangency conditions for the Rayleigh line through the initial state point and the Hugoniot curve on a pressure-volume diagram. The end state is thus given by the Chapman-Jouguet point as illustrated in Figure 1.

This led to the concept of Chapman-Jouguet (C.J.) detonations. Implicit in the definition of a C.J. detonation is the idea of a steady, one dimensional wave with an infinitely thin reaction zone.

While the Chapman-Jouguet concept does yield fairly accurate values for the experimentally observed gross properties of a steady detonation such as its velocity and pressure[6], it does not throw any light on the extent of the chemical reaction zone behind the shock wave. Moreover the reaction occurring in the shocked gas is controlled by finite chemical reaction rates, and hence the reaction zone cannot be infinitely thin. A more realistic model was therefore proposed independently by Zeldovich[7], von Neumann[8], and Doering[9], (Z.N.D. Model) in which the detonation is visualized as a shock transition followed by a finite region of chemical reaction, which is supposed to reach equilibrium at the Chapman-Jouguet plane. The C.J. plane also defines

the plane where all the heat of combustion has been released. This model allows the description of a finite, albeit arbitrary, reaction zone thickness, since the actual chemical reactions proceed at a slower rate as they shift toward the equilibrium composition, and in reality reach complete equilibrium only after some time. Therefore there is no unambiguous definition for the reaction zone length at the present time[10,11].

The stability of a detonation and its propagation velocity are intimately linked to the phenomena occurring within the reaction zone, since it is here that the major portion of the heat release takes place. Factors such as the reaction zone thickness, the reaction rate, rate of heat release, and the interaction of the kinetics with the flow control the underlying mechanisms for the sustenance or failure of the detonation. Furthermore it is in this reaction zone that instabilities appear and grow to form transverse waves that travel across the detonation front[12,13,14]. The production of these transverse waves and their periodic collision to reinforce the lead shock wave is of paramount importance to the survival and stability of a detonation. The lead shock, the transverse wave and the mach stem existing at their intersection form a triple shock configuration, and it is the intersection point namely the triple point, which traces out the characteristic "cell" of a detonation wave. This has been verified by various investigators[16,17]. The size of this cell, i.e., the distance between two adjacent transverse waves propagating in the same direction measured in a direction perpendicular to the flow, is a unique parameter for a given detonation propagating in a large diameter tube, and is dependent on the initial pressure and composition of the gas.

Since these transverse waves do not appear in non-reactive systems and there is no characteristic cell spacing in these systems, the key to

understanding the properties of transverse waves and the detonation as a whole lies in the chemistry of the problem and its interaction with the hydrodynamics of the flow. The phenomenon however is exceedingly complex and does not readily admit to a simple examination. The detonation front is far from one-dimensional due to the presence of the transverse wave complex moving across its surface, and any quantitative analysis of the propagation mechanism should involve the front as a whole. It shall be the aim of this thesis to investigate the relation between the chemistry and hydrodynamics of the flow as linked to the shock motion in a simplified manner, quite apart from the existence of the transverse waves, so as to understand this basic mechanism.

The first investigations in detonation phenomena were aimed primarily at understanding its gross properties and were limited in their scope as it was tacitly assumed that the wave was one-dimensional in nature and that it consisted of a shock transition followed by an infinitely thin reaction zone. With the realization that chemical kinetics demands a finite reaction zone length much greater than the order of the shock thickness, there was the advent of the Z.N.D. model. Analyses were for some time thereafter based on the Z.N.D. model and the Chapman-Jouguet concept[7,12,18,19]. Various investigators[20,21,22] soon began to discover that the detonation front was not one-dimensional and that transverse waves in a complex three dimensional pattern existed at the front. It was therefore sought to analyze the nature and properties of these transverse waves. Denisov and Troshin[23] in their work used a high speed schlieren photographic technique to study transverse wave structure. They showed that the lead shock strength fluctuates in a periodic manner as the detonation traces out its characteristic cell structure, and that this phenomenon plays a principal role in controlling the character

of the reaction wave behind it. Thus although the detonation front as a whole propagates at a time-integrated constant average velocity, it is highly non-steady within the period of each cell length. Measurement by Crooker[24] and Steel[25] has shown that in marginal detonations the velocity of the lead shock varies from 1.8 C.J. velocity at the beginning to about 0.6 C.J. velocity at the end of the cell. This variation is larger as the detonation approaches its lowest mode of propagation, i.e., as the cell length grows larger for a particular tube geometry. In the case of steady detonations this variation is about 20 percent of the C.J. velocity. Crooker also found by the device of sprinkling sand grains on a smoked mylar plate on which the detonation leaves its characteristic cellular imprint, that the lead shock wave is highly curved at the beginning of the cell and flattens out as it moves down the cell. Hence these curved shock fronts may be conceived to be cylindrical waves whose radius of curvature increases as the shock proceeds down the cell. Also it has been experimentally observed[26,27] that expanding detonations that are first overdriven by passing them through the convergent section of a convergent-divergent nozzle are indeed cylindrical, with no transverse structure.

Since the interaction of chemical kinetics and the hydrodynamics of the flow produced by the fluctuating lead shock, and the periodic collision of transverse waves, together contain the pertinent parameters necessary for the existence and stability of detonation waves, the trend of current research effort is to isolate these major elements constituting the multifront detonation and to study each element in detail. There is therefore a great deal of interest at the present time in the behavior of unsteady cylindrical and spherical detonations, both in their own right and also in an attempt to shed new light on the basic mechanism of propagation of multifront detonation waves.

Lundstrom and Oppenheim[28] have investigated the effect of non-steadiness on the induction thickness of a detonation wave by modeling the lead shock as a decaying blast wave with a constant decay parameter determined by matching with their experimentally measured shock velocity. By assuming a power law density variation along a particle path, and by suitable approximations, they calculate the induction zone thickness based on parameters evaluated at the shock front. They note that as the shock decays, the induction zone thickness increases markedly approaching large magnitudes as the lead shock nears the end of the cell, whereby they conclude that the detonation is quenched. While their results are qualitatively correct, they do not allow heat release in the flow. The effects of the interaction between the gasdynamics and the chemical kinetics are therefore not taken into account in their calculations.

In his experiments on cylindrical expanding detonation waves Soloukhin[29] has shown that under conditions favorable for stable propagation, the detonation preserves its cell structure. The experimental apparatus consisted of two circular glass plates joined together to form a narrow cylindrical vessel A tube attached at the center served to direct a plane detonation initiated in it into the cylindrical vessel. Open shutter photographs obtained as the cylindrical detonation propagates outwards in equal-volume acetylene-oxygen mixtures showed that below certain pressures the detonation is quenched and no transverse waves were generated. However above this limit pressure the detonation traveled at a constant velocity maintaining a uniform cell size even as the front area increased. This showed that even in the absence of wall reflections, the spontaneous generation and interaction of transverse waves traveling in opposite directions, reinforced the wave thus enabling it to maintain a constant speed.

In similar experiments on the diffraction of multifront waves Mitrofanov and Soloukhin[30] demonstrated that when a stable detonation encounters a sudden increase in channel area, the mechanism of transverse wave collisions can re-establish the detonation in the increased section under suitable conditions.

Struck and Reichenback[31] have conducted a photographic investigation of freely expanding spherical detonation waves in acetylene-oxygen mixtures, using both streak schlieren and interferometric techniques.

Lee, Lee and Knystautas[32] have conducted a theoretical and experimental investigation of unconfined spherical expanding waves in acetylene-oxygen mixtures. The detonations were initiated using a spark-laser source. They have proposed a reacting blast wave model based on the initiation energy, to predict the trajectories of the shock and reaction wave fronts. They assume that the hydrodynamic motion is not influenced by chemical reaction but include the effects of finite kinetic rates. Various regimes of shock propagation, characterized by the amount of energy deposited in the gas from the laser source, have been investigated. Their conclusions however are based on observations involving a fairly short length traveled by the detonation wave. Also the analysis fails to take into account the interaction of the hydrodynamics and the chemical reaction.

Boussard, Manson and Niollet[33] have studied the propagation of cylindrical detonations in narrow diverging sectors, in mixtures of propane and oxygen diluted with nitrogen, and have established the limits of propagation as a function of the composition of the mixture and the thickness of the sector.

Cylindrical unconfined detonations have also been studied by Lee, Lee and Shanfield[34] and by Lee, Lee and Knystautas[35] in equi-molar acetylene-oxygen mixtures. Using a similarity analysis based on the assumption that the wave is a C.J. detonation, they have calculated the flow properties

immediately behind the expanding detonation front. In their experiments on spark ignition of converging cylindrical detonation waves, Knystautas and Lee[36,37] have shown that the collision of transverse waves is essential to the establishment of a stable detonation.

Recently Zajac and Oppenheim[38] have studied the non-steady gasdynamic effects of a reacting explosive hot spot surrounded by a gas of fixed composition. The hot spot is considered to be composed of a hydrogen-oxygen mixture. They postulate that within the reactive kernel, all state properties are independent of the space coordinate and are functions of time only. Using the method of characteristics and a "bulk expansion" model, they have calculated the salient features of the resultant flow field generated by the pressure pulses from the expanding hot spot. Since it is considered that the occurrence of hot spots in the flow, e.g., by the collision of transverse waves serves to regenerate the attenuating lead shock, this gives some idea of the flow produced by such hot spots.

Non-reactive, non-steady flow fields resulting from expanding cylindrical and spherical shock fronts have engaged the attention of many investigators[39-45], especially in connection with blast waves from various sources including atomic explosions. Closed form solutions obtained by these investigators are usually based on a similarity approach, while numerical solutions invariably employ the method of characteristics.

We may summarize the foregoing observations thus:

(1) Steady detonations are in general complex three dimensional phenomena, and derive their "steady" nature from the reinforcing collision of transverse waves.

(2) While the detonation appears steady as a time-integrated process, it is indeed highly non-steady within the period of each cell length.

(3) The lead shock strength can vary from as much as 1.8 C.J. velocity to 0.6 C.J. velocity in its course from the beginning to the end of the cell. It is thus continuously attenuating.

(4) The incident shock curvature decreases as it travels through a cell and may be adequately modeled as a cylindrical wave (at least at the shock front).

(5) This last observation has led a number of researchers to investigate the properties of cylindrical detonation waves, in an attempt to understand how the dynamics of the continually attenuating lead wave controls the overall propagating mechanism.

However, the researches conducted so far fail to study the complex coupling mechanism between the gasdynamics of the flow and the chemical reaction that occurs behind the incident wave. Since this interaction between the chemical kinetics and the flow field within the reaction zone significantly influences the propagation of the detonation as a whole, it is the object of this thesis to study the non-steady reacting flow field behind a cylindrical expanding detonation. A method of characteristics approach is employed using the experimentally measured reaction rates for the important recombination reactions of the hydrogen-oxygen system, in the presence of argon as a third body. The hydrogen-oxygen system is used in our calculations because its kinetics are well understood at the present time. This system undergoes an induction period before it begins to react. A piston velocity calculated on the basis of ordinary blast wave theory is used as the only input parameter.

In the next section we shall deal with the underlying theoretical considerations and the method of calculation. The last two sections deal with the discussion of results and conclusions respectively.

2. THEORETICAL CONSIDERATIONS

2.1 The Governing Equations

The object of our computations is the calculation of the gasdynamic and thermodynamic parameters of the flow field in a cylindrical expanding detonation wave in an argon diluted hydrogen-oxygen mixture. The problem is best solved in a cylindrical coordinate system. The flow field is non-steady and the entropy is nowhere constant in the flow. The radius of the lead shock wave increases monotonically as the lead shock wave attenuates. Immediately adjacent to the shock front is a non-reactive region comprising the induction zone of the hydrogen-oxygen system. Having passed through the induction zone, the hydrogen-oxygen mixture undergoes recombination reactions which are exothermic. Thus at every point in this reactive region the chemical composition of the gas is continuously changing while the mixture as a whole shifts towards an equilibrium composition. These chemical effects interact with the gasdynamics as the non-steady flow expands radially.

The Rankine-Hugoniot equations for non-reactive flow apply across the shock transition while the flow within the induction zone may be assumed to be governed by the inviscid, frozen flow conservation equations. The reactive flow at the end of the induction zone involves the additional specifying equation for the rate processes. No assumption regarding the constancy of specific heats is made anywhere in the calculations.

The conservation equations for non-steady, reactive cylindrical flow in Eulerian coordinates in the absence of transport phenomena and body forces are

$$\text{Continuity} \quad \frac{\partial \rho}{\partial t} + u \frac{\partial \rho}{\partial r} + \rho u \frac{\partial u}{\partial r} + \frac{\rho u}{r} = 0 \qquad (1)$$

$$\text{Momentum } \rho \frac{\partial u}{\partial t} + \rho u \frac{\partial u}{\partial r} + \frac{\partial p}{\partial r} = 0 \tag{2}$$

$$\text{Energy } \frac{\partial s}{\partial t} + u \frac{\partial s}{\partial r} = - \frac{1}{T} \sum_{i=1}^{S} \left(\frac{\mu i}{Mi}\right) \frac{DX_i}{Dt} \tag{3a}$$

or

$$\rho \frac{Dh}{Dt} - \frac{Dp}{Dt} = 0 \tag{3b}$$

$$\text{Rate } \frac{\partial X_i}{\partial t} + u \frac{\partial X_i}{\partial r} = \frac{\omega_i}{\rho} \tag{4}$$

$$\text{State } p = \rho \sum_i X_i R_i T \tag{5}$$

The specifying equation for the rate processes has been derived for the special case of chemical reaction by B. T. Chu[46] and Wood and Kirkwood[61]. It is a composite form of the rate equation, the equation of state and the energy equation, and may be written as follows

$$\frac{D\rho}{Dt} = \frac{1}{a_f^2} \frac{Dp}{Dt} - \sum_{i=1}^{S} \left[\left(\frac{\partial p}{\partial X_i}\right)_{p,T,X_j} - \frac{\rho}{C_{p_f} T} \left(\frac{\partial h}{\partial X_i}\right)_{p,T,X_j}\right] \frac{DX_i}{Dt} \tag{6}$$

Equation (6) may also be written as

$$\frac{D\rho}{Dt} = \frac{1}{a_f^2} \frac{Dp}{Dt} + W_c \tag{7}$$

where

$$W_c = \sum_{i=1}^{S} - \left[\frac{\rho}{C_{p_f} T} \left(\frac{\partial h}{\partial X_i}\right)_{p,T,X_j} + \left(\frac{\partial \rho}{\partial X_i}\right)_{p,T,X_j}\right] \frac{DX_i}{Dt}$$

is the term due to the occurrence of chemical reaction.

2.2 The Characteristic Directions and the Compatibility Equations

The above set of quasi-linear partial differential equations is hyperbolic and has three characteristic directions which are

$$\frac{dr}{dt} = u + a_f$$

$$\frac{dr}{dt} = u - a_f$$

and $$\frac{dr}{dt} = u.$$

The derivation of the characteristic directions for the non-equilibrium case of chemical reaction is given in Appendix A.

Equations (3) and (4) are the compatibility equations along the third characteristic direction, i.e., along the particle path $\frac{dr}{dt} = u$. The compatibility equations along the characteristic directions $\frac{dr}{dt} = (u \pm a_f)$ can be easily derived as follows:

From equation (1) we have

$$\frac{\partial \rho}{\partial t} + u \frac{\partial \rho}{\partial r} = \frac{Dp}{Dt} = - \rho \frac{\partial u}{\partial r} - \frac{\rho u}{r} \tag{8}$$

Substituting equation (8) into equation (7) and rearranging

$$\frac{\partial p}{\partial t} + u \frac{\partial p}{\partial r} + a_f^2 \rho \frac{\partial u}{\partial r} = -a_f^2 \left(W_c + \frac{\rho u}{r}\right) \tag{9}$$

Multiplying the momentum equation (2) by the frozen sound velocity a_f and rearranging we have

$$a_f \frac{\partial p}{\partial r} + a_f \rho \frac{\partial u}{\partial t} + a_f \rho u \frac{\partial u}{\partial r} = 0 \tag{10}$$

Adding equations (9) and (10) we get

$$\frac{\partial p}{\partial t} + (u + a_f)\frac{\partial p}{\partial r} + a_f \rho[\frac{\partial u}{\partial t} + (u + a_f)\frac{\partial u}{\partial r}] = -a_f^2 (W_c + \frac{\rho u}{r}) \quad (11)$$

while subtracting (10) from (9) we get

$$\frac{\partial p}{\partial t} + (u - a_f)\frac{\partial p}{\partial r} - a_f \rho[\frac{\partial u}{\partial t} + (u - a_f)\frac{\partial u}{\partial r}] = -a_f^2 (W_c + \frac{\rho u}{r}) \quad (12)$$

Equations (11) and (12) are the compatibility equations along the characteristic directions $\frac{dr}{dt} = (u + a_f)$ and $\frac{dr}{dt} = (u - a_f)$ respectively.

Let

$$\frac{\delta^+}{\delta t} = \frac{\partial}{\partial t} + (u + a_f)\frac{\partial}{\partial r}$$

and

$$\frac{\delta^-}{\delta t} = \frac{\partial}{\partial t} + (u - a_f)\frac{\partial}{\partial r}$$

Then equations (11) and (12) may be written as

$$\frac{\delta^+ p}{\delta t} + a_f \rho \frac{\delta^+ u}{\delta t} = - a_f^2 (W_c + \frac{\rho u}{r}) \quad (13)$$

along $\frac{dr}{dt} = (u + a_f)$

and

$$\frac{\delta^- p}{\delta t} - a_f \rho \frac{\delta^- u}{\delta t} = - a_f^2 (W_c + \frac{\rho u}{r}) \quad (14)$$

along $\frac{dr}{dt} = (u - a_f)$.

The pressure p and velocity u have been used in the compatibility equations as the most convenient flow variables under the present non-equilibrium condition of chemically reactive flow. If the flow is non-reactive, the equations are unaltered except for the fact that $W_c = 0$.

2.3 The Kinetic Scheme and the Partial Equilibrium Concept

The explosion kinetics of the hydrogen-oxygen system has been studied extensively for a number of years and is fairly well understood[47-52]. The important reaction steps are

I Initiation

$$H_2, O_2, M \longrightarrow H, O, \text{ or } OH \tag{15}$$

II Chain Branching

$$H + O_2 \xrightarrow{c_1} OH + O \tag{16}$$

$$O + H_2 \xrightarrow{c_2} OH + H \tag{17}$$

$$OH + H_2 \xrightarrow{c_3} H_2O + H \tag{18}$$

III Recombination

$$H + H + M \xrightarrow{k_{1_f}} H_2 + M \tag{19}$$

$$H + OH + M \xrightarrow{k_{2_f}} H_2O + M \tag{20}$$

$$H + O_2 + M \xrightarrow{k_{3_f}} HO_2 + M \tag{21}$$

The species HO_2 which is produced according to equation (21) is unstable and is used up according to the equation:

$$HO_2 + H + M \longrightarrow 2\ OH + M$$

Therefore equation 21 plus the above equation has the overall stoichiometry

$$2\ H + O_2 + M \longrightarrow 2\ OH + M \qquad (21a)$$

Equations (16) - (18) constitute the steps of the chain branching mechanism of the hydrogen-oxygen reaction which gives rise to an induction period during which the radicals H, O and OH appear. The effective chain carrier here is the H atom. The overall rate of the induction process is controlled by equation (16). The induction process is almost thermally neutral for all practical purposes, although equation (16) is endothermic. It has been found[47] that the hydrogen-oxygen mixture contains a large excess of the species O, H and OH at the end of the induction period and that the OH radical and H atom go through a maximum at this point. The time elapsed up to this point is defined as the induction time. The rapid, pressure independent bi-molecular reactions (16) - (18) which have predominated during the induction period are now essentially in equilibrium, towards the close of the induction process.

Induction times for the hydrogen-oxygen reaction have been measured by various investigators[47,49], and it is found that the logarithm of the product of the induction time and the oxygen concentration is linearly related to the inverse temperature. The equation employed for the

calculation of induction time in this work is taken from Reference 49 and is given by the equation

$$10^9 \times \log_{10} \tau_i \, [O_2] = \left(\frac{3565}{T} - 1.162\right) \quad \frac{\text{moles}}{\text{liter sec.}} \tag{22}$$

where τ_i is the induction time, sec., and $[O_2]$ is the oxygen concentration, moles/liter. In order to find the reaction front at the end of the induction zone the quantity

$$\Sigma \Delta\phi = \Sigma \frac{\Delta t}{\tau_i} \tag{23}$$

was calculated along a particle path until the sum equaled unity. The point where $\Sigma \frac{\Delta t}{\tau_i} = 1$ was taken to be a point on the reaction front. Here Δt is the increment in time along two points on a particle path and τ_i is the mean induction time in the interval Δt.

The induction period of the hydrogen-oxygen system is essentially thermally neutral. We have therefore assumed that the gas composition is frozen during the induction period.

At the close of the induction period, the rapid bi-molecular exchange reactions are in equilibrium, while the slow recombination process that now sets in is not. Thus the mixture may be conceived to be in a state of partial equilibrium. It has been shown[52] that the three recombination reactions (19) - (21) adequately depict the behavior of the system during the recombination process. Thus the reacting hydrogen-oxygen mixture is considered to pass through a series of partial equilibrium states to a state of full equilibrium, during the slow

recombination regime governed by the equations (19) - (21). Since there is no net mole change resulting from the bi-molecular exchange reactions, while there is a decrease in the total number of moles of the hydrogen-oxygen system during the slow recombination process toward full equilibrium, it is possible to adequately describe the state of the system during recombination by specifying a single recombination parameter defined in terms of the change in the number of moles. Therefore for any system where we know the unreacted hydrogen stoichiometry ϕ, and the temperature, the state of the system, namely its chemical composition during recombination, is completely described by specifying a recombination parameter ν which is defined as follows

$$\nu = \frac{N - Neq.}{N_i - Neq.} \tag{24}$$

where N_i = number of moles initially present in the unreacted system, and Neq = number of moles at equilibrium.

From the definition of ν it is seen that its value is unity at the close of the induction period before any recombination has occurred. At full equilibrium, ν has a value of zero, where all the recombination possible has taken place. Should the temperature be high enough to cause dissociation of the hydrogen and oxygen present, ν increases beyond unity and has a maximum value of $2\phi + 2$, 4 or $\frac{3\phi + 1}{\phi}$ according as ϕ is greater than, equal to or less than unity.

Calculation of the mixture composition based on the partial equilibrium hypothesis is thus independent of the detailed previous history of the system and its pressure. The kinetic scheme is much simplified and it

is less time consuming than the integration of the entire set of rate equations which entails a full knowledge of the rates of all the participating reactions. Moreover the application of the partial equilibrium hypothesis is found to give realistic results in practical applications[53].

The partial equilibrium composition is determined by a set of three pressure independent, bi-molecular, equilibrium equations for given values of the variables ϕ, ν and T. The temperature T specifies the composition of the mixture through the equilibrium constants for the equations (16) - (18) while the recombination parameter ν specifies the extent of recombination of the system. The calculation of the species composition during recombination therefore reduces to the solution of three non-linear algebraic equations in three unknowns, which is performed in the numerical analysis by a three variable Newton-Raphson iterative technique.

2.4 The Recombination Rate

Getzinger and Schott[50] have shown that the recombination rate of the hydrogen-oxygen system in the presence of third bodies is given by the equation

$$R_{Rec} = \sum_{j=1}^{S} \{k_{jf}[A_j][B_j][C_j]\} - \sum_{j=1}^{S} k_{jr}\,[D_j][C_j] \qquad (25)$$

where R_{Rec} is the recombination rate, k_{jf} is the effective forward reaction rate for the recombination reaction j in the presence of third

bodies for a reaction of the type

$$A + B + C \underset{k_{jr}}{\overset{k_{jf}}{\rightleftharpoons}} D + C \tag{26}$$

k_{jr} is the effective reverse reaction rate. The effective reaction rate is the reaction rate considering all species not participating in the reaction as third bodies for that particular reaction. The forward and reverse reaction rates for the recombination reactions (19) to (21) are related to the equilibrium constant of the individual reaction by the expression

$$k_{jr} = \frac{k_{jf}}{K_{pj} RT} \tag{27}$$

The values of k_{jf} used in the calculation for the reactions (19) to (21) are

$$k_{1_f} = 4.0 \times 10^{14} \left[1 + 4 \left(X_{H_2O} + X_{H_2} \right) \right] \text{ cc}^2/\text{mole}^2\text{sec.}$$

$$k_{2_f} = 5.5 \times 10^{15} \text{ cc}^2/\text{mole}^2\text{sec} \tag{28}$$

$$k_{3_f} = 1.42 \times 10^{15} \left[1 + 4 X_{H_2} + 29 X_{H_2O} \right] \text{ cc}^2/\text{mole}^2\text{sec}$$

The above rates are for hydrogen-oxygen mixtures diluted with argon.

In calculating the reverse rates, the third recombination equation namely equation (21) poses a problem in that the species HO_2 is unstable and does not enter into the reverse reaction in a simple way. We have therefore ignored the reverse rate for this reaction in the calculations.

Written in terms of the parameter ν the recombination rate equation becomes

$$\frac{d\nu}{dt} = \frac{\rho^2 N}{M_w^2 (Neq - N_i)} X_H \left[\frac{k_{1_f}}{2} X_H + k_{2_f} X_{OH} + k_{3_f} X_{O_2}\right]$$

$$- \frac{\rho}{M_w} \frac{N}{(Neq - N_i)} \left[k_{1_r} X_{H_2} + k_{2_r} X_{H_2O}\right] \qquad (29)$$

where M_w is the molecular weight of the mixture, gms., and ρ is the density, gms/cc. The recombination rate as defined above is negative for recombination and positive for dissociation. The rate of change of the hydrogen atom concentration in equation (19) is twice the rate k_{1_f}, and since k_{1_f} as used in equation (29) refers to a change in hydrogen atom concentration, the rate is divided by two as shown in equation (29).

Equation (29) is the form used for the rate equation (4) in the numerical analysis.

2.5 The Detonation Model

The detonation model used in this calculation is similar to the familiar Z.N.D. model, with the exception that no C.J. plane is specified for the completion of the chemical reaction. The model is illustrated for the case of a plane, steady detonation in Figure 2. The temperature and pressure of the hydrogen-oxygen mixture is discontinuously increased as it passes through the shock whose thickness is of the order of a few mean free paths. At the end of the induction zone the hydrogen-oxygen mixture is assumed to be in a state of partial equilibrium with no recombination. However the temperature at the end of the induction period calculated on

the assumption that the gas has suddenly reached the partial equilibrium state is somewhat different from the temperature calculated on the assumption that the gas composition is frozen. In order to overcome this discrepancy in the value of the temperature at the end of the induction zone a correction was added to the calculated temperature along a particle path in the region $0.8 < \tau_i < 1$. This is elucidated further on in the method of calculation.

As the gas recombines at the completion of the induction period, the temperature rises rapidly, due to the heat releasing recombination reactions, until it attains a fairly constant value as the mixture nears its final equilibrium composition. The value of ν, the recombination parameter falls from unity at the end of the induction zone to the equilibrium value ν_{eq}.

In the present calculation, the detonation is neither plane nor steady, but the intrinsic nature of the model is still valid. The lead shock front is given by the curve OS in an r-t co-ordinate system as shown in Figure 3. II' is the line representing the reaction front and is the locus of points where $\Sigma \Delta \phi = 1$ along all the particle paths passing through the shock.

OP is the initial particle path passing through the point O where the calculation was initiated. This point does not lie at the origin of co-ordinates. The velocity along the initial particle path OP is specified by assuming that the lead shock OS is an unreactive blast wave and using the equations of blast wave theory. The exact method of calculation is explained later on in this section.

2.6 The Method of Calculation

In this section is described the salient features of the numerical calculation.

The working fluid is an argon-diluted hydrogen-oxygen mixture. A total of seven species namely H_2, O_2, H_2O, OH, H, O and Ar enter into the calculations. The thermodynamic properties of the constituent gases are calculated from a five parameter curve fit to the JANAF thermodynamic tables[54].

The input quantities to the computer program are

(1) The shock mach number at the starting point 0 (Figure 3)

(2) The initial radius r_1 at which the calculation is started and the final radius r_2 at which it is stopped

(3) The initial unreacted mixture composition in mole fractions

(4) The initial ambient temperature and pressure

(5) The thermodynamic coefficients for all the reacting species

(6) A set of stream function parameters characteristic of the particle paths along which the flow properties are to be studied, and which must therefore be printed out by the machine. The stream function is defined as the radius at which the particle first entered the shock

(7) A parameter R_o, which controls the rate of decay of the lead shock. This is calculated from blast wave theory and is explained further on in this section.

Depending on the particular problem that is being studied, we may hold various input quantities constant and then change one parameter to study a specific phenomenon of interest. For example, to study the effect of the initial pressure on the flow field and shock decay, we may simply change the

input ambient pressure through a series of values, or the effect of mixture composition and stoichiometric ratio is easily studied by varying the initial mixture composition. The influence of the rate of decay of the lead shock on the resultant flow field and kinetics can be studied by changing the parameter R_o controlling the rate of decay of the shock wave. Thus by varying the appropriate parameters in the calculation, we may study how they control the dynamics of motion of the shock and the gasdynamic properties of the flow behind it.

In our investigation of the flow field behind cylindrical expanding detonation waves, we shall make two sets of calculations. In the first set we shall study the effect of initial pressure and rate of shock decay for a fixed initial composition in the particular case of the marginal detonation wave experimentally investigated by Crooker[24]. The second set of calculations will concern itself with the study of the effect of stoichiometric ratio and lead shock decay in cases representing more closely the situation of an ordinary steady detonation wave. The details of the calculation will now be illustrated using as an example the parameters pertinent to the first set of calculations as outlined above. The method of calculation for the second case is essentially similar except for the preliminary evaluation of the input parameters.

The problem is defined thus:---

Given an experimentally measured mach number versus radius curve, such as that observed by Crooker (Figure 4), in the case of a marginal detonation propagating in a stoichiometric hydrogen-oxygen mixture diluted with 50 percent by volume of argon at an ambient pressure of 58 mm of mercury and an ambient temperature of 300^{o}K., we seek the gasdynamic description of the unsteady reacting flow behind this cylindrical detonation wave.

The system of quasi-linear partial differential equations (1) to (7) governing the flow may be solved by the method of characteristics iteratively to furnish a unique solution[55]. The independent variables for non-steady cylindrical flow are the radial co-ordinate r and the time t. The minimum number of dependent variables that determine the flow field is the same as the minimum number of differential equations[56]. Accordingly we have combined various governing equations and have employed three equations, namely the continuity equation, the momentum equation and the specifying equation to obtain three compatibility equations along three characteristic directions. The dependent variables we have chosen to work with are the pressure p, the velocity u and the recombination parameter ν. The species composition X_j are determined from the partial equilibrium hypothesis once ν and the temperature T are known. Also

$$T = f(p, u, \nu) \tag{30}$$

The data curves used in the method of characteristics solution are the particle path OP through the initial starting point O (Figure 3), and the shock trajectory OS. Values of ν are specified along the particle path OP, in an implicit way through the compatibility equation (29). We also choose to specify the particle velocity u on the curve OP. Since the curve POS is crossed twice by both the left running and right running characteristics with compatibility equations (11) and (12), and we have already specified the value of u on OP, it is possible to prescribe the value of p alone on the data curve OS. This is done indirectly by solving the relevant compatibility equation (11) and the Rankine-Hugoniot equations obtaining across the shock discontinuity OS.

By specifying the velocity u and recombination parameter ν on the initial particle path, we have in effect prescribed a piston velocity causing the shock motion, together with the law of chemical reaction along this piston path. All quantities are normalized in the numerical computations. Seventeen variables are stored for each point in the calculation. These are the space co-ordinates r, t, the velocity u, the sound velocity a, the recombination parameter ν, the temperature T, the pressure p, the enthalpy h, the fractional induction time, the stream function and the seven chemical species in mole fractions.

The initial point O (Figure 3) does not lie at the origin of co-ordinates, and hence it is necessary to first find the co-ordinates of this point. Using the equations of blast wave theory[57] it is possible to obtain the co-ordinates of this point. According to blast wave theory, the shock trajectory in a shock mach number versus radius plot is given by the equation

$$\frac{1}{M^2}\left(\frac{R_o}{R_s}\right)^2 = J_o\left(1 + \frac{\lambda_1}{M^2} + \cdots\right) \quad \text{for a cylindrical shock} \qquad (31)$$

where M is the shock mach number at radius R_s, $R_o = \left(\frac{E}{p_o}\right)^{1/2}$ where E is the energy per unit length supplied at the center of explosion, p_o = initial pressure, and J_o, λ_1 are constants dependent on the specific heat ratio of the gas. The shock radius R_s is measured from the center of the explosion.

If we have a shock mach number versus radius curve in an arbitrary co-ordinate system as in Figure 4, the corresponding radius of the cylindrical shock modeled as a blast wave is obtained as follows:

Let M_1 be the shock mach number at radius x_1 in the arbitrary co-ordinate system and let M_2 be the mach number at radius x_2. Let r_1 and r_2 be the corresponding shock radii for the blast wave model with the origin of

co-ordinates at the center of explosion. If b is the distance between the origin of co-ordinate in the two systems (Figure 5) then

$$r_1 = x_1 + b$$
$$r_2 = x_2 + b$$

and from equation (31)

$$\frac{1}{M_1^2}\left(\frac{R_o}{x_1 + b}\right)^2 = J_o\left(1 + \frac{\lambda_1}{M_1^2}\right)$$

$$\frac{1}{M_2^2}\left(\frac{R_o}{x_2 + b}\right)^2 = J_o\left(1 + \frac{\lambda_1}{M_2^2}\right)$$

from which we can solve for the unknown quantities R_o and b. The quantity b enables us to transform the co-ordinates from the arbitrary system in which the experimental curve is plotted to one consistent with the blast wave model. The parameter R_o fixes the scale of the explosion and controls the rate of decay of the shock wave. If r_1 is the radius of the shock at the starting point O, then the corresponding time t_1 is calculated from the equation[57]

$$\frac{a_o t_1}{R_o} = \sqrt{J_o}\, k \qquad (32)$$

where a_o = velocity of sound at ambient temperature and $k = \frac{1}{J_o \lambda_1}\left[\sqrt{1 - J_o \lambda \left(\frac{r_1}{R_o}\right)^2} - 1\right]$

This gives us the co-ordinates (r_1, t_1) of the initial point O. The values used for J_o and λ_1 are 0.878 and -1.989 respectively[57] corresponding to a value of specific heat ratio $\gamma = 1.4$. This gave good agreement between the calculated

shock trajectory and the experimental curve as shown in Figure 4. Also the value of gamma changes along the shock front and has a mean value of about 1.4.

The velocity along the piston path which is used as an input quantity is also obtained from the mechanics of blast wave motion. Based on the similarity solution of Sakurai[57], it is possible to calculate the velocity, pressure and density along a particle path such as OP. Thus the particle velocity u is given by

$$u = U \left[f_o + \frac{1}{M^2} f_1 + \cdots \right] \tag{33}$$

where u is the particle velocity at the point (r,t) and U is the shock velocity at time t. f_o is defined by the equation

$$2 \ln f_o = \frac{\alpha(\alpha+3)(\gamma-1)}{(\alpha+1)\gamma-(\alpha-1)} \ln z + \frac{(\alpha+1)(\gamma-1)}{2\gamma+\alpha-1} \ln (\gamma f_o - z)$$

$$- \frac{(\alpha^2 + 2\alpha + 5)\gamma^2 + (-3\alpha^2 + 2\alpha + 1)\gamma + 4(\alpha^2 - 1)}{(2\gamma + \alpha - 1)\{(\alpha + 1)\gamma - (\alpha - 1)\}} \quad x$$

$$\ln \left| \frac{x - (\alpha + 1)\gamma - (\alpha - 1)}{(\alpha + 3)} f_o \right| + \ln C \tag{34}$$

where $\alpha = 0$, 1 or 2 according as the wave is plane, cylindrical or spherical, and $z = \frac{r}{R_s}$, R_s = radius of the shock at time t, and

$$\ln C = 2 \ln \frac{2}{\gamma+1} - \frac{(\alpha+3)(\gamma-1)}{2\gamma+\alpha-1} \ln \left(\frac{\gamma-1}{\gamma+1}\right)$$

$$+ \frac{(\alpha^2+2\alpha+5)\gamma^2 + (-3\alpha^2+2\alpha+1)\gamma+4(\alpha^2-1)}{(2\gamma+\alpha-1)\{(\alpha+1)\gamma-(\alpha-1)\}} \ln \left| \frac{3\alpha+1 - (\alpha-1)\gamma}{(\alpha+3)(\gamma-1)} \right| \tag{35}$$

In the solution given by Sakarai, f_1 is in the form of a series. Only the first term of the series has been used in the present computation. Hence

$$f_1 = (z-f_o)\phi_1 \tag{36}$$

where approximate values of ϕ_1 are chosen as follows:

$$\phi_1 = 5.5 \text{ if } z \leq 0.9$$
$$\phi_1 = 6.5 \text{ if } z > 0.9$$

Since the numerical solution of the reactive nonsteady flow field is exceedingly complex and time consuming, even if the initial piston velocity is furnished as a simple mathematical function, it was felt that these approximations in the second coefficient of the series solution for the particle velocity was justified.

Given the co-ordinates (r,t) of a point on the particle path OP, the velocity at the point is calculated as follows The shock mach number M corresponding to time t and the shock radius R were obtained from the simultaneous solution of equations (31) and (32). This enables us to find the shock velocity U and also the quantity $z = \frac{r}{R}$ Equation (34) above is then solved iteratively for f_o, and f_1 is found from equation (36). Finally the particle velocity u is obtained from equation (33). The points on the particle path are located successively as the net points are calculated in the method of characteristic analysis

The calculations are begun by first calculating the gasdynamic properties at the point O immediately downstream of the incident shock, using the Rankine-Hugoniot equations for steady, one-dimensional constant area flow:

$$\rho_1 u_1 = \rho_2 u_2 \text{ where } u_1 = M_1 a_1 \tag{37}$$

$$p_1 + \rho_1 u_1^2 = p_2 + \rho_2 u_2^2 \tag{38}$$

$$h_1 + 1/2\ u_1^2 = h_2 + 1/2\ u_2^2 \tag{39}$$

along with the equations of state

$$p = \rho RT \tag{40}$$

The subscript 1 refers to the conditions ahead of the shock and subscript 2 refers to the shocked conditions. The gas composition does not change as it passes through the shock. Gas properties such as enthalpy and specific heat ratio used in the velocity of sound calculations are computed for the particular mixture composition employed. The Rankine-Hugoniot equations are solved by assuming a range of density ratios across the shock $\eta = \frac{\rho_2}{\rho_1}$. For a given assumed density ratio, u_2 is calculated from (37) and p_2 from (38). The density ρ_1 is known and hence ρ_2 can be calculated from the current value of η. The temperature T_2 is calculated from equation (40) using the computed values of p_2 and ρ_2. Next h_2 is found for the particular value of T_2. The initial temperature is constant, so that for a particular point ($h_1 + 1/2\ u_1^2$) is constant. The velocity u_1 changes from point to point along the shock trajectory. A check on the assumed value of η is made on the basis of equation (39). If the values of the two sides of equation (39), do not agree within specified limits, the iteration is continued until they do so. The computed values of u_2, p_2, ρ_2, T_2 and h_2 are the required downstream shock values.

The method of calculation of various types of net points encountered in the analysis is now illustrated.

2.6.1 Calculation of a Shock Point such as H in the Net GHK

All seventeen quantities that are carried in the program are known at the points 1, 1′ and 2 in Figure 6 from previous calculations. The points 1 and 3 lie on the decaying shock. Values at the point 3, upstream of the shock are the known ambient conditions specified at the outset. We require the properties at the point 3′ downstream of the incident shock and also the shock strength at point 3 and the location of point 3. The line 2-3′ is the (u+a) characteristic through 2 and the line 1′-2 is the (u-a) characteristic through 1′. In the numerical calculations the values used for these slopes were the averages at the points 2 and 3′ for (u+a) and of the points 1′ and 2 for (u-a).

The slope of the shock line 1-3 is known once the velocity of the shock is known. Using the co-ordinates of the points 1 and 2 and the slopes of the lines 1-3 and 2-3 we now solve for the co-ordinates of the point 3. The compatibility equation across the characteristic 2-3′ is

$$\frac{\delta^+ p}{\delta t} + a_f \rho \frac{\delta^+ u}{\delta t} = - a_f^2 \frac{\rho u}{r}$$

i.e.,
$$\frac{p_3' - p_2}{t_3' - t_2} + (a_f \rho)_{23'} \frac{u_3' - u_2}{t_3' - t_2} = - \left(\frac{a_f^2 \rho u}{r} \right)_{23'} \qquad (41)$$

where

$$(a_f \rho)_{23'} = \frac{(a_f \rho)_2 + (a_f \rho)_{3'}}{2} \qquad \text{etc} \qquad (42)$$

Also the Rankine-Hugoniot equations apply across the shock transition 33′, namely

$$\rho_3 u_3 = \rho_3' u_3'$$

$$p_3 + \rho_3 u_3^2 = p_3' + \rho_3 u_3'^2$$

$$h_3 + 1/2\ u_3^2 = h_3' + 1/2\ u_3'^2 \qquad (43)$$

The simultaneous solution of equations (41) and (43) was obtained by a double loop iteration technique by first assuming a value of the shock mach number at the point 3 and solving the Rankine-Hugoniot equations for T_3', p_3', ρ_3', u_3' h_3'. Next a check was made to see if these values satisfied the compatibility equation (41). If not the iteration was continued with new values for the shock mach number until the compatibility equation was satisfied within the limits of accuracy specified.

The net size was found to be a very critical factor in the overall accuracy of the program. If the gasdynamic properties of the flow varied slowly and by small amounts, it was found that a larger net size could be employed. However if any of the gasdynamic parameters varied rapidly, it was necessary to have as small a net size as possible consistent with the overall accuracy and machine time employed. A check was therefore made to see if the length 13 was within certain limits. If this was not the case, point 2 was brought closer to point 1 and the entire calculation for point 3 was repeated until the length 13 was such that the best accuracy was obtained.

2.6.2 Calculation of Net Points such as N in the Reactive Region and N in the Non-reactive Region

The solution of the compatibility equations for net points located in the reactive and non-reactive regions are essentially similar. Calculation of a reactive net point is more complicated and time consuming than the corresponding calculation for a non-reactive point because the composition of the gas is continuously changing in the reactive region. The reactive point calculation will therefore be outlined first, followed by the simpler details for the non-reactive point.

Let 1235 in Figure 7 be a typical net in the region of chemical reaction. Since all points on the previous (u-a) line are known, the pertinent values at the points 3 and 5 are therefore stored in the computer memory. Point 1 has just been calculated from the evaluation of the previous net point. The thermodynamic and gasdynamic variables at points 1 and 3 are now used to calculate the required values at point 2.

The compatibility equation along the (u+a) characteristic 3-2 written in finite difference form is

$$\frac{p_2-p_3}{t_2-t_3} + (a_f\rho)_{32}\frac{u_2-u_3}{t_2-t_3} = -a_{f_{32}}^2\left(W_c + \frac{\rho u}{r}\right)_{32} \tag{44}$$

Along the (u-a) characteristic 1-2 we have

$$\frac{p_2-p_1}{t_2-t_1} - (a_f\rho)_{12}\frac{u_2-u_1}{t_2-t_1} = -a_{f_{12}}^2\left(W_c + \frac{\rho u}{r}\right)_{12} \tag{45}$$

and along the particle path 4-2, the compatibility equation (29) applies,

i.e.,

$$\frac{d\nu}{dt} = f\ (\rho,T,\nu) \text{ or } \frac{\nu_2-\nu_4}{t_2-t_4} = f\ (\rho,T,\nu) \tag{46}$$

The points 1 and 3 have been completely determined. The point 2 is located from known values at points 1 and 3 by purely geometric considerations. The evaluation of the requisite quantities at point 2 involves four sets of iterations and is performed in elemental steps in eight subroutines, some of which are common to other steps in the overall calculations. Two iterations are required to satisfy the three compatibility equations above, and the calculation of the temperature T and the species composition at 2 require one iteration each, making four iterations in all.

Values for u_2, a_2, ν_2, p_2 and T_2 are first assumed as the average of the corresponding values at points 1 and 3; of these the values of u_2, p_2 and ν_2 are taken to be reference values to be compared with calculated values at the end of the iteration. Using the assumed values of ν_2, T_2 and p_2, the species composition in mole fractions of the reacting mixture is calculated by invoking the partial equilibrium subroutine, and the term

$$W_c = \sum_{i=1}^{S} \left[-\left(\frac{\partial\rho}{\partial X_i}\right)_{p,T,X_j} + \frac{\rho}{C_{p_f} T} \left(\frac{\partial h}{\partial X_i}\right)_{p,T,X_j} \right] \frac{DX_i}{Dt}$$

is first obtained. W_c may be written in terms of the recombination parameter ν, in a form more convenient for numerical evaluation as follows:

$$W_c = \left[-\left(\frac{\partial\rho}{\partial\nu}\right)_{p,T} + \frac{\rho}{C_{p_f} T} \left(\frac{\partial h}{\partial\nu}\right)_{p,T} \right] \frac{d\nu}{dt} \tag{47}$$

The term $\left(\frac{\partial h}{\partial\nu}\right)_{p,T}$ is evaluated locally at each of the points 1, 2 and 3 by

allowing a small variation of ν from its current value at these points, calculating the new compositions corresponding to these new values of ν and finding $(\frac{\partial h}{\partial \nu})$. The quantity $(\frac{\partial \rho}{\partial \nu})$ is more easily calculated from the expression

$$(\frac{\partial \rho}{\partial \nu})_{p,T} = \rho \, N \, \frac{\partial (\frac{1}{N})}{\partial \nu} \tag{48}$$

$\frac{d\nu}{dt}$ is calculated at each point from equation (29).

At this point all the terms involved in the compatibility equations (44) and (45) are known except p_2 and u_2. We therefore solve equations (44) and (45) to find new values of p_2 and u_2. The point 4 on the particle path through 2 is now located and values of p_4, T_4, ν_4 and τ_{i_4} are found. The third compatibility equation (46) along the particle path is solved to find a new value for ν_2, after which the temperature T_2 is calculated by iteration on the basis of the energy equation (3b). A check is now made to see if the new values of p_2, u_2 and ν_2 agree simultaneously within specified limits with the chosen reference values so labeled at the outset of the calculation. If this condition is not satisfied, the newly obtained values of p_2, u_2 and ν_2 are now labeled as reference values and the iteration is repeated, until the values of p_2, u_2 and ν_2 at the end of an iteration agree within the specified limits with the corresponding values at the beginning of the iteration. The increment in induction time for the segment 4-2 is now found and added on to τ_{i_4} to find the induction time τ_{i_2} at point 2.

A calculation is now made to see by how much the values of p_2, u_2 and ν_2 have changed with reference to the values at point 1. If the variation in any one of the quantities p_2, u_2 or ν_2 is more than five percent of the values at point 1, then a new point is added midway between points 5 and 3,

the whole numbering sequence along the (u-a) characteristic 5-3 is changed, and the point 2 is recalculated. This control on the mesh size is necessary to secure good overall accuracy in the results. If, however the variation in the calculated values of p_2, u_2 and ν_2 is less than one percent of the values at point 1, the point 2 is recalculated using the next highest point above 3 on the previous (u-a) characteristic. As the total time for a single problem took anywhere from thirty to ninety minutes on the IBM 360/70 computer, it was expedient to maintain the net size at its optimum value, so that it was neither too small to consume excess computer time nor too large to cause spurious results.

The calculation of a net point in the non-reactive region within the induction zone is simpler because the composition of the gas remains unchanged. The term W_c in the compatibility equations need not be calculated. The third compatibility equation for ν is therefore not used. The compatibility equations for this case are

$$\frac{\delta^+ p}{\delta t} + a_f \rho \frac{\delta^+ u}{\delta t} = - a_f^2 \frac{\rho u}{r} \quad \text{along} \quad \frac{dr}{dt} = u + a \tag{49}$$

$$\frac{\delta^- p}{\delta t} - a_f \rho \frac{\delta^- u}{\delta t} = - a_f^2 \frac{\rho u}{r} \quad \text{along} \quad \frac{dr}{dt} = u - a \tag{50}$$

and

$$\rho \frac{Dh}{Dt} - \frac{Dp}{Dt} = 0 \qquad \text{along} \quad \frac{dr}{dt} = u \tag{51}$$

The method of calculation of a net point in this region is essentially similar to the case with chemical reaction.

Since the temperature at the end of the induction zone based on a frozen gas composition is not equal to the temperature calculated according to the partial equilibrium hypothesis, a temperature correction is applied along the particle path within the induction zone in the region $0.8<\tau_i<1$. This is done in the computer program by checking to see if τ_2 lies in this region between 0.8 and 1. If so, the temperature at point 2 is calculated again on the assumption that the partial equilibrium hypothesis obtains at point 2. Let T_{2p} be this new value. Then the current value of T_2 assigned to point 2 is given by

$$T_{2c} = T_2 + (T_{2p} - T_2)(\tau_2 - \tau_4) \times \frac{0.8}{0.2} \tag{52}$$

2.6.3 Calculation of the $\tau=1$ Point on the Reaction Front

The calculation of a point on the reaction front presents certain problems because it lies on the boundary separating the reactive and non-reactive regions of the flow. The net size should be as small as possible in such a calculation, in order to get good results. Let 5-3′ and 1-2′ be two (u-a) characteristics and let 5-1, 3-2 and 3′-2′ be (u+a) characteristics (Figure 8). Points 5, 3, 3′ and 2′ all lie in the reactive region while point 1 lies in the non-reactive region. Points 5 and 2 lie on the reaction front line where $\tau_i = 1$. In the process of calculation of points along a (u-a) characteristic, the situation usually arises that as the reaction front is approached, a net such as 12′3′5 is encountered. Such a net calculation is first made on the assumption that the points 3′ and 2′ lie in the non-reactive region, in order to ascertain that the point 2′ does indeed lie in the reactive region. A calculation involving the points 12′3′5 is not really valid, because the reaction boundary is crossed by this net.

Therefore it is desirable to locate the point 2 on the reaction front. This is done by an iterative procedure using various points along the segment 5-1, i.e., the (u+a) characteristic through the last point 5 on the reaction line. Particle paths are drawn through a series of points on 5-1 to intersect the (u-a) characteristic through 1, such as the line 4-2, and the induction time at 2, τ_{i_2} is calculated from the value τ_{i_4} at point 4, until the following inequality is satisfied

$$\left| \tau_{i_2} - 1.00 \right| < 0.005 \tag{53}$$

Using this location of point 2, point 3 on the previous (u-a) line is found from purely geometric considerations. All the properties at point 3 are known since all the points on line 5-3′ have been previously calculated. Point 2 is now evaluated by considering that the characteristic 1-2 lies in the non-reactive region, while the characteristic 3-2 lies in the reactive region. The compatibility equations used are

$$\frac{\delta^+ p}{\delta t} + a_f \rho \frac{\delta^+ u}{\delta t} = - a_f^2 \left(W_c + \frac{\rho u}{r} \right) \quad \text{along 3-2}$$

$$\frac{\delta^- p}{\delta t} - a_f \rho \frac{\delta^- u}{\delta t} = - a_f^2 \frac{\rho u}{r} \quad \text{along 1-2}$$

and

$$\rho \frac{Dh}{Dt} - \frac{Dp}{Dt} = 0 \quad \text{along 4-2} \tag{54}$$

2 6 4 Calculation of a Boundary Point such as D in Figure 3

Let points 1 and 2 in Figure 9 be points on the initial particle path OP. The properties at point 1 are known and the properties at point 3 have just been calculated. Line 1-3 is the (u+a) characteristic through 1 and line 3-2 is the (u-a) characteristic through 3. Using the co-ordinates of points 1 and 3 and the slopes of lines 1-2 and 3-2, the location of point 2 is established. The compatibility equations to be satisfied are

$$\frac{d\nu}{dt} = f(\rho, T, \nu) \tag{55}$$

$$\rho \frac{Dh}{Dt} - \frac{Dp}{Dt} = 0 \tag{56}$$

along the particle path 1-2 and

$$\frac{\delta^- p}{\delta t} - a_f \rho \frac{\delta^- u}{\delta t} = - a_f^2 \left(\frac{\rho u}{r} + W_c\right) \quad \text{along 3-2} \tag{57}$$

It is necessary to furnish the particle velocity at point 2. The velocity u_2 is therefore calculated from blast wave theory as outlined previously Equation (55) is now applied along 1-2 to find ν_2, and W_c for the segment 1-2 is calculated. The compatibility equation (57) along 3-2 is solved iteratively for p_2 and the temperature T_2 is found from Equation (56). If the point 2 lies in the non-reactive region, the procedure is essentially similar, with the exception of the evaluation of the quantities ν and W_c.

A specific problem is begun at a radius r_1 with a given value for the input mach number at this point and a value for the parameter R_o controlling the rate of shock decay. The calculation is terminated when the shock radius has reached a particular specified value.

The evaluation of the entire flow field in (r,t) co-ordinates is accomplished by calculating the points on successive (u-a) characteristics, each beginning with a shock point and ending with a point on the initial piston path OP. Owing to the long machine times involved in the calculation a problem was usually computed in sections by terminating a part of the calculation at a (u-a) characteristic after the elapse of a certain time, and using the points on this line to start the next part of the calculations. This procedure is continued until the lead shock attains the limit radius for the problem.

Two sets of calculations were made. The first group enables us to study the effect of initial pressure and the rate of lead shock decay on the gas-dynamic parameters of the flow field, using as the basis of comparison, the flow behind the lead shock of an experimentally measured marginal detonation. The shock mach number in this case varies from 1.8 C.J. at the beginning to about 0.6 C.J. at the end of the detonation cell. But in the case of ordinary steady detonations, the lead shock mach number varies only from about 1.2 C.J. to 0.8 C.J. from the beginning to the end of the cell. The scale of the corresponding blast wave model and the variation of the flow parameters is therefore noticeably different from those of marginal detonations.

In order to study the flow field behind a lead shock whose characteristics are similar to the lead shock of a steady detonation wave, a second set of calculations were made. However in this case the shock mach number versus radius curve is not available and so we must secure the input parameters to the computer program by using additional theory and a different method of approach, employing the experimentally measured cell spacing from smoke track records. A rich mixture with a stoichiometric ratio of 2.12 and a lean mixture with a stoichiometric ratio of 0.36, both diluted with 60 percent of argon, were chosen. Smoke track records with these mixtures at an ambient

pressure of 150 mm of mercury had been taken previously. We must now elicit from these smoke records the input parameters to the computer program, to begin our calculations.

It can be shown[58] by applying the Rankine-Hugoniot equations across the three shock transitions of a typical mach stem configuration (Figure 10a), that the mach numbers of the three shocks involved satisfy the relation

$$\frac{M_M}{M_I} = M_R \tag{58}$$

to within an accuracy of seven percent. With a knowledge of the initial pressure and mixture composition, the mach number of the transverse wave M_R can be calculated using a computer program developed by Strehlow and Biller[59] Now from the dynamics of Mach stem interactions, from which the detonation derives its steady nature, it is seen[24,60,58] that the lead shock is a mach stem shock at the beginning of the cell and an incident shock at the end of the cell (Figure 10b). However the conditions at the very beginning of the cell are identical with the conditions at the extreme end of the cell i.e., at the points P and O in Figure 10b. Thus the equation (58) holds for the lead shock at these two positions in the cell. Since the lead shock can be modeled as a blast wave with a fixed center of explosion we can write

$$\frac{1}{M_M^2}\left(\frac{R_o}{r_1}\right)^2 = J_o\left[1 + \frac{\lambda_1}{M_M^2}\right] \tag{59}$$

$$\frac{1}{M_I^2}\left(\frac{R_o}{r_2}\right)^2 = J_o\left[1 + \frac{\lambda_1}{M_I^2}\right] \quad \text{where } r_2 = r_1 + \ell \tag{60}$$

$$\frac{M_M}{M_I} = M_R \tag{58}$$

Further we assume that very close to the center of the cell, the mach number of the lead shock is equal to the C.J. mach number of the detonations. Therefore

$$\frac{1}{M_{CJ}^2} \quad \frac{R_o^2}{(r_1 + \frac{\ell}{2})^2} = J_o \left[1 + \frac{\lambda_1}{M_{CJ}^2} \right] \tag{61}$$

M_{CJ} is known from the given ambient conditions and initial mixture composition, and M_R is calculated from the computer program developed by (59). The cell length ℓ is measured from available smoke track records. To begin the calculations for a given set of ambient conditions and mixture composition we need to know the initial radius r_1 and the shock mach number there, i.e., M_M; also the final radius r_2 and the final shock mach number M_I and the decay parameter R_o. We can therefore solve for these unknown quantities r_1, r_2, M_M, M_I and R_o from the algebraic equations (58) to (61). Using the calculated values of M_M and r_1 at the starting point, the required input parameters are supplied to the program and the computations are begun in a manner similar to the case of the marginal detonation discussed above.

3 RESULTS AND DISCUSSION

3.1 Effect of Chemical Reaction on the Flow Field

The first problem investigated was the flow field corresponding to the shock trajectory of the marginal detonation observed by Crooker (Figure 4). The curve representing the mean of the experimental values was modeled as an unreactive blast wave to obtain a value of 37.154 for the decay parameter R_o representing the scale of the explosion. The calculations were initiated at a mach number of 9 and an initial radius of 4.4755 cms, and were terminated at a radius of 15.6 cm. The initial gas mixture consisted of stoichiometric hydrogen and oxygen diluted with fifty percent by volume argon. The initial temperature and pressure corresponded to the experimental conditions of 58 torr and 300^{o}K respectively.

Although the measured shock mach number is higher to begin with, an initial mach number of 9 was chosen for computational purposes, because the resulting shocked gas temperature was near the upper limit of the thermodynamic data available in reference 54. The temperature usually dropped quickly in this hot region behind the strong initial shock, so that the major part of the flow lay away from this high temperature limit. Because of the rapid expansion of the flow field near the center of explosion, the gasdynamic parameters of the flow varied rapidly in this region, and the net size had to be kept as small as possible to obtain reliable results. Further on where the lead shock was weaker and its rate of decay less marked, a larger net size could be employed. This control of net size was established by a checking procedure in the calculation of a shock point as described in the previous section. The correct net size was one which did not change the flow parameters when varied by small amounts around this optimum value.

To study the effect of initial pressure on the resulting flow field, calculations were made with the value of R_o fixed at 37.154 cms but with initial pressures of one-fifth the experimental value, i.e., 11.6 torr, and five times the experimental value namely 280 torr. This gives a set of three calculations with the shock decay parameter fixed at 37.154 cms. Calculations of the flow field were also made for the same three values of pressure viz. 11.6 mm, 58 mm and 280 mm of mercury, with the decay parameter first held at 18.577 cms and then at 74.308 cms. This gives a set of nine calculations of the flow field from which we can study the effect of the rate of shock decay and the initial pressure on the gasdynamic parameters.

To compare the flow field with chemical reaction to the non-reactive flow field produced by the same shock trajectory, the problem was calculated for the three values of R_o and an initial pressure of 58 torr. Since the flow field is self similar in the non-reactive case, it is not necessary to make any additional calculations.

The variation of temperature T, reaction co-ordinate ν, pressure p, enthalpy H and local flow mach number M along particle paths entering the attenuating shock at different radii is shown in Figures 11 to 15 respectively, for the case corresponding to the experimentally measured marginal detonation with R_o = 37.154 cms. The number on each curve in Figure 11 indicates the value of the non-dimensional radius or stream function at which the particle was first engulfed by the shock. The first curves in Figures 11 and 12 correspond to the initial particle path. From the first curve in Figure 11 we see that close to the center of explosions, the temperature drops sharply before it levels off. This is due to the high rate of expansion of the flow. Another contributory reason is that the temperature of the shocked gas at this mach number is high enough to cause dissociation of the gas as shown in Figure 12. The radial distance travelled by a particle within the induction zone

in this region is small because of the high temperatures involved. Further on as the shock decays and the temperature behind the shock front falls off, the radial distance traversed by the particles in the induction zone increases. The particles entering the shock at the end of its trajectory are not heated sufficiently to reach the recombination stage. Thus in an actual detonation cell, the lead shock has become weak towards the end of the cell and is unable to ignite the gas in this region. In order to secure the chemical energy latent in this gas, it is necessary that the gas be reheated by one of the transverse waves to further shorten the induction period and cause the gas to undergo recombination. Thus the rates of decay of the three shocks involved at a triple shock intersection could be intimately linked to the chemical reaction rates such that the correct shock strengths would be re-established by the collision of the oppositely travelling transverse waves. This would discontinuously increase the lead shock strength to its value at the beginning of the cell and the cycle would begin again. From Figures 11, 12 and 16 we see that towards the center of the explosion, the radial expansion of the gas is more pronounced and hence although heat is being liberated by the hydrogen-oxygen mixture in the reactive region, the cooling effect of the gas expansion dominates causing the temperature of the gas to remain fairly constant. As the shock decays, the heat release at the end of the induction period dominates over the cooling effects of the flow expansion and the temperature of the gas rises in the recombination region. Particles that entered the shock close to the center of the explosion have essentially reached equilibrium by the time the shock has traversed one cell length, while changes in temperature and composition continue to occur in the gas that has been engulfed by the shock towards the end of the cell.

The chemical composition of the gas as described by the recombination parameter ν is shown in Figure 12, for the different particle paths. The

curves all begin on the ν equals one line as it is at this value of the reaction co-ordinate that the recombination process begins. The length of the horizontal portion of each curve indicates the radial distance travelled by a particle within the induction zone. It is seen that particles entering the shock where it is weaker undergo longer induction periods than particles which were swallowed by the shock where it was still strong. For this particular case where the initial mach number is nine the temperature behind the shock is initially high enough to cause dissociation of the hydrogen-oxygen mixture. The rate of dissociation is almost an order of magnitude higher than the rate of recombination as shown in Figure 22. Thus the gas dissociates rapidly, causing a quick drop in the temperature. As the shock attenuates, the gas is not compressed to so high a temperature as to cause dissociation, and it forthwith recombines at the end of the induction zone. From Figure 12 we see that although the gas engulfed by the shock in the early stages of the expansion has the maximum amount of time available for recombination, it still does not undergo the maximum extent of recombination, as evidenced by the values of ν at the extreme radius represented. The lowest value of ν and hence the highest extent of recombination is attained by the particle which was hit by the shock at a non-dimensional radius of 0.65. This particle also has the greatest slope $\frac{d\nu}{dr}$ at the end of the induction zone as can be readily seen from Figure 12. An examination of the calculations reveals that the region immediately adjacent to the reaction front is one where the recombination rate is high. The recombination rate as given by equation 29 is a function of the density and the recombination parameter ν, and is a maximum when ν is unity. Thus the longer a particle stays in this region of high recombination, the higher will be the extent of recombination and the greater the heat release. Particles that enter the shock close to the center of explosion have a high velocity imparted to them which carries them quickly through this region of high recombination into cooler, less

dense areas. Particles that enter the shock at some optimum position attain the lowest values of ν because their gasdynamic properties are such that they spend the most time in this region of high recombination, while particles that enter the shock where it is weak do not have sufficient time to recombine fully. Besides in this region where the density behind the shock is lower, the recombination rate $\frac{d\nu}{dt}$ is at its lowest value. The lowest value of ν attained in this case at an initial pressure of 58 mm of mercury and R_o = 37.154 cms corresponding to the marginal detonation is 0.675, i.e., 32.5 percent.

Thus we see that the extent of recombination or the amount of chemical energy released to the flow is intimately connected with the dynamics of the shock motion. In the case just discussed the mixture is stoichiometric with fifty percent argon dilution. The heat release and the specific variation of the heat release with position and time all combine to influence the gasdynamic parameters of the flow, which in turn affect the strength and rate of decay of the lead shock. Thus the attenuation of the lead shock in a detonation cell is governed by all these factors. At the end of the cell a regenerative mechanism becomes operative which discontinuously increases the shock strength to the value it had at the beginning of the cell and the process repeats. At this time this regenerative mechanism is considered to be effected by the collision of transverse waves and the sudden explosion of the gas at the end of the cell. In the case of a marginal detonation the discontinuous increase in lead shock strength at the end of the cell is a maximum and hence the strength of the regenerative mechanism is also a maximum. Since the process is a non-steady one, the rate and extent of lead shock decay is connected with the rate and extent of the re-establishing mechanism, which are together connected with the gasdynamic and rate processes occurring in the flow.

The variation of pressure along different particle paths is shown in Figure 13. The pressure decreases rapidly in the region near the center of explosion due to rapid flow expansion and the effect of heat addition is thus not apparent. However, as the rate of flow expansion decreases, a distinct change in slope occurs at the end of the induction zone. It will be noticed that the rate of decrease of pressure is less in the reactive region generally than in the non-reactive induction zone.

The pressure curve corresponding to a particle that entered the shock at a radius of 0.85 shows some interesting effects. The induction period for this particle ends at a radius of about 1.07 (Figure 12). The rise in the enthalpy curve before this radius in Figure 14 is due essentially to the temperature correction applied at the end of the induction zone in this calculation. The pressure curve exhibits an increased drop rate just in this region around a radius value of 1.05 because the flow is subsonic at this radius (Figure 15). However, beyond a radius of 1.07 the pressure decreases slowly again, being controlled mainly by flow expansion processes. The effect of heat addition due to chemical recombination on the flow mach number is shown in Figure 15. It is seen that a combination of area effects and heating effects control the variation of the mach number as evidenced by a comparison of Figures 15 and 18. Since no chemical effects are present in the non-reactive case (Figure 18), the mach number along the particle paths is controlled entirely by the flow expansion.

To compare the reactive flow field with the non-reactive frozen composition flow, a calculation was made for the same value of the parameter R_o as in the case just discussed, namely 37.154 cms. The initial composition was the same, as also the initial shock mach number and initial radius at which the calculations were begun. The calculation of points in the flow field within the induction zone is identical to the calculation of similar

points in the induction zone of the reactive case. However for the non-reactive calculation, the chemical reaction is suppressed at the end of the induction zone, and the entire flow field is calculated as if the gas is of fixed frozen composition.

Figures 16, 17 and 18 illustrate the temperature, pressure and Mach number variation along particle paths, for the same input piston trajectory as the reactive problem just discussed. The figures show that the temperature, pressure and mach number decrease smoothly without any effects due to exothermic chemical reaction. Each curve starts at a lower point on the vertical scale, because of the decaying shock, as in the case with chemical reaction.

3.2 Effect of Pressure on the Flow Field.

In order to study the effect of pressure on the flow variables in the presence of chemical reaction, calculations were made keeping all other input parameters constant but changing the initial pressure first to 280 torr and then to 11.6 torr. The decay parameter R_o remained at 37.154 cms and the composition was unchanged. Figures 19, 20 and 21 show the variation of temperature T, reaction co-ordinate ν and pressure p along particles that entered the shock at the same points as in the case where the initial pressure was 58 torr. Comparing Figures 11 and 19 and Figures 12 and 20 it can be seen that because of the prevailing higher densities within the induction zone the radial distance travelled by particles within it is very much reduced. The temperature at the end of the induction zone increases very rapidly even close to the center of explosion where the cooling effect of flow expansion is more pronounced. The equilibrium temperature is higher in the case where the initial pressure is 280 torr. The reaction rate which is an order of magnitude higher at the higher pressure enables the recombination

to proceed further in this case. The recombination parameter ν has a lowest value of about 0.4 indicating a recombination of 60 percent. Figure 20 shows that recombination processes release sufficient heat that the temperature rises high enough for dissociation processes to compete with the recombination as exemplified by the curves corresponding to stream function values of 0.55 and 0.65.

A comparison of Figures 12 and 20 reveals that although the rate of dissociation is at least five times larger in the high pressure case (Figure 22) the actual magnitude of the dissociation is lower viz. 1.446 as against 1.4931 at an initial pressure of 58 torr. The amount of dissociation at the higher pressure is lower because Figure 22 shows that at the higher pressure the recombination rate $\frac{d\nu}{dt}$ changes from dissociation to recombination closer to the center of explosion at the higher initial pressure. This is offset to some extent by the fact that the flow velocity decreases faster in the high pressure case, so that the time the particle remains in the dissociative region is longer. However the velocity does not decrease sufficiently rapidly so that the extent of dissociation in each case is almost the same. This represents a dissociation of roughly sixteen percent.

Figure 20 shows that recombination at the higher pressure is accomplished extremely rapidly as illustrated by the steepness of the ν versus radius curves. The radial distance travelled by a particle in the reaction zone following induction is of the order of one to two centimeters before the particle attains a value of ν close to the equilibrium value.

At the lower pressure of 11.6 torr, the recombination rate as illustrated in Figure 22 is much lower and hence the extent of recombination along the particle trajectories is quite small. This is shown in Figure 23. Very little chemical energy is released to the flow during the time that the lead shock takes to travel through the length of the detonation cell.

The pressure versus radius curve along particle paths for the higher initial pressure of 280 torr is shown in Figure 21. The pressure decays rapidly behind the lead shock wave. The high heat release rates at this high pressure cause perceptible changes in the slopes of these curves even for particles that entered the shock close to the center of explosion. This shows that the rapid release of chemical energy at the higher pressures strongly influences the flow characteristics.

3.3 Effect of Pressure on Lead Shock Decay

The variation of shock mach number versus the shock radius for a value of R_o of 37.154 cms and initial pressures of 11.6 mm, 58 mm and 280 mm of mercury is shown in Figure 24. The shock mach number for the non-reactive case at an initial pressure of 58 torr is also shown in the figure. It is seen that at this initial pressure the shock front decays faster when there is chemical reaction than in the non-reactive case. A higher initial pressure of 280 torr produces an even faster lead shock decay, and a reduction in pressure to 11.6 torr gives the slowest rate of shock decay. The shock strength is found to be sensitive to the effective "piston velocity" behind the shock that sustains it. A comparison of Figures 15 and 18 shows that the mach number of the flow decreases faster with chemical reaction. This is to be expected, since heat is added to the flow as the exothermic recombination occurs in the gas, causing a more rapid decay in the flow velocity than in the non-reactive case. At higher pressures increased rates of heat release produce an even faster decrease of flow velocity. Due to heat addition therefore, the "piston velocity" sustaining the shock is decreased and the shock attenuates faster. Thus the decay of the shock front increases with pressure in a chemically reactive gas.

3.4 Effect of Rate of Lead Shock Decay on the Flow Field

Since the flow field behind expanding cylindrical detonations is non-steady and the rates of a number of simultaneously occurring processes all interact to produce the final flow pattern, a study was made to see how the rate of lead shock decay influenced the characteristics of the flow. Calculations were made of the flow field keeping the pressure constant at each of the three values used in this study, but varying the parameter R_o controlling the velocity along the piston trajectory and hence dictating the rate of shock decay. For example, at a pressure of 58 torr, the flow field was calculated at values of R_o fixed at 37.154, 74.308 and 18.577 cms. Since the input piston velocity along the initial particle path calculated from blast wave theory is dependent on the value of R_o, this change in input velocity suitably alters the shock trajectory. Increasing the value of R_o reduces the rate of shock decay and vice versa. The parameter R_o is representative of the amount of energy introduced into the flow field by the power source initiating the explosion. A large value of R_o signifies a greater amount of energy deposited in the flow field, producing a stronger shock which decays less rapidly.

Figures 25 and 26 show the variation of temperature T and reaction co-ordinate ν along particle paths for the same initial conditions of 58 torr pressure and 300°K temperature. The value of R_o is now 74.308 cms, i.e., the shock front decays half as fast as before. Comparing Figures 25 and 26 with Figures 11 and 12 we can see how the reduced rate of shock decay affects the flow. In the flow field behind expanding cylindrical detonations, the gas-dynamic expansion processes vie with the chemical rate processes. A reduced rate of shock decay reduces the rate at which the temperature, pressure and flow velocity behind the shock fall off. The quenching effects of rapid

expansion are present to a lesser degree and the chemical reaction takes place under less adverse flow conditions than if the lead shock decayed rapidly. A slower decay of the shock front also provides more time for the recombination processes. Thus Figures 11 and 25 show that once the recombination processes set in, the temperature rise along particle paths is greater, in the case with the slower rate of shock decay. The temperature at the outermost radius for the same extent of lead shock decay is higher for corresponding particle paths. The lowest value of ν is 0.58 when R_o is 74.308 cms as against 0.675 when R_o is 37.154 cms. It is interesting to note that the lowest value of ν is attained by the particle that entered the shock at a stream function value of 0.65 when R_o is 37.154 cms and by the corresponding particle with a stream function value of 1.30 when R_o = 74.308 cms.

If the value of R_o is now kept constant at 74.308 cms but the initial pressure is increased to 280 torr, we have the combined effect of the low rate of gas expansion and the high rate of chemical recombination. These two effects still further increase the rate of temperature rise along particle paths in the recombination region. The recombination processes progress further to give a value of ν of 0.36. Now if the rate of lead shock decay is increased by a factor of 4, by reducing R_o to 18.577 cms. while still maintaining the initial pressure at 280 torr, the lowest value of ν attained becomes 0.44. Thus we see that at an initial pressure of 280 torr, where the recombination rate is higher, the temperature rise along particle paths and the extent of recombination is controlled almost entirely by the rapid, dominant, exothermic chemical reaction. Although at the higher rate of shock decay, the particles have less time available for recombination for the same reduction in shock mach number, the difference in the maximum extent of recombination as described by the

lowest values of ν attained is less marked. Thus the amount of heat given to the flow is almost entirely controlled by the chemical rate processes at the higher pressures.

3.5 Effect of Rate of Shock Decay and Pressure on the Reaction Zone Thickness

The experimental measurement of reaction zone thickness in detonation waves is usually made by schlieren or interferometric techniques, and is taken to be the distance from the lead shock to the region of strong density gradient. From the present calculations we see that the strongest density gradient is produced in the region immediately adjacent to the end of the induction zone. This is because the recombination rate and hence the heat release rate is greatest in this region, as evidenced by the steep drop in the ν values. After this initial rapid decrease, the ν values however continue to drop at a slower rate until they reach an almost constant equilibrium value. The extent of the reaction zone strictly speaking is the distance from the shock front to the point where the particle is essentially in equilibrium. To attain complete equilibrium would indeed take a long time. However from the calculations we see that the particles attain values of ν close to the equilibrium value in fairly short times of the order of 40 microseconds. It is seen from the graphs that the radial distance travelled by the particles before they reach equilibrium values of ν decreases with the pressure, but increases as the rate of shock decay decreases. For slower rates of shock decay, the cooling effects of flow expansion are not present to such an extent as to cause freezing of the composition sooner, so that chemical effects continue to be felt thus increasing the radial distance travelled by the particle within the reaction zone.

3.6 Effect of Pressure on the Induction Zone

Figure 27 shows the radial distance travelled by particles in the induction zone plotted against the stream function or the radial co-ordinate at which they entered the shock. R_o was kept constant at 37.154 cms, as also the initial Mach number at which the calculations were begun. The three curves represent the radial distance travelled by particle paths for the three reactive cases where the initial pressure is 11.6, 58 and 280 torr respectively, and for the non-reactive case for an initial pressure of 58 torr. It is seen from the figure that the radial distance travelled by a particle within the induction zone is greater in the reactive case than in the non-reactive case, all other conditions remaining the same. At smaller radii the difference is not readily apparent. Two factors contribute towards the increase of radial distance travelled by a particle within the induction zone. As illustrated by Figure 24, the shock front decays more rapidly when chemical recombination follows the induction period, reducing the effective piston velocity driving the shock. At any given radius the shock mach number with chemical reaction is consistently lower, and hence the temperature, pressure and flow velocity behind the shock are also lower. The induction time as given by equation 22 is dependent on the temperature and density, and therefore increases at the lower temperatures and pressures behind the shock with chemical reaction. Although the particles have a slightly lower flow velocity in the reactive case the distance travelled in the induction zone is still higher. This is because the induction time as calculated from equation 22 is highly pressure sensitive. This fact is borne out by the curves for the lower and higher pressure in Figure 27.

In the present calculations a temperature correction was made towards the close of the induction period. It was found that the radial distance travelled by a particle within the induction zone was very sensitive to this

temperature correction. The reaction front could be made to move appreciably closer to the shock front by increasing the temperature correction.

3.7 Effect of Mixture Composition on the Flow Field Behind Steady Detonation Waves

So far we have studied the effect of the rate of lead shock decay and the initial pressure on the gasdynamic parameters of the flow behind the lead shock, using as our standard of comparison the lead shock corresponding to an experimentally observed marginal detonation in a stoichiometric hydrogen-oxygen mixture. To study the effects of chemical reaction on the flow field behind shock waves corresponding to normal "steadily" propagating detonations, in particular to study the effect of mixture composition on the flow field in these cases, a second set of calculations were made as outlined towards the close of the section on theoretical considerations.

Two mixture compositions were selected for which experimental smoke track data had been taken earlier. One was a fuel lean mixture with a stoichiometric ratio of 0.36, diluted with 60 percent argon, and the second was a fuel rich hydrogen-oxygen mixture with a stoichiometric ratio of 2.12, again with the same argon dilution of 60 percent by volume. The initial conditions for the test data were the same for both mixtures, namely $300^{o}K$ and an initial pressure of 150 torr. Figure 28 shows the cellular experimental smoke track records for these mixtures. From the calculations we find that the lead shock decays from a mach number of 4.64 to 3.88 from the beginning to the end of the cell for the lean mixture with $\phi = 0.36$. The Chapman-Jouguet mach number is 4.23. This constitutes a decrease of 0.76 in the mach number or eighteen percent of the C.J. value. For the rich mixture with $\phi = 2.12$ the lead shock mach number decreases from 4.56 to 3.812 representing a variation of 14.7 percent of the

C.J. mach number which is 4.374. The mach number variation of the lead shock is therefore quite small in the case of steady detonations.

The values of the decay parameter R_o calculated from the blast wave theory model using the experimental cell lengths from Figure 28 were 64.7 cms and 112.0 cms for the lean and rich mixtures respectively. To study the effect of the rate of lead shock decay in these off-stoichiometric mixtures, the decay parameter R_o was varied in each case to cause a shock decay twice as fast and half as fast as in the actual physical situation.

Figures 29 to 32 show the variation of temperature, reaction co-ordinate ν, enthalpy H and mach number M along particle paths in the lean mixture with $\phi = 0.36$ and $R_o = 64.7$ cms, and Figures 33 and 34 represent the temperature and reaction co-ordinate along particle paths for the rich mixture with $\phi = 2.12$ and $R_o = 112.0$ cms.

Figures 29 and 30 show that the lead shock variation is such that conditions are optimum for the exothermic recombination reactions to occur rapidly. After a brief induction period, the major part of the recombination occurs within a radial distance of about 2 millimeters, causing the temperature to rise sharply at the end of the induction zone. Although the mixture is lean, the gasdynamic flow conditions are favorable for rapid recombination. Figure 30 shows that there is no dissociation in the gas that entered the shock close to the center of explosion as in the case of Figure 12 for a marginal detonation. The maximum recombination occurs along the particle path that first entered the shock, demonstrating that the recombination rate is fairly uniform throughout the flow, and that the amount of time available for recombination controls the extent of recombination. It is seen from Figure 30 that recombination is almost complete, i.e., almost all the hydrogen present is used up. The temperature along gas particles soon reaches the equilibrium value as illustrated in

Figure 29. A comparison of Figures 14 and 31 shows that the enthalpy rises sharply in the region of exothermic chemical reaction for the "steady" detonation before falling off on account of the flow expansion.

Figure 33 and 34 illustrate the variation of temperature T and reaction co-ordinate ν along particle paths for the rich mixture with $\phi = 2.12$. The reaction is almost complete in this case also as evidenced by the low values of ν attained by the particles in Figure 34. The flow field is very much similar to the case when the hydrogen-oxygen mixture was lean. It is interesting to note that in the case of these steady detonations, that the ratio of R_o for the lean and rich mixtures which is 0.592 is very nearly equal to the ratio of the cell lengths which is 0.578.

The rate of shock decay influences the flow field in a manner similar to the case with the stoichiometric mixture described above.

In Figure 35 is plotted the shock mach number against the radius of the lead shock corresponding to the detonation cell of Figure 28a. This is a lean mixture with $R_o = 64.7$. On the same graph is plotted the radial distance travelled by a particle in the induction zone against the radius at which the particle first entered the shock. A careful examination of the mach number versus radius curve shows that there is a sharp change in the slope of the curve at a radius of about 1.410. Shortly thereafter there is a marked increase in the radial distance travelled by a particle in the induction zone. Thus there appears to be two different regimes controlling the flow and influencing the shock propagation. The location of the changes in slope of these curves corresponds extremely well to the location in the cell where the triple point path defining the cell boundary changes its direction. The radial distance travelled by a particle within the induction zone remains quite small and the reaction front stays close to the shock front. During the latter half of the shock travel, the radial distance travelled

by a particle within the induction zone increases markedly, but the rate of shock attenuation decreases. Thus the influences of the re-establishing mechanism appear to be felt during the latter half of the shock trajectory.

In Figure 36 are plotted the total time available for reaction and the induction time experienced by a particle, against the radial location at which the particle enters the shock. From the figure we see that towards the latter end of the shock trajectory, close to the end of the detonation cell the gas particles have very little time available for recombination. Indeed at the very end of the cell, the gases are still unreacted and must be heated by additional transverse waves to undergo reaction.

4. CONCLUSIONS

The results presented hitherto lead to a number of observations. The interaction of the chemical kinetics and heat release phenomena with the gasdynamics of the flow appreciably alters the temperature, density and flow velocity in a space-time co-ordinate system behind the incident shock wave (Figures 11-18). This in turn influences the strength and decay rate of the lead shock at later times as shown in Figure 24. Thus the strength and attenuation of the curved lead shock of a "steady" detonation modeled as a cylindrical blast wave, is controlled by the chemical rate processes and the hydrodynamics of the flow downstream of the lead shock wave. This is illustrated in the present calculation with special reference to the marginal detonation observed by Crooker[24].

In an actual detonation cell, a regenerative transverse wave collision mechanism at the end of the cell ensures that the lead shock strength is suddenly increased to its initial value at the beginning of the cell. In their investigation of transverse waves in detonations, it has been shown by Strehlow and co-workers[62] that at fairly high argon dilutions, the interaction of colliding triple shock configurations can be adequately described as a regular reflection of a single mach stem structure subject to an unreactive-unreactive slip stream balance condition. Therefore, while the energetics of the collision mechanism may in some cases be studied on the unreactive gas assumption, the present study shows that the rate of lead shock decay and its strength at any particular location is controlled by the reactive flow field behind the shock. The process being unsteady, the detonation cell spacing is thus dependent on the unsteady kinetic rate processes in the shocked gas.

The results of the present study show that the overall effects of the chemical processes in the hydrogen-oxygen system are strongly dependent on the initial pressure and to a lesser degree on the mixture composition, dilution and rate of shock decay. In limit situations, it is to be expected that the chemical composition of the gas and the shock decay rate will also enter strongly into the picture. Belles[63] has calculated the composition limits of detonation of hydrogen-oxygen mixtures using the criterion that the lead shock strength should be of such a magnitude as to cause spontaneous explosion of the shocked gas behind it. At the detonation limit the shock is unable to cause the gas behind it to explode. It would appear on the basis of what we now know of the complex detonation structure that the agreement obtained by Belles with the experimentally measured composition limits is fortuitous and is more likely influenced by the fact that the collision of transverse waves at the end of the detonation cell does indeed cause the gas to explode spontaneously, strengthening the lead shock wave in the process. However the lead shock strength and decay rate is coupled to the strength and rate of change of the individual shocks of the triple shock configuration. It is possible that this decay rate, which is also dependent on the chemical rate process, adjusts itself so that the effectiveness of the regenerative transverse wave collision process is still governed by the kinetic explosion limit criterion.

Thus in the present study for the lean mixture with $\phi = 0.36$ and the rich mixture with $\phi = 2.12$ we see that the lead shock strength varies by less than 20 percent and the decay rate is kept down to a minimum. Almost all the heat of reaction is released to the flow in the time available for the lead shock decay. Thus the detonation wave spontaneously avails itself of the optimum lead shock strength and decay rate such that the collision mechanism is effective within the detonation limits.

A similar argument could be presented for the pressure limits of detonation. The present study illustrates the strong influence of the initial pressure on the shock front decay (Figure 24), and hence on the pressure explosion limit of the transverse wave mechanism. This is confirmed by the experiments of Knystautas[32] on spherical detonations where the expanding detonation front fails to break up into a multifront detonation as the pressure limit of explosion is approached.

The present investigation shows that the reaction time decreases with pressure, all other conditions remaining the same, as can be seen from Figures 12, 20 and 23. The reaction zone thickness is thus reduced as the pressure increases. These results are in qualitative agreement with the observations of Jost, Just and Wagner[66], who have made optical measurements of the reaction zone behind steady waves in hydrogen-oxygen and hydrocarbon-oxygen mixtures. Their measured thicknesses are however considerably larger than calculated reaction zone thicknesses[11]. The present investigation goes further in that it reveals that during the time the shock travels through one cell length, different particles entering the shock at different radii have different induction and reaction times (Figure 36). An evaluation of the gross time as made by Jost et al can at best be taken as an average value.

The position of the reaction front is dependent on the shock strength and initial pressure as shown in Figure 27 for the experimentally observed marginal detonation. Lundstrom and Oppenheim[28] have calculated the position of the reaction front for the particular case of the detonation observed by Steel. They modeled the detonation front as a decaying blast wave, which is not purely cylindrical as in the present calculation. The interaction

of the gasdynamics with the chemical kinetics is not taken into account in their calculations, i.e., no heat release effects are considered. The position of the reaction front is not obtained by numerical integration along particle paths as in the present investigation, but is computed on the basis of the gasdynamic parameters of the flow immediately downstream of the decaying shock front. Their calculations therefore do not include the influence of chemical reaction on the shock front at later times, so that the influence of the increased shock decay rate is not reflected in their results. Also the effects of flow expansion within the induction zone is not taken into account. The present calculations show that the real kinetic behavior of the hydrogen-oxygen system results in a longer induction period than if the interaction of the chemical kinetics and the hydrodynamics be neglected.

Figure 24 shows that the rate of decay of the lead shock is greater when chemical reaction is present. It is seen from Figure 4 that the cylindrical blast wave model used in this study does indeed give a fairly close agreement with the measured shock trajectory of Crooker[24]. Figure 24 shows that by the time the shock has reached a non-dimensional radius of 0.8 the increased shock decay rate has caused the shock mach number in the reactive mixture to decrease by about 0.95 more than in the non-reactive case, for the same initial pressure of 58 torr. It was observed by Crooker that in the vicinity of this radius the mach number versus radius curve on a semi-log plot exhibited a distinct change in slope. The present calculations show that beyond this radius, the decay of the shock in the reactive gas is the same as that of the shock in the frozen composition gas. Figure 27 also shows that near this radius of 0.8 there is a marked increase in

the radial distance travelled by a particle within the induction zone. Thus it would appear that as far as the shock front is concerned, there is a decoupling of the shock front from the reaction front at this point in the shock trajectory. This decoupling of the shock and reaction fronts lowers the rate of shock decay and the shock front behaves as if it were propagating in a non-reactive medium. This same effect is also observed in Figure 35 in the case of a steady detonation in the lean mixture with $\phi = 0.36$.

A similar effect has been observed by Bach, Knystautas and Lee[65]. In their experiments on spherical detonations in acetylene-oxygen mixtures they find that the shock and reaction fronts become decoupled when the energy deposited in the flow by the laser spark source initiating the explosion is a critical value. The shock wave which is initially overdriven as in our observations, first decays and the reaction front subsequently decouples from the shock front. It is also observed from the experimental shock trajectory of Bach et al that following this decoupling, the shock front decays at a reduced rate, followed finally by the breaking up of the spherical shock wave into a multifront detonation.

It would be worthwhile investigating whether the lead shock mach number at this point where decoupling occurs is such that it fails to cause the gas to explode spontaneously behind it. It would also be interesting to see if the shock decay rate from this point to the end of the cell is related to the strength of the transverse wave mechanism at the end of the cell, such that the collision of transverse waves just enables the gas to spontaneously explode.

The present study shows that not all the latent chemical energy is released to the flow if the gas is processed by the lead shock alone. Thus for the cylindrical detonation model used in this study, the calculations

show that for the detonation propagating in the rich mixture with $\phi = 2.12$, the lowest value of ν attained by a particle is 0.2, while for the lean mixture with $\phi = 0.36$, the lowest value of ν is 0.15. Or in other words, about eighty percent of the available chemical energy is imparted to the flow in the case of the rich mixture and eighty-five percent in the case of the lean mixture when the gas is processed by the lead shock alone. The exact amount of energy given to the flow is dependent on the ν values as well as the stoichiometry of the mixture. In the case of the marginal detonation studied in this work the lowest value of ν attained along the particle paths is only 0.675, i.e., 32.5 percent of the energy has been released to the flow.

It has already been mentioned that the strength of the transverse wave regenerating mechanism is high in the case of the marginal detonation. The lead shock wave is regenerated by the sudden release of explosive chemical energy brought about by the interaction of colliding transverse waves. In the case of the marginal detonation a large part of the chemical energy is still available as evidenced by the high values of ν attained by the particles. This energy is utilized or released by the colliding transverse waves to strongly boost the lead shock strength. In the case of "steady" detonations, the major part of the chemical energy has already been released to the flow as the gas is traversed by the lead shock. The lead shock decay is small and the transverse wave regenerating mechanism has only a small portion of the chemical energy available to bolster the lead shock strength. This is just sufficient to increase the mach number of the lead shock to its value at the beginning of the cell.

Thus the underlying propagating mechanism of the detonation avails itself of the correct lead shock strength and decay rate in conjunction with

the prevailing chemical, thermodynamic and gasdynamic constraints. This is evidenced by the fact that very regular cell spacings are observed in such systems as the hydrogen-oxygen system, the ethylene and acetylene systems, but the spacings are not regular in other systems such as the propane system, where the chemistry of the heat release is markedly different. However even for those cases where the structure is regular the process is non-steady and any quantitative study should be integrated with respect to time. Thus it would be interesting to evaluate the chemical energy given to the flow, integrated along all the particle paths, during the time that the lead shock traverses one cell length to see if this is related in any way to the difference in blast wave energy of the lead shock wave from the beginning to the end of the cell. It would also be interesting to see if the rate of energy release through chemical reaction is related to the enthalpy change across the lead shock at the point where decoupling of the reaction front occurs.

APPENDIX

CHARACTERISTIC DIRECTIONS IN ONE DIMENSIONAL NON-STEADY REACTIVE FLOW

The governing equations for one dimensional non-steady reactive flow are

$$\text{Continuity:} \quad \frac{\partial \rho}{\partial t} + u \frac{\partial \rho}{\partial r} + \rho \frac{\partial u}{\partial r} + \frac{\rho u}{r} = 0 \tag{1}$$

$$\text{Momentum:} \quad \rho \frac{\partial u}{\partial t} + \rho u \frac{\partial u}{\partial r} + \frac{\partial p}{\partial r} = 0 \tag{2}$$

$$\text{Energy:} \quad \rho \frac{Dh}{Dt} - \frac{Dp}{Dt} = 0 \tag{3}$$

$$\text{Rate:} \quad \frac{d\nu}{dt} = \omega\ (p, \rho, \nu) \tag{4}$$

$$\text{State:} \quad h = h\ (p, \rho, \nu) \tag{5}$$

We can use the equation of state (5) to find $\frac{Dh}{Dt}$ in the energy equation (3). Therefore differentiating equation (5) w.r.t.r and t and substituting in (3) we get

$$- \frac{1}{a_f^2} \frac{\partial p}{\partial t} - \frac{u}{a_f^2} \frac{\partial p}{\partial r} + \frac{\partial \rho}{\partial t} + u \frac{\partial \rho}{\partial r} + \frac{h_\nu}{h_\rho} \frac{\partial \nu}{\partial t} + \frac{u h_\nu}{h_\rho} \frac{\partial \nu}{\partial r} = 0 \tag{6}$$

where the frozen sound velocity

$$a_f = \frac{\rho h_p - 1}{\rho h_\rho} \tag{7}$$

and $h_p = \frac{\partial h}{\partial p}$ etc.

We have three basic dependent variables namely p, ρ and ν and need three differential equations to work with. Hence the three differential equations chosen are the continuity equation (1), the momentum equation (2) and the combined equation (6).

Let us transform these three equations to (ξ,η) co-ordinates. We then have:

Continuity Equation: $$\frac{\partial \rho}{\partial \xi}\left(\frac{\partial \xi}{\partial t} + u\frac{\partial \xi}{\partial r}\right) + \frac{\partial u}{\partial \xi}\,\rho\,\frac{\partial \xi}{\partial r}$$

$$= -\left(\frac{\partial \rho}{\partial \eta}\,\frac{\partial \eta}{\partial t} + u\frac{\partial \rho}{\partial \eta}\frac{\partial \eta}{\partial r} + \rho\frac{\partial u}{\partial \eta}\frac{\partial \eta}{\partial r} + \frac{\rho u}{r}\right) \qquad (8)$$

Momentum Equation: $$\frac{\partial p}{\partial \xi}\frac{\partial \xi}{\partial r} + \frac{\partial u}{\partial \xi}\left(\frac{\partial \xi}{\partial t} + u\frac{\partial \xi}{\partial r}\right)\rho = -\left(\frac{\partial p}{\partial \eta}\frac{\partial \eta}{\partial r} + \rho\frac{\partial u}{\partial \eta}\,\frac{\partial \eta}{\partial t} + \right.$$

$$\left.\rho u\frac{\partial u}{\partial \eta}\,\frac{\partial \eta}{\partial r}\right) \qquad (9)$$

Combined Energy and State Equation:

$$\frac{\partial p}{\partial \xi}\left(\frac{\partial \xi}{\partial t} + u\frac{\partial \xi}{\partial r}\right)\left(-\frac{1}{a_f^2}\right) + \frac{\partial \rho}{\partial \xi}\left(\frac{\partial \xi}{\partial t} + u\frac{\partial \xi}{\partial r}\right) =$$

$$\frac{1}{a_f^2}\,\frac{\partial p}{\partial \eta}\,\frac{\partial \eta}{\partial t} + \frac{u}{a_f^2}\,\frac{\partial p}{\partial \eta}\,\frac{\partial \eta}{\partial r} - \frac{\partial \rho}{\partial \eta}\,\frac{\partial \eta}{\partial t} - u\frac{\partial \rho}{\partial \eta}\,\frac{\partial \eta}{\partial r} - \frac{h_\nu}{h_\rho}\frac{\partial \nu}{\partial t} -$$

$$\frac{h_\nu}{h_\rho}\,u\,\frac{\partial \nu}{\partial r} \qquad (10)$$

The first derivatives of the quantities p, ρ, ν can be discontinous across the characteristic lines. Therefore from equations (8), (9) and (10) we have the determinant

$$\begin{vmatrix} \frac{\partial \xi}{\partial r} & 0 & \rho\left(\frac{\partial \xi}{\partial t} + u\,\frac{\partial \xi}{\partial r}\right) \\ 0 & \left(\frac{\partial \xi}{\partial t} + u\,\frac{\partial \xi}{\partial r}\right) & \rho\,\frac{\partial \xi}{\partial r} \\ \left(\frac{\partial \xi}{\partial t} + u\,\frac{\partial \xi}{\partial r}\right)\left(-\frac{1}{a_f^2}\right) & \left(\frac{\partial \xi}{\partial t} + u\,\frac{\partial \xi}{\partial r}\right) & 0 \end{vmatrix} = 0 \qquad (11)$$

from whence we get

$$a_f^2 \left(\frac{\partial \xi}{\partial r}\right)^2 = \left(\frac{\partial \xi}{\partial t} + u\,\frac{\partial \xi}{\partial r}\right)^2$$

i.e., $$a_f \frac{\partial \xi}{\partial r} = \pm \left(\frac{\partial \xi}{\partial t} + u\,\frac{\partial \xi}{\partial r}\right)$$

from which we get the relation along the characteristic direction as

$$\frac{dr}{dt} = (u \pm a_f)$$

From equation (3) we see that

$$\frac{dr}{dt} = u$$

is already a characteristic direction.

Therefore the characteristic directions for one-dimensional, non-steady, reactive flow are

$$\frac{dr}{dt} = u + a_f \qquad (12)$$

$$\frac{dr}{dt} = u - a_f \tag{13}$$

and

$$\frac{dr}{dt} = u \tag{14}$$

The characteristic relations which apply along these directions may be derived from the above determinant system, but are obtained more easily in the body of the text.

LIST OF REFERENCES

1. A.J. Laderman, P.A. Urtiew and A.K. Oppenheim, On the Generation of a Shock Wave by a Flame in an Explosive Gas, Ninth Symposium (Intl.) on Combustion, p. 265, Academic Press, N.Y., 1963.

2. W.J.M. Rankine, Transactions Royal Society (London) 160, 277, 1870.

3. H. Hugoniot, J. de Lecole Polyl., 58, 1, 1889.

4. D.L. Chapman, Phil. Mag., 5, 47, 90, 1889.

5. E. Jouguet, J. Pure and Applied Mathematics, 1, 347, 1905; 2, 1, 1906.

6. H. Gg. Wagner, "Fundamental Data Obtained from Shock Tube Experiments", p. 329, Pergamon Press, New York, 1961.

7. Y. B. Zel'dovich, J. Exptl. Theor. Phys. (U.S.S.R.), 10, 542, 1940.

8. J. Von Neumann, O.S.R.D., Report No. 549, Ballistic Research Laboratory File No. X-122, Aberdeen Proving Ground, Maryland, (1962).

9. W. Doring, Annalen der Physik, 43, 421, 1943.

10. H. Gg. Wagner, Reaction Zone and Stability of a Gaseous Detonation, Ninth Symposium (Intl.) on Combustion, p. 454, Academic Press, N.Y., 1963.

11. R. A. Strehlow, Gas Phase Detonations; Recent Developments, Combustion and Flame, V. 12, No. 2, 1968.

12. K. I. Shchelkin and Ya. K. Troshin. "Gasdynamics of Combustion", p. 12, Mono Book Corporation, Baltimore, 1965.

13. R. A. Strehlow and F. D. Fernandes, Combustion and Flame, 9, 109, 1965.

14. H. O. Barthel and R. A. Strehlow, Physics of Fluids, 9, 1896, 1966.

15. P. A. Urtiew and A. K. Oppenheim, Detonative Ignition by Shock Merging, Eleventh Symposium (Intl.) on Combustion, p. 665, The Combustion Institute, 1967.

16. Yu. N. Denisov and Ya. K. Troshin, On the Mechanism of Detonative Combustion, Eight Symposium (Intl.) on Combustion, p. 600, Williams and Wilkins Co., Baltimore, 1962.

17. A. K. Oppenheim, Private Communication, 1969.

18. W. W. Wood, Physics of Fluids, 6, 1081, 1963.

19. D. B. Spalding, Ninth Symposium (Intl.) on Combustion, p. 417, Academic Press, N.Y., 1963.

20. D. R. White, Physics of Fluids, 4, p. 465-480, 1961.

21. R. I. Soloukhin, Soviet Physics - Uspekhi, 6, p. 523-541, 1964.

22. K. I. Shchelkin, The Nature of a Detonation, U. S. Dept. of Commerce, TT: 66-30504, 1966.

23. Yu. N. Denisov and Ya. K. Troshin, Structure of Gaseous Detonation in Tubes, Translation from Zhurnal Tekhnicheskoi Fiziki Vol. 30, No. 4, p. 450-459, April, 1960.

24. A. J. Crooker, Phenomenological Investigation of Low Mode Planar Detonations, Ph.D. Thesis, Univ. of Illinois, Urbana, 1969.

25. G. B. Steel, Experimental Study of the Wave Structure of Marginal Detonations in a Rectangular Tube, Report No. 3, College of Engineering, University of California, Berkeley, 1966.

26. G. J. Mullaney and R. Arave, Determination of Induction times in One-Dimensional Detonations, Report D1-82-0 324, Boeing Scientific Research Laboratories, 1963.

27. D. R. White, Physics of Fluids, 6, p. 749 and 1011, 1963.

28. E. A. Lundstrom and A. K. Oppenheim, On the Influence of Non-Steadiness on the Thickness of the Detonation Wave, Proceedings Royal Society, Series A, No. 1503, Vol. 310, June, 1969.

29. R. I. Soloukhin, "Shock and Detonation Waves in Gases", p. 138, Mono Book Corporation, Baltimore, 1966.

30. V. V. Mitrofanov and R. I. Soloukhin, Soviet Physics, Doklady, Vol. 9, No. 12, p. 1055, 1964.

31. W. G. Struck and H. W. Reichenbach, Eleventh Symposium (Intl.) on Combustion, p. 677, The Combustion Institute, 1967.

32. R. Knystautas, An Experimental Study of Spherical Gaseous Detonation Waves, MERL Report 69-2, Dept. of Mech. Engg., McGill University, Montreal, Canada, 1969.

33. J. Brossard, N. Manson and M. Niollet, Eleventh Symposium (Intl.) on Combustion, p. 623, The Combustion Institute, 1967.

34. J. H. Lee, B. H. K. Lee and I. Shanfield, Tenth Symposium (Intl.) on Combustion, p. 805, 1965.

35. J. H. Lee, B. H. K. Lee and R. Knystautas, Physics of Fluids, Vol. 9, No. 1, p. 221, 1966.

36. R. Knystautas and J. H. Lee, A.I.A.A. Journal, Vol. 5, No. 6, p. 209, 1967.

37. J. H. Lee and R. Knystautas, A.I.A.A. Journal, Vol. 7, No. 2, p. 312, 1969.

38. L. J. Zajac and A. K. Oppenheim, Dynamics of an Explosive Hot Spot, College of Engineering, Univ. of California, Berkeley, 1969.

39. L. I. Sedov, "Similarity and Dimensional Methods in Mechanics", Edited by M. Holt, Academic Press, 1959.

40. G. I. Taylor, The Formation of a Blast Wave by a Very Intense Explosion, I. Theoretical Discussion, Proc. Roy. Society, (London) A201, 159-174, 1950.

41. S. C. Lin, Cylindrical Shock Waves Produced by Instantaneous Energy Release, J. Appl. Physics, 25, 54-57, 1954.

42. P. C. Chou, R. P. Karpp and S. L. Huang, Numerical Calculation of Blast Waves by the Method of Characteristics, A.I.A.A. Journal, Vol. 5, No. 4, p. 618, 1967.

43. V. P. Korobeinikov, N. S. Melnikova and E. V. Ryazanov, "Theory of Point Explosions" (in Russian). Goz. Izdot. Fiz.-Mat., Mowcow, 1961.

44. A. Sakurai, "Blast Wave Theory", in "Basic Developments in Fluid Dynamics", Vol. 1, Ed. Maurice Holt, Academic Press, 1965.

45. K. Oshima, Rept. Aeronautical Res. Inst. Univ. of Tokyo, No. 358, 1960.

46. B. T. Chu, "Wave Propagation and the Method of Characteristics in Reacting Gas Mixtures with Applications to Hypersonic Flow", W.A.D.C. TN. 57-213, 1957.

47. G. L. Schott and J. C. Kinsey, Kinetic Studies of Hydroxyl Radicals in Shock Waves II. Induction times in the Hydrogen-Oxygen Reaction, J. Chem. Physics, Vol. 29, No. 5, p. 1177, 1958.

48. G. L. Schott, Kinetic Studies of Hydroxyl Radicals in Shock Waves III. The OH Concentration Maximum in the Hydrogen-Oxygen Reaction, The Journal of Chemical Physics, Vol. 32, No. 3, 1960.

49. R. A. Strehlow and A. Cohen, Initiation of Detonation, Physics of Fluids, Vol. 5, No. 1, Jan., 1962.

50. R. W. Getzinger and G. L. Schott, Recombination via the $H + O_2 + M \longrightarrow HO_2 + M$ Reaction in Lean Hydrogen-Oxygen Mixtures, J. Chem. Phys., Vol. 43, No. 9, 1965.

51. G. L. Schott and P. F. Bird, Recombination Rates in Rich Hydrogen-Oxygen Mixtures, J. Chem. Phys., Vol. 41, No. 9, 1964.

52. R. W. Getzinger, A. Shock Wave Study of Recombination in Near-Stoichiometric Hydrogen-Oxygen Mixtures, Eleventh Symposium (Intl.) on Combustion, p. 117, 1967.

53. R. A. Strehlow and P. M. Rubins, Experimental and Analytical Study of H_2-Air Reaction Kinetics Using a Standing Normal Shock, Paper No. 67-479, A.I.A.A. 3rd Propulsion Joint Specialist Conference, Washington, July, 1967.

54. D. R. Stull, JANAF Thermochemical Tables, Dow Chemical Company, Midland, Michigan.

55. R. Courant, "Partial Differential Equations", Vol. II of Methods of Mathematical Physics, p. 466, Interscience Publishers, 1962.

56. J. J. Der, Theoretical Studies of Supersonic Two-Dimensional and Axisymmetric Non-Equilibrium Flow, including Calculations of Flow through a Nozzle", NASA TR 164, 1963.

57. A. Sakurai, "Blast Wave Theory", in "Basic Developments in Fluid Dynamics", Vol. 1, Ed. by M. Holt, Academic Press, 1965.

58. R. A. Strehlow, To be published.

59. R. A. Strehlow and J. R. Biller, "On the Strength of Transverse Waves in Detonations", Comb. and Flame, 13, (in press).

60. R. I. Soloukhin, "Shock Waves and Detonations in Gases", Mono. Book Corp., Baltimore, p. 145, 1966.

61. W. W. Wood and J. Kirkwood, Applied Physics, Vol. 28, No. 4, p. 395, 1957.

62. R. A. Strehlow, R. Liaugminas, R. H. Watson and J. R. Eyman, "Transverse Wave Structure in Detonations", Eleventh Symposium (Intl.) on Combustion, The Combustion Institute, 1967.

63. F. E. Belles, "Detonability and Chemical Kinetics: Prediction of the Limits of Detonability of Hydrogen", Seventh Symposium (Intl.) on Combustion, Butterworths Scientific Publications, 1959.

64. R. A. Strehlow, "Multidimensional Detonation Wave Structures", To be published.

65. G. G. Bach, R. Knystautas, and J. H. Lee, "Direct Initiation of Spherical Detonations in Gaseous Explosives", McGill University, Montreal, Canada, 1969.

66. W. Jost, Th. Just and H. Gg. Wagner, "Investigation of the Reaction Zone of Gaseous Detonations", Eighth Symposium (Intl.) on Combustion, Williams and Wilkins Company, 1962.

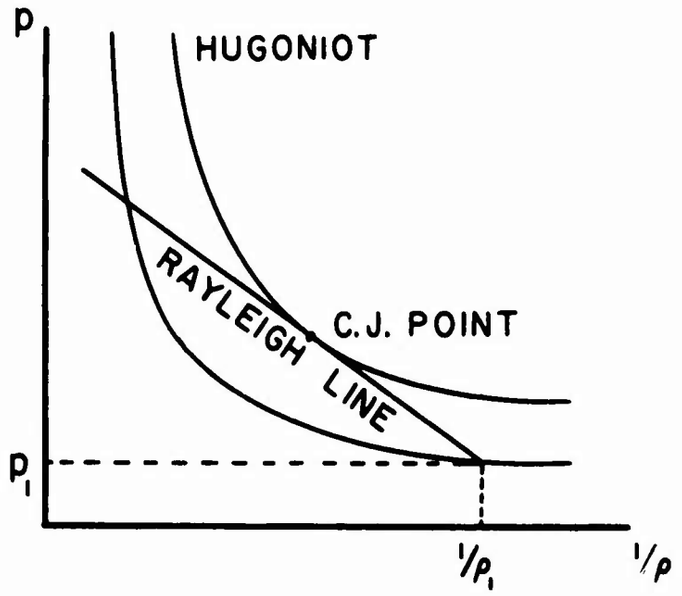

FIGURE 1

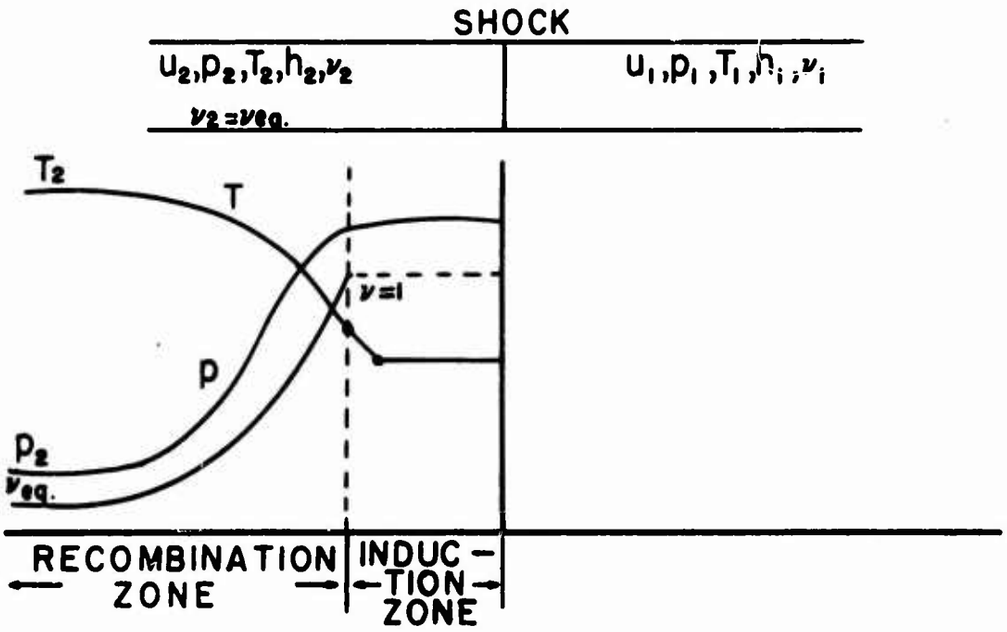

FIGURE 2

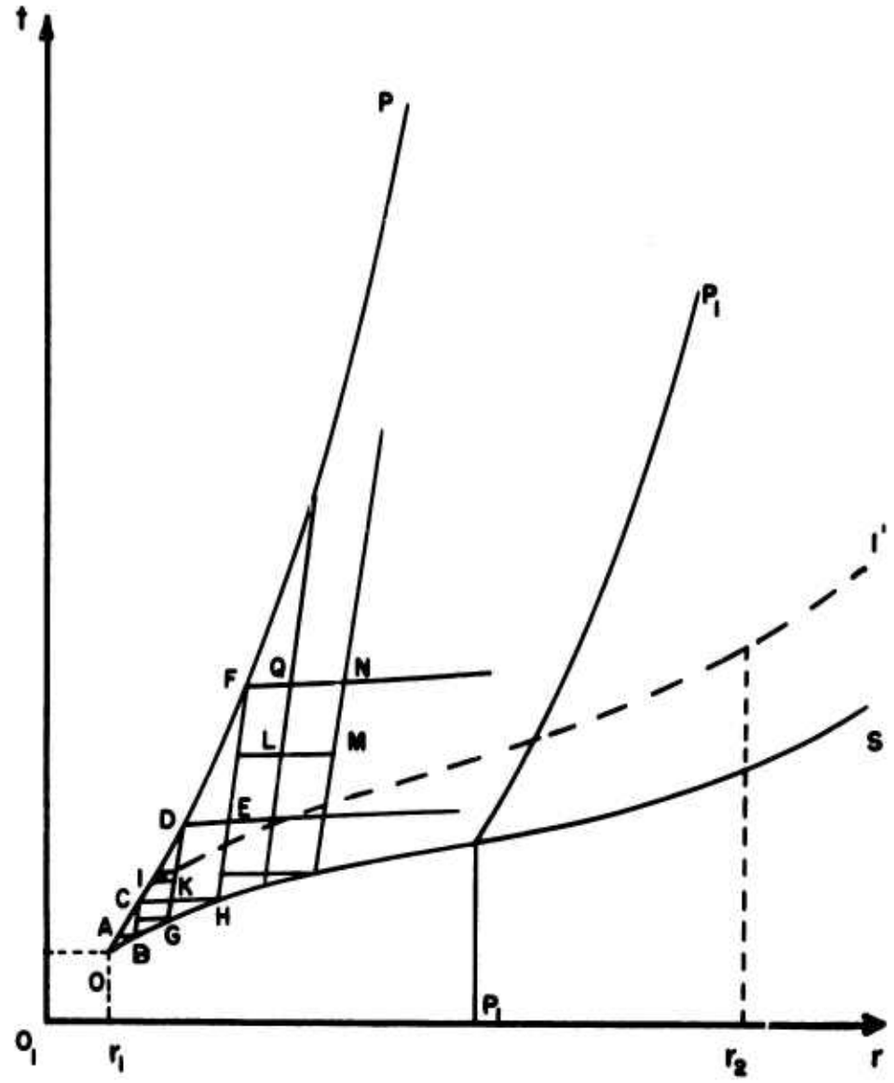

FIG. 3

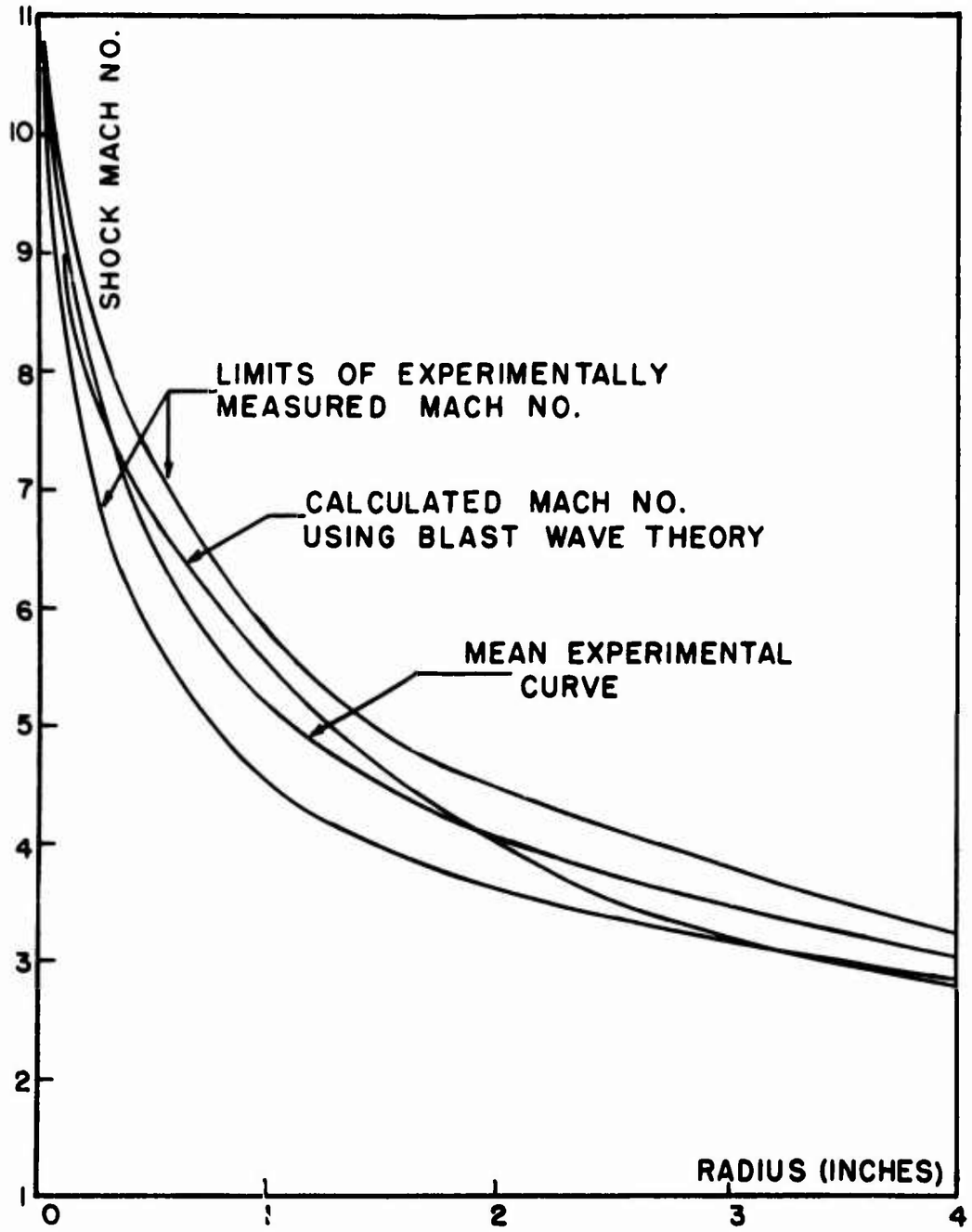
SHOCK MACH NO.
LIMITS OF EXPERIMENTALLY MEASURED MACH NO.
CALCULATED MACH NO. USING BLAST WAVE THEORY
MEAN EXPERIMENTAL CURVE
RADIUS (INCHES)
11
10
9
8
7
6
5
4
3
2
1
0
1
2
3
4

FIGURE 4

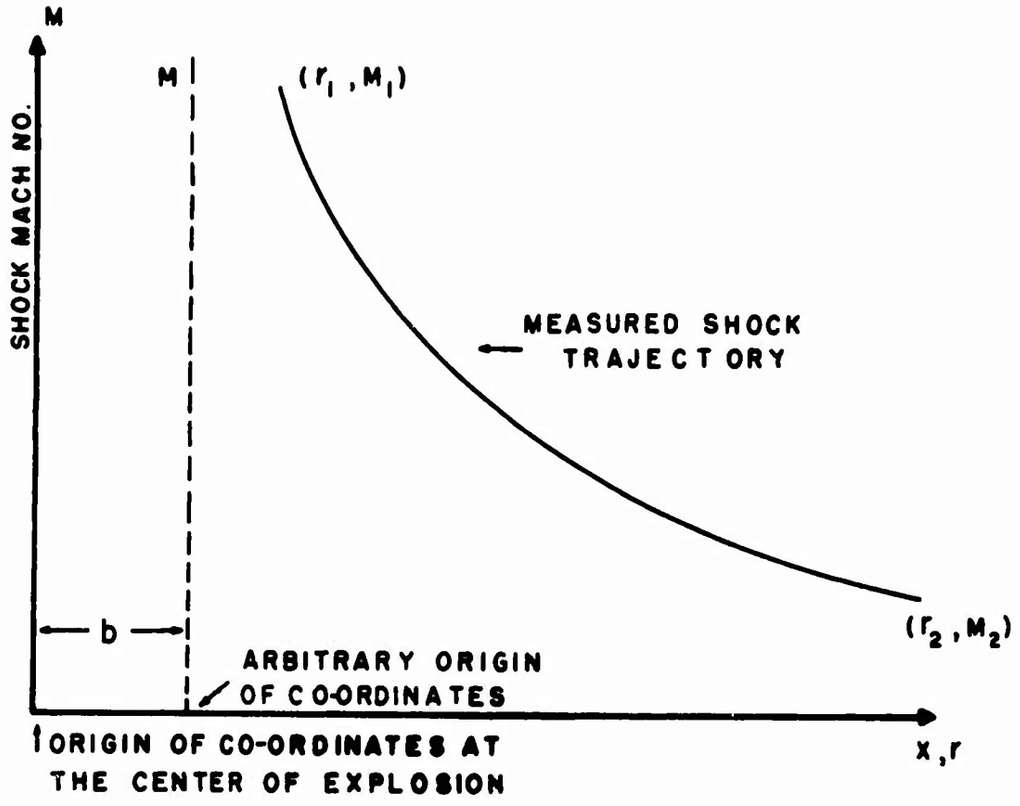
M
SHOCK MACH NO.
M
(r_1, M_1)
MEASURED SHOCK TRAJECTORY
(r_2, M_2)
b
ARBITRARY ORIGIN OF CO-ORDINATES
ORIGIN OF CO-ORDINATES AT THE CENTER OF EXPLOSION
x, r

FIGURE 5

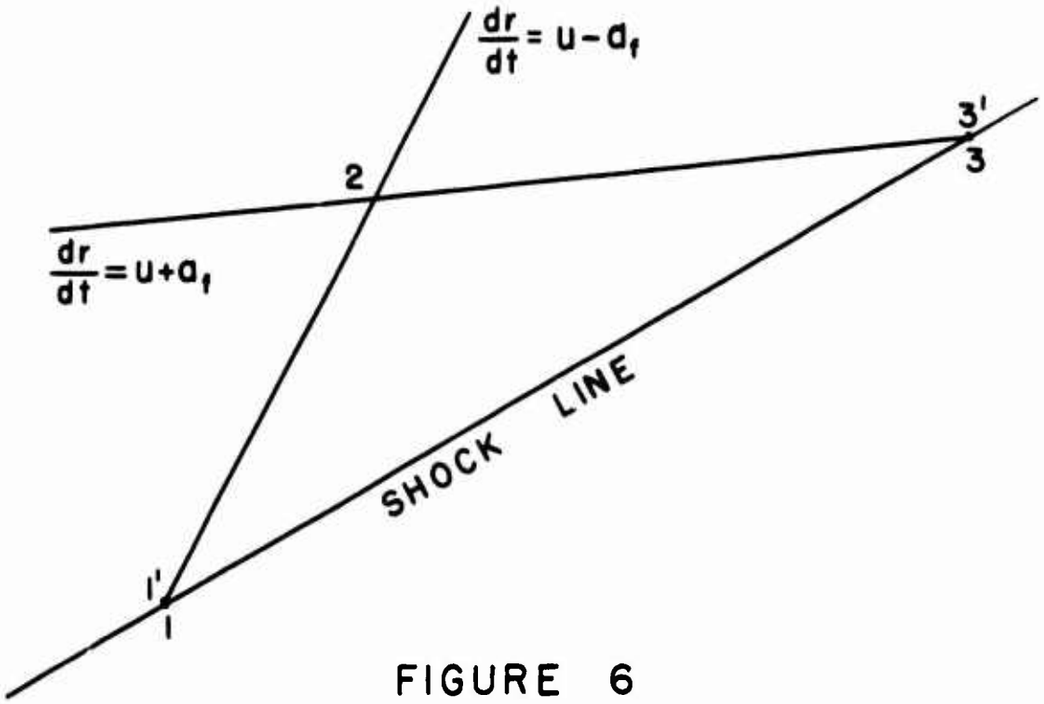

FIGURE 6

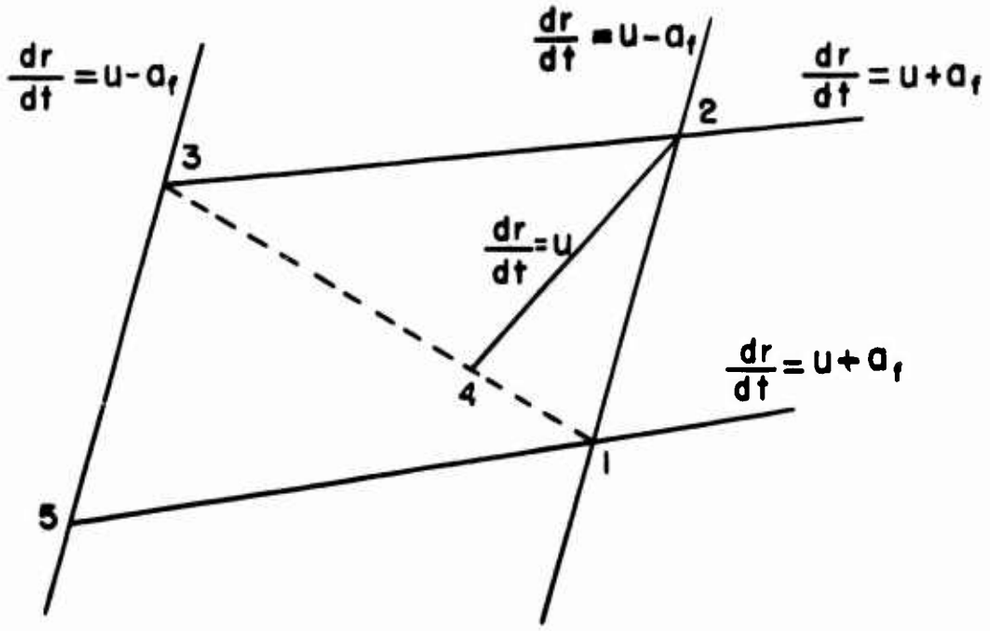

FIGURE 7

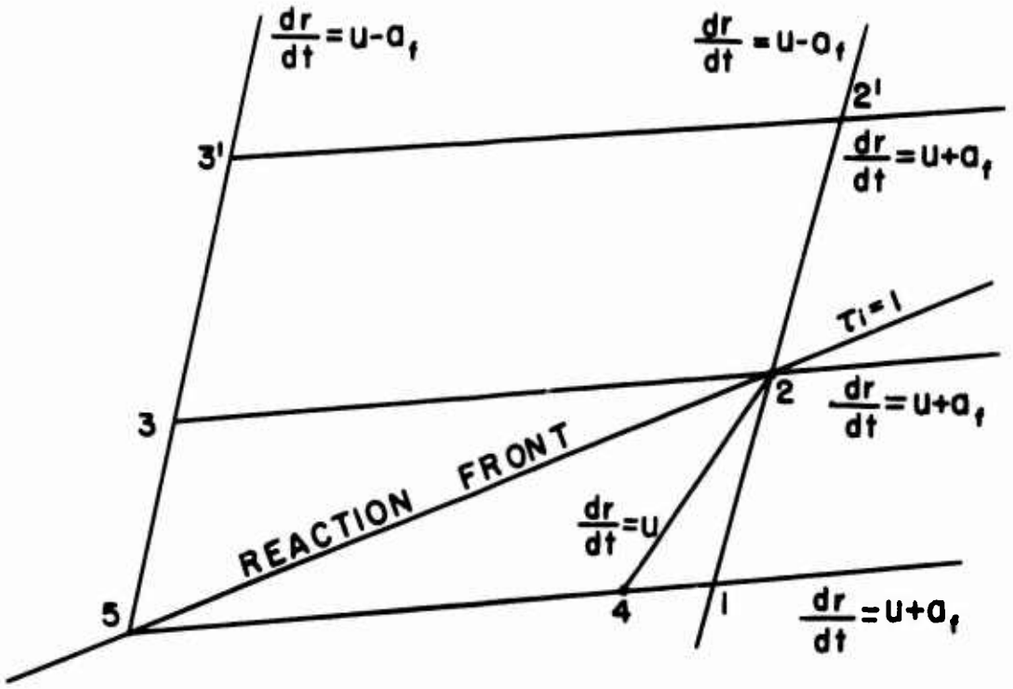

FIGURE 8

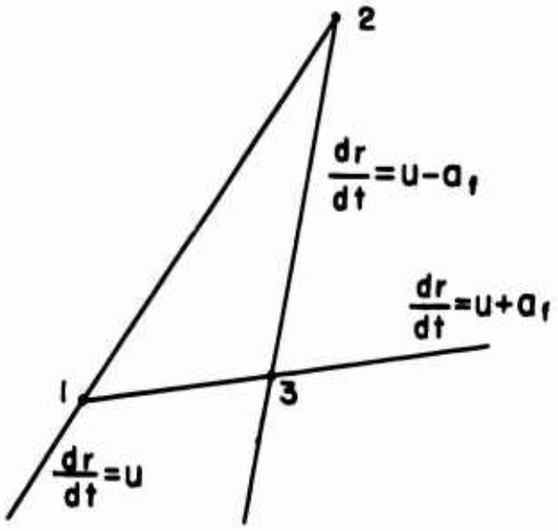

FIGURE 9

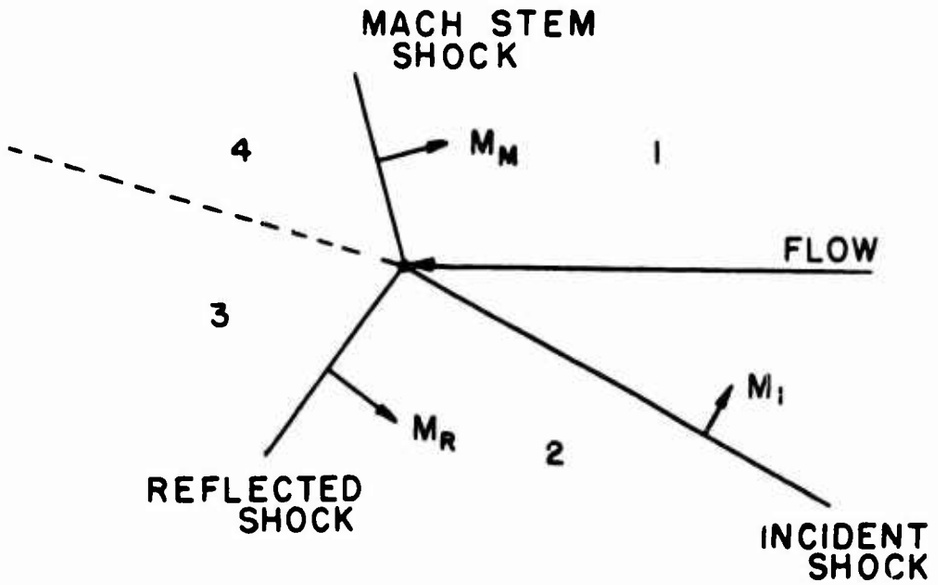

(a) STEADY MACH STEM CONFIGURATION

FIGURE 10

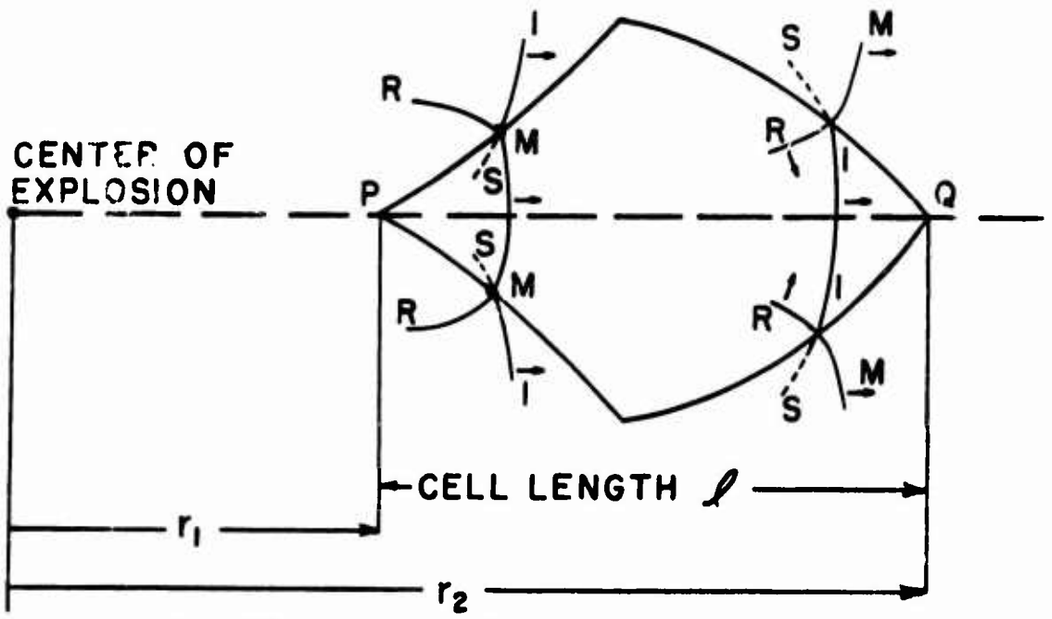

(b) TYPICAL DETONATION CELL

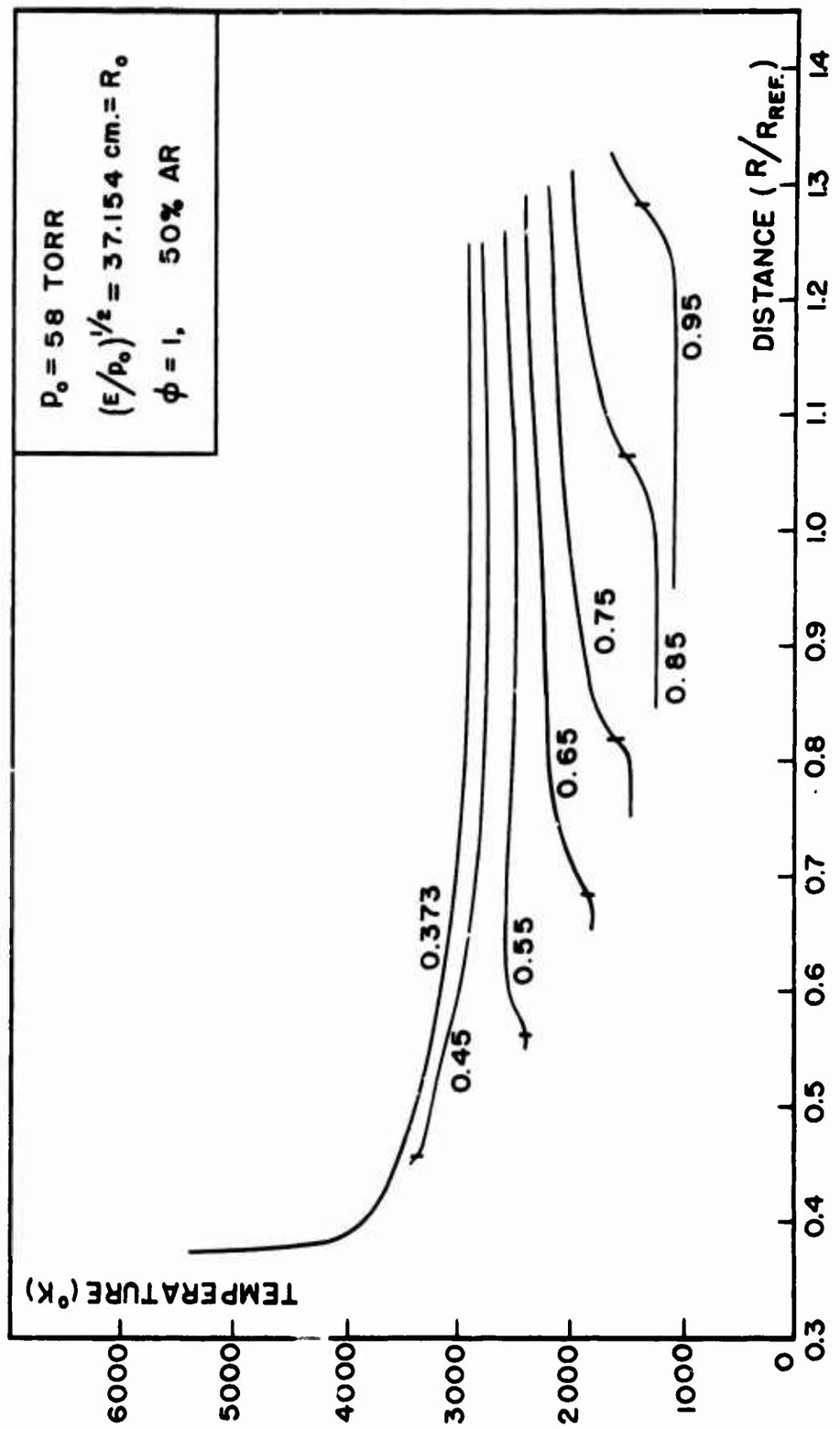
P_o = 58 TORR
$(\varepsilon/p_o)^{1/2}$ = 37.154 cm. = R_o
ϕ = 1, 50% AR
TEMPERATURE (°K)
DISTANCE ($R/R_{REF.}$)
0.373
0.45
0.55
0.65
0.75
0.85
0.95
6000
5000
4000
3000
2000
1000
0
0.3
0.4
0.5
0.6
0.7
0.8
0.9
1.0
1.1
1.2
1.3
1.4

FIGURE 11

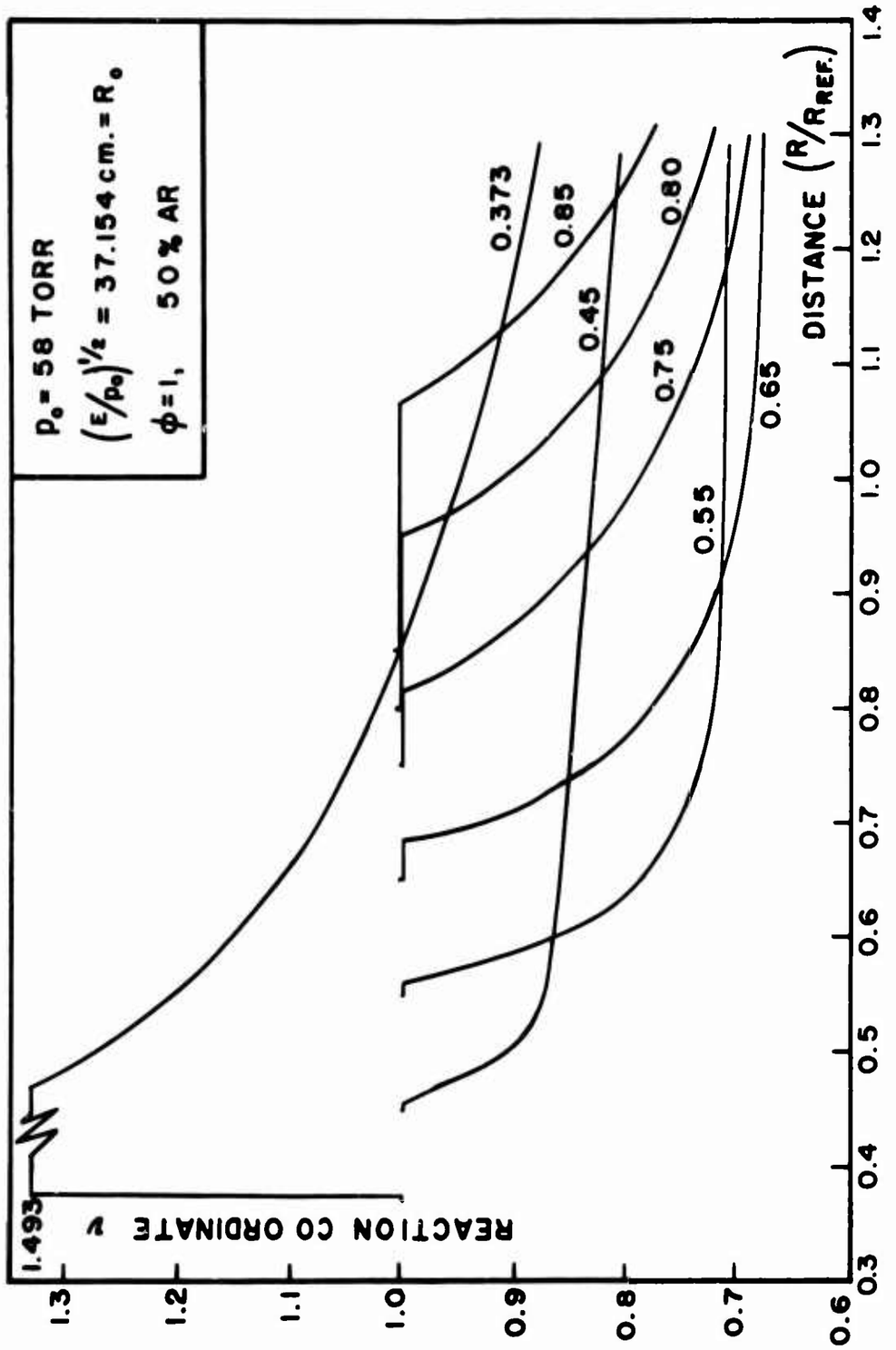
p_o = 58 TORR
$(E/p_o)^{1/2}$ = 37.154 cm. = R_o
ϕ=1, 50% AR
0.373
0.85
0.45
0.80
0.75
0.65
0.55
1.493
REACTION CO ORDINATE
DISTANCE $(R/R_{REF.})$
0.3 0.4 0.5 0.6 0.7 0.8 0.9 1.0 1.1 1.2 1.3 1.4
0.6 0.7 0.8 0.9 1.0 1.1 1.2 1.3

FIGURE 12

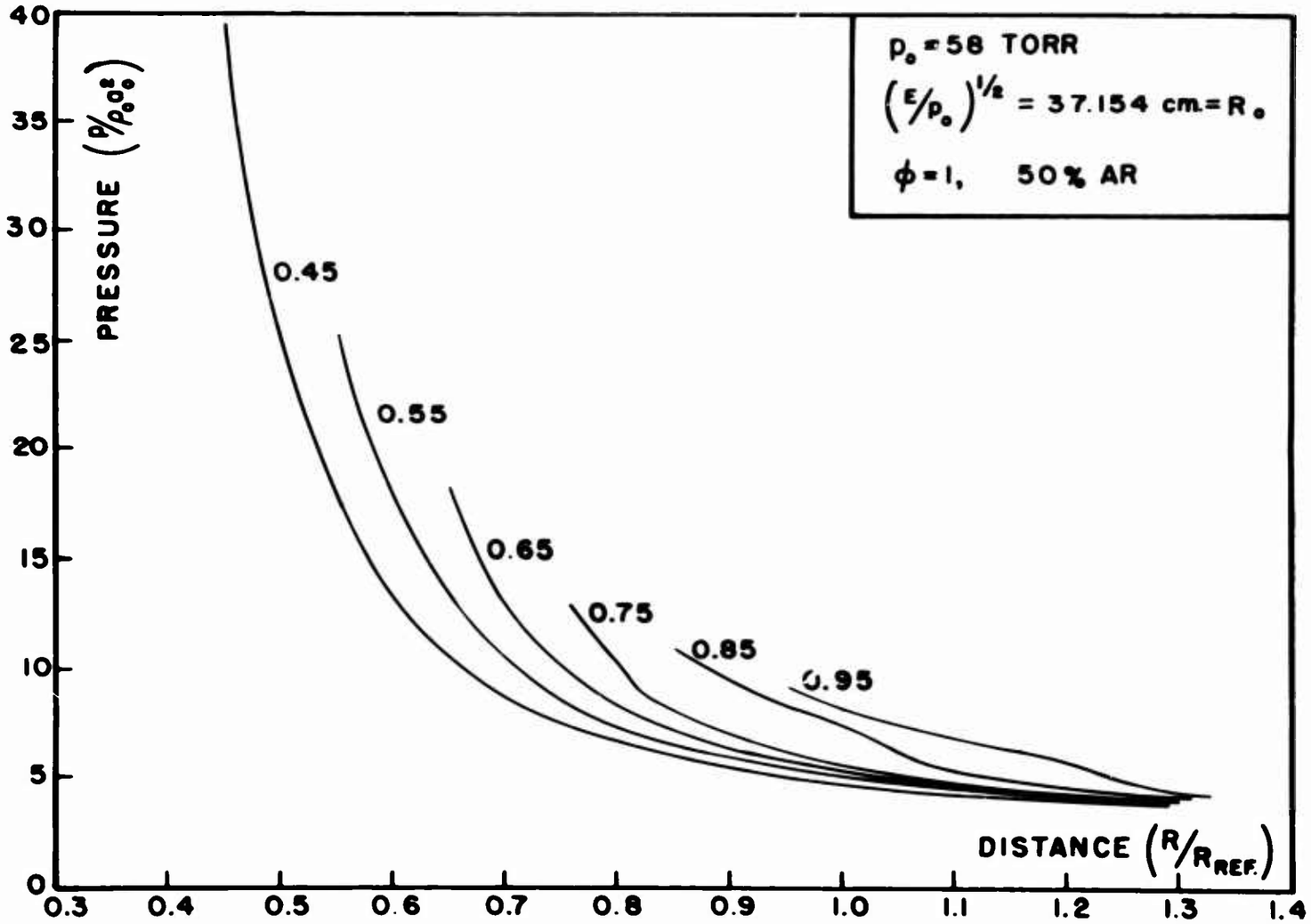
p_o = 58 TORR
$(E/p_o)^{1/2}$ = 37.154 cm = R_o
ϕ = 1, 50% AR
0.45
0.55
0.65
0.75
0.85
0.95
PRESSURE (%p_{00})
DISTANCE ($R/R_{REF.}$)
0
5
10
15
20
25
30
35
40
0.3
0.4
0.5
0.6
0.7
0.8
0.9
1.0
1.1
1.2
1.3
1.4

FIGURE 13

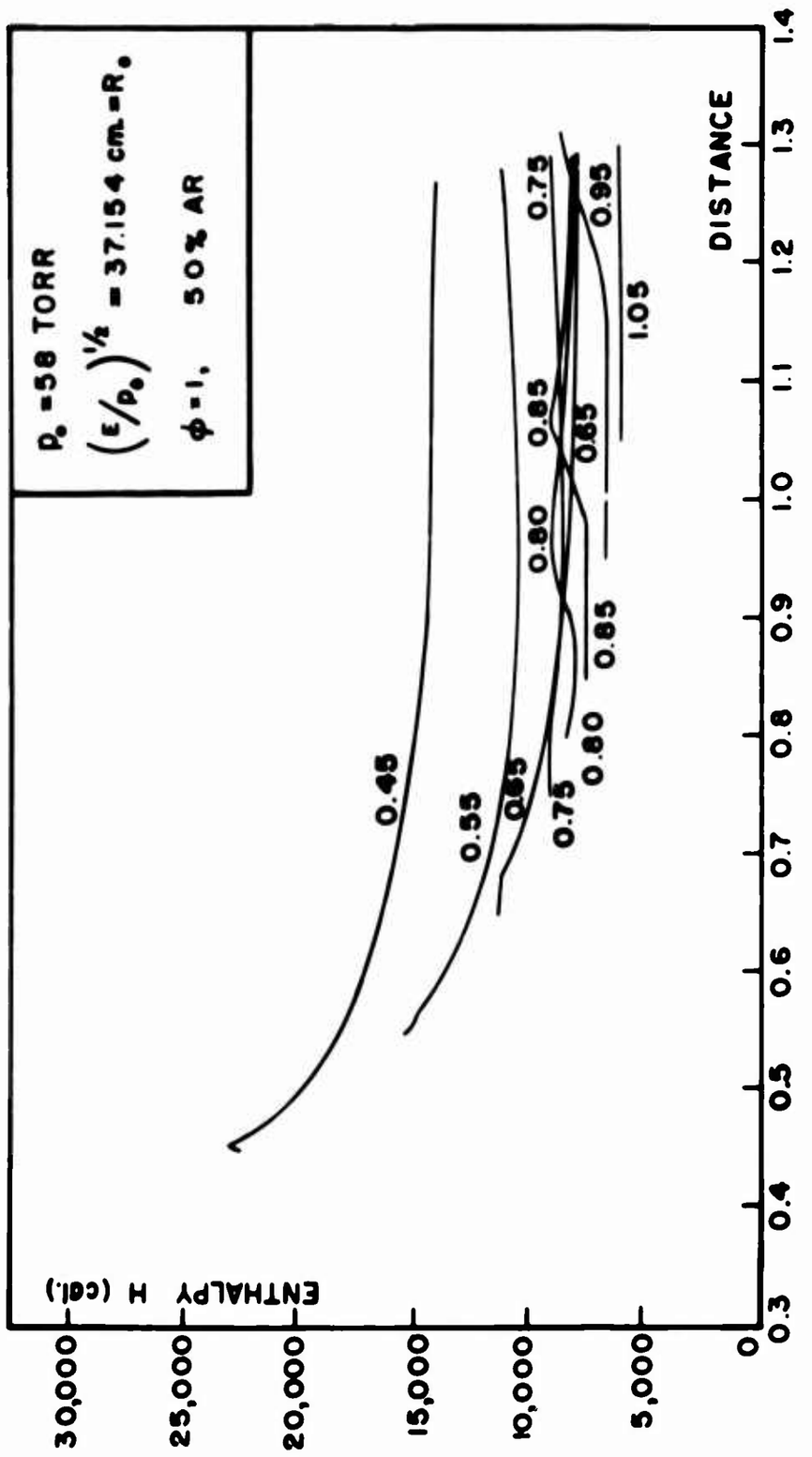
p_o = 58 TORR
$(\varepsilon/p_o)^{1/2}$ = 37.154 cm = R_o
ϕ = 1, 50% AR
ENTHALPY H (cal.)
DISTANCE
30,000
25,000
20,000
15,000
10,000
5,000
0
0.3
0.4
0.5
0.6
0.7
0.8
0.9
1.0
1.1
1.2
1.3
1.4
0.45
0.55
0.65
0.75
0.80
0.85
0.75
0.80
0.85
0.85
0.95
1.05

FIGURE 14

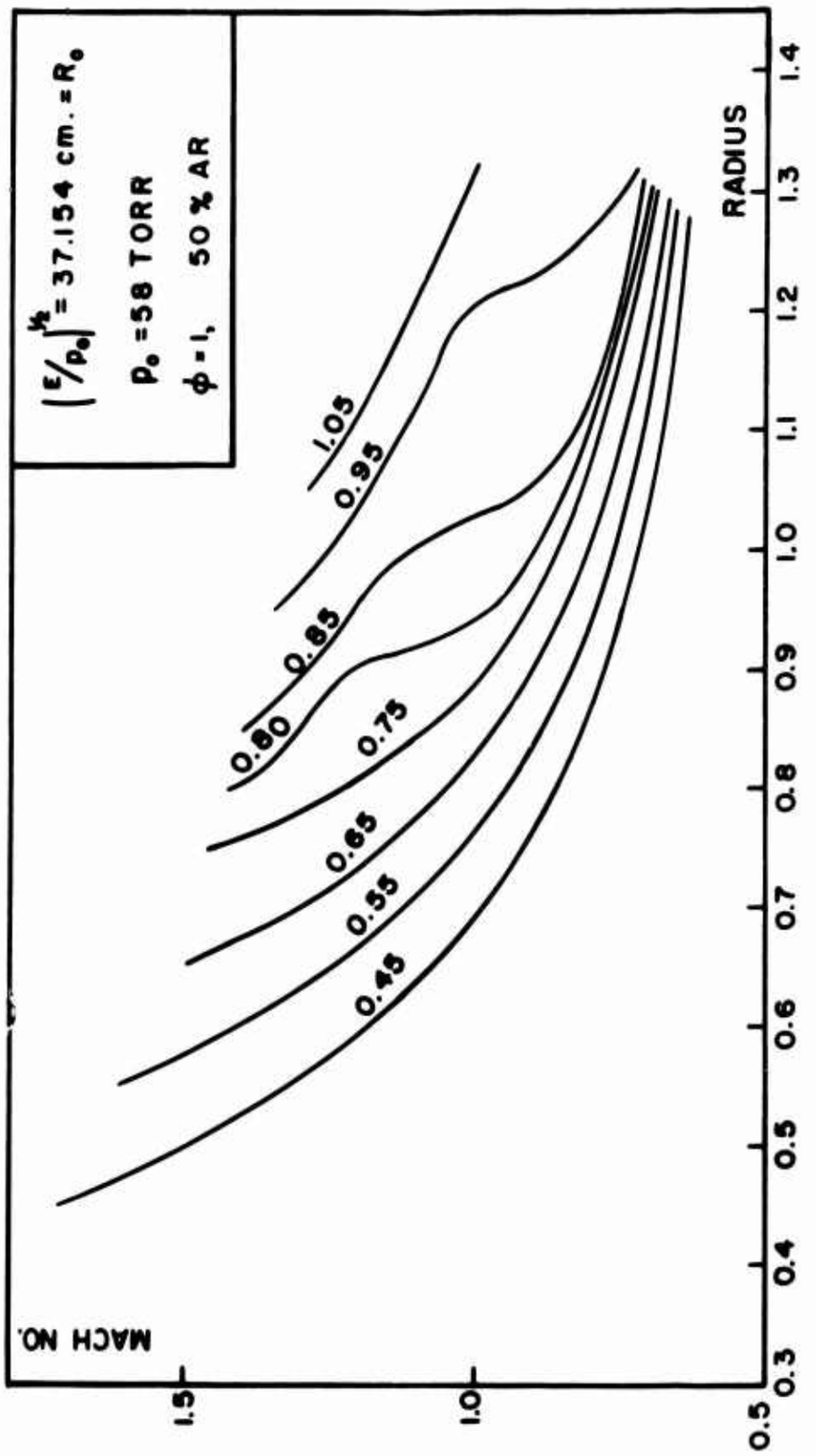
$\left|E/p_0\right|^{1/2} = 37.154$ cm. $= R_0$
$p_0 = 58$ TORR
$\phi = 1$, 50 % AR
1.05
0.95
0.85
0.80
0.75
0.65
0.55
0.45
MACH NO.
RADIUS
0.5
0.3
0.4
0.5
0.6
0.7
0.8
0.9
1.0
1.1
1.2
1.3
1.4
1.0
1.5

FIGURE 15

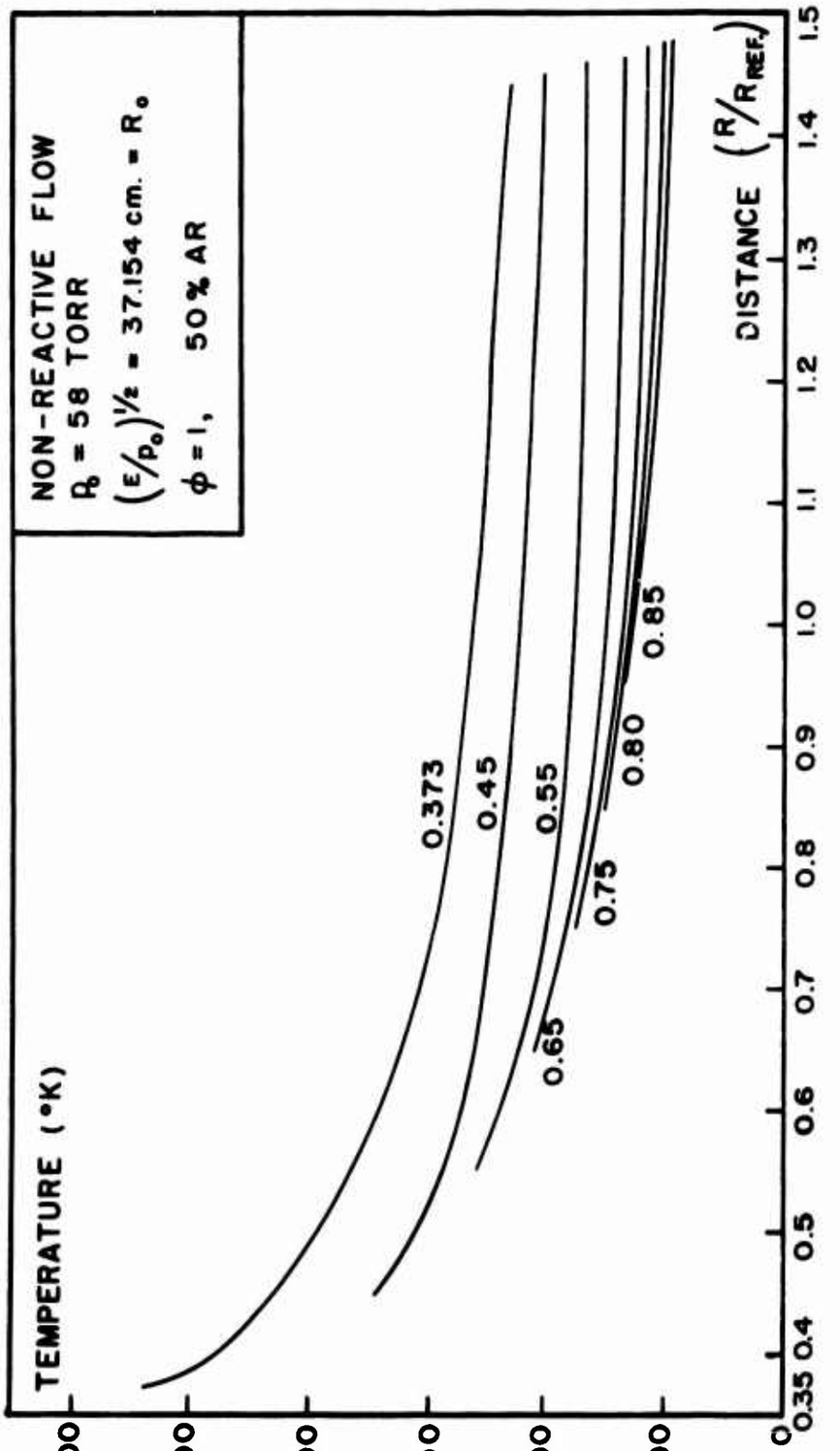
NON-REACTIVE FLOW
P_o = 58 TORR
$(\epsilon/\rho_o)^{1/2}$ = 37.154 cm. = R_o
ϕ = 1, 50% AR
TEMPERATURE (°K)
DISTANCE ($R/R_{REF.}$)
0.373
0.45
0.55
0.65
0.75
0.80
0.85
0
1000
2000
3000
4000
5000
6000
0.35
0.4
0.5
0.6
0.7
0.8
0.9
1.0
1.1
1.2
1.3
1.4
1.5

FIGURE 16

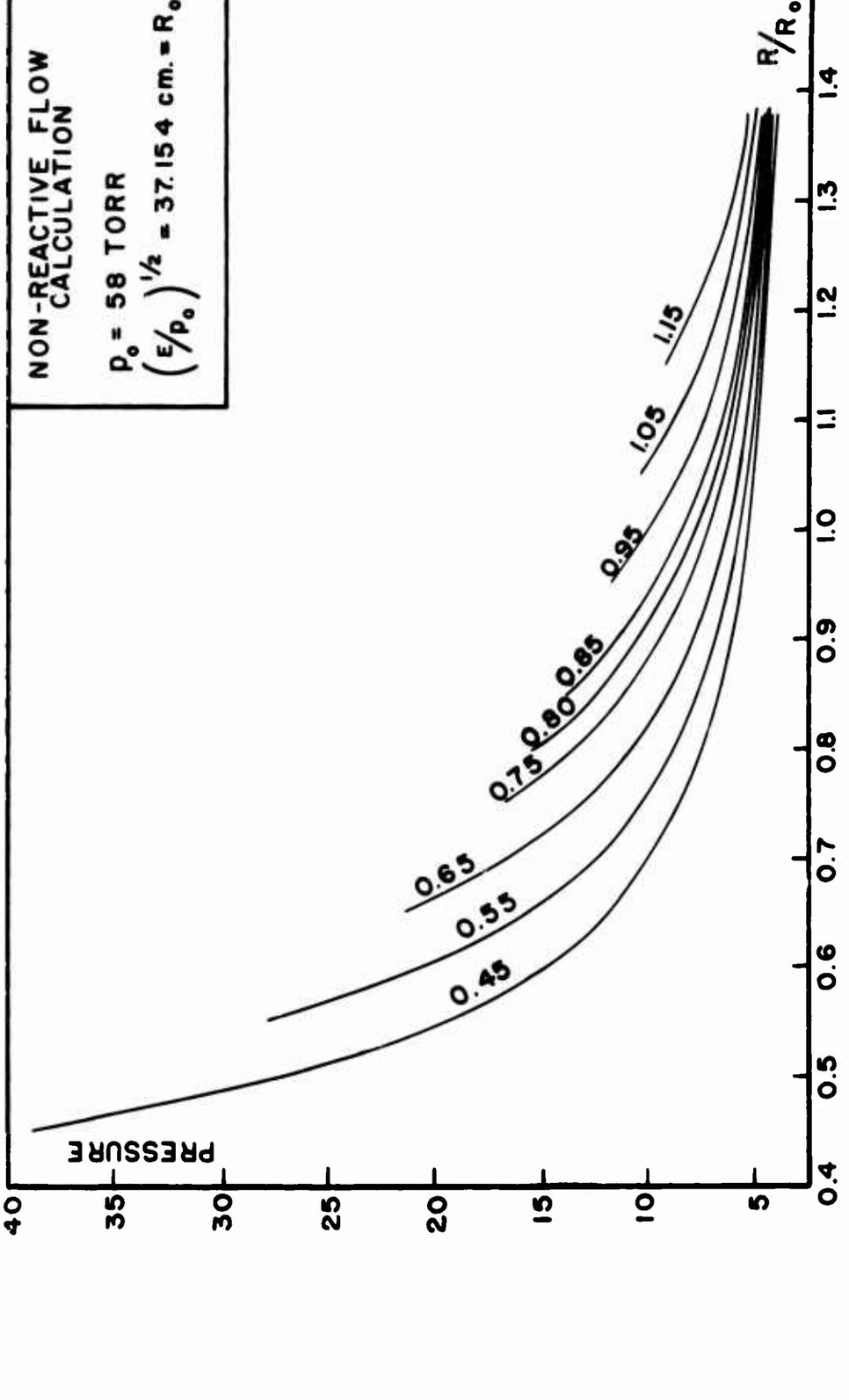
NON-REACTIVE FLOW
CALCULATION
p_o = 58 TORR
$(\varepsilon/p_o)^{1/2}$ = 37.154 cm. = R_o
PRESSURE
R/R_o
0.45
0.55
0.65
0.75
0.80
0.85
0.95
1.05
1.15
40
35
30
25
20
15
10
5
0.4
0.5
0.6
0.7
0.8
0.9
1.0
1.1
1.2
1.3
1.4

FIGURE 17

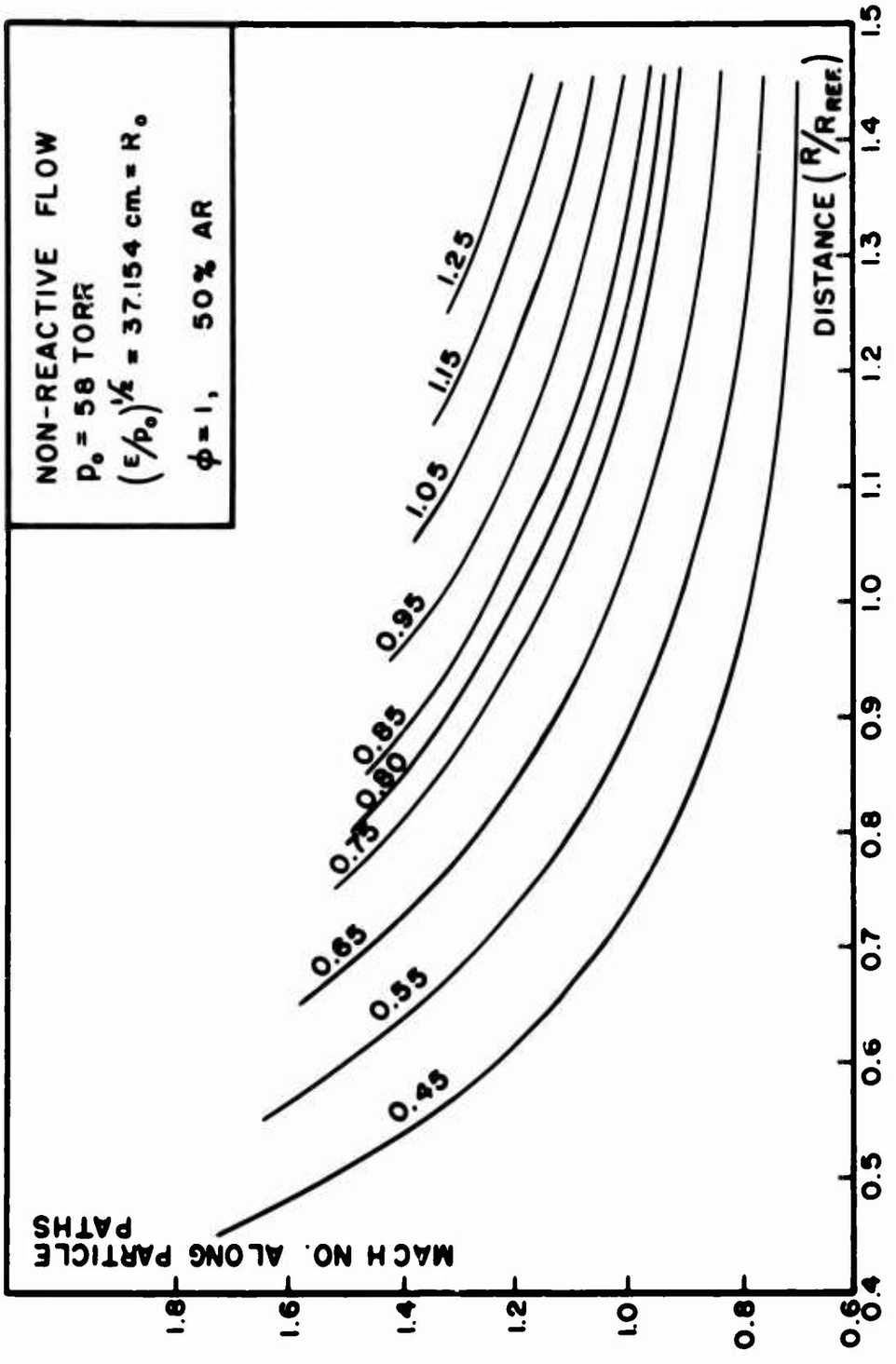
NON-REACTIVE FLOW
p_o = 58 TORR
$(\epsilon/p_o)^{1/2}$ = 37.154 cm = R_o
ϕ = 1, 50% AR
MACH NO. ALONG PARTICLE PATHS
DISTANCE ($R/R_{REF.}$)
0.45
0.55
0.65
0.75
0.80
0.85
0.95
1.05
1.15
1.25
0.4
0.5
0.6
0.7
0.8
0.9
1.0
1.1
1.2
1.3
1.4
1.5
0.6
0.8
1.0
1.2
1.4
1.6
1.8

FIGURE 18

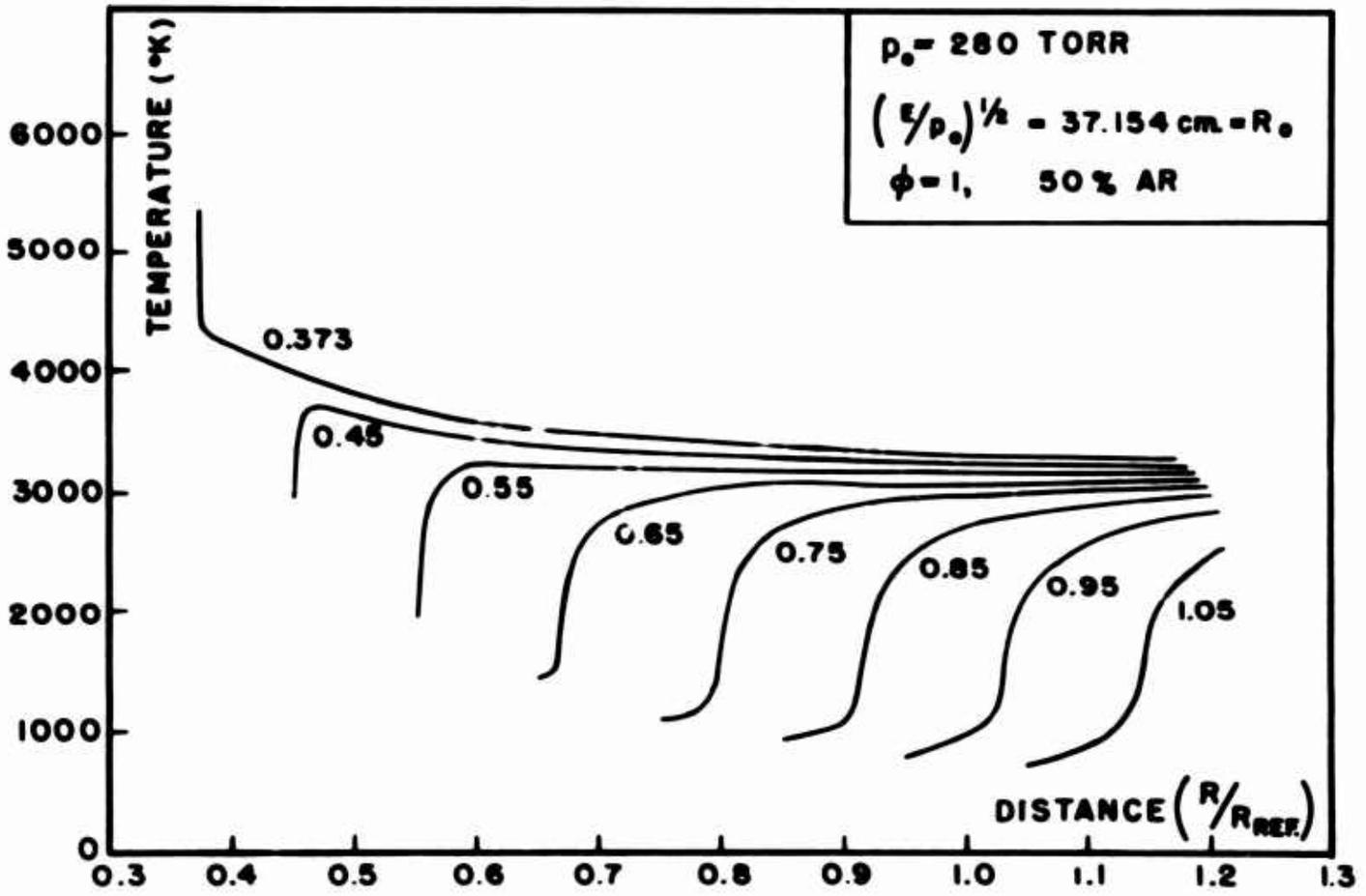
p_o= 280 TORR
$(E/p_o)^{1/2}$ = 37.154 cm. = R_o
ϕ = 1, 50% AR
TEMPERATURE (°K)
6000
5000
4000
3000
2000
1000
0
0.373
0.45
0.55
0.65
0.75
0.85
0.95
1.05
DISTANCE $(R/R_{REF.})$
0.3
0.4
0.5
0.6
0.7
0.8
0.9
1.0
1.1
1.2
1.3

FIGURE 19

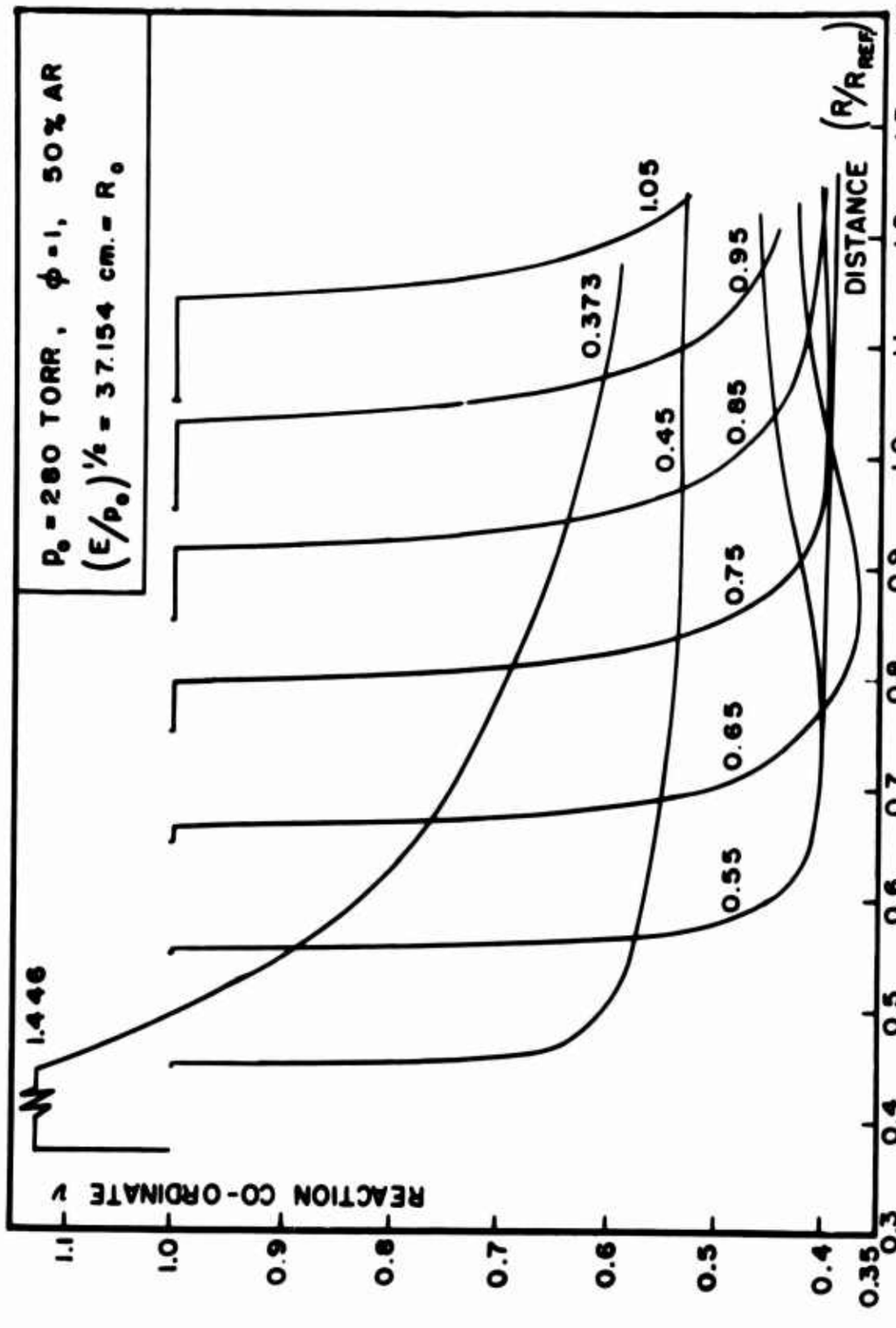
P_o = 280 TORR, ϕ = 1, 50% AR
$(E/p_o)^{1/2}$ = 37.154 cm. = R_o
1.446
0.373
0.45
0.55
0.65
0.75
0.85
0.95
1.05
REACTION CO-ORDINATE y
DISTANCE (R/R_{REF})
1.1
1.0
0.9
0.8
0.7
0.6
0.5
0.4
0.35
0.3
0.4
0.5
0.6
0.7
0.8
0.9
1.0
1.1
1.2
1.3
1.4

FIGURE 20

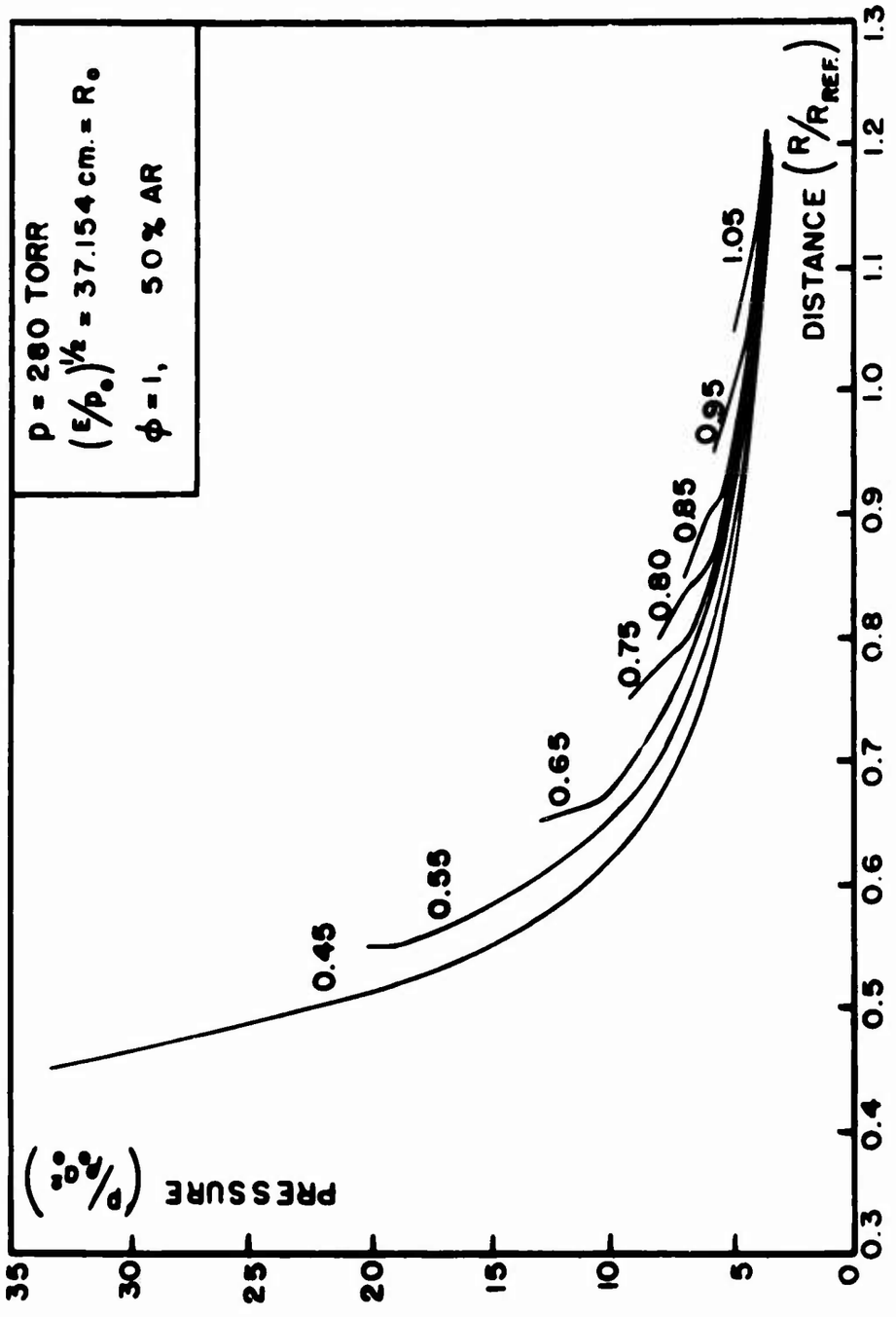
p = 280 TORR
$(E/p_o)^{1/2}$ = 37.154 cm. = R_o
ϕ = 1, 50% AR
PRESSURE (p/p_{max})
DISTANCE $(R/R_{REF.})$
0.45
0.55
0.65
0.75
0.80
0.85
0.95
1.05
0
5
10
15
20
25
30
35
0.3
0.4
0.5
0.6
0.7
0.8
0.9
1.0
1.1
1.2
1.3

FIGURE 21

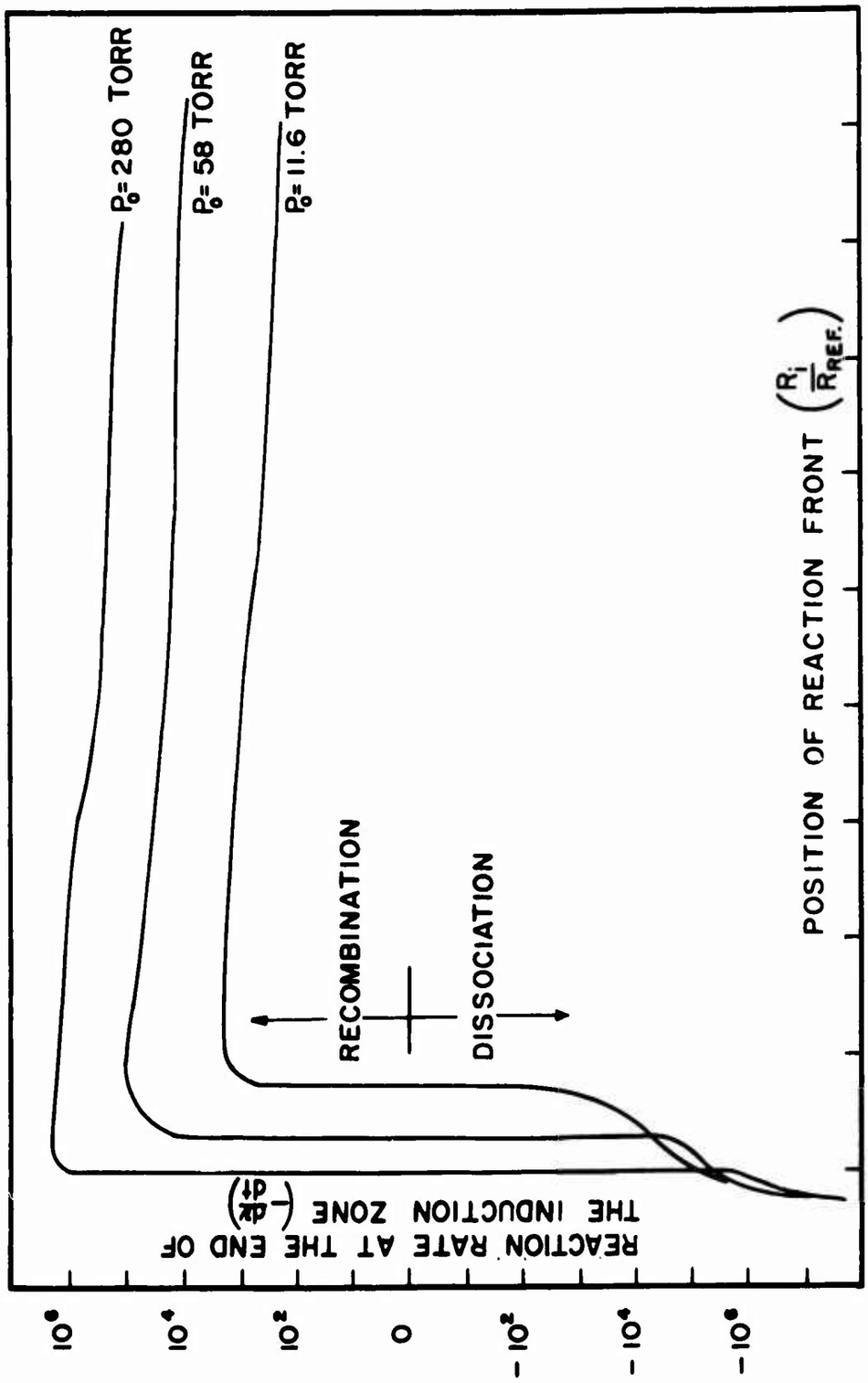
P_o= 280 TORR
P_o= 58 TORR
P_o= 11.6 TORR
RECOMBINATION
DISSOCIATION
POSITION OF REACTION FRONT $\left(\frac{R_i}{R_{REF.}}\right)$
0.4
0.6
0.8
1.0
1.2
REACTION RATE AT THE END OF THE INDUCTION ZONE $\left(-\frac{d\alpha}{dt}\right)$
10^6
10^4
10^2
0
-10^2
-10^4
-10^6

FIGURE 22

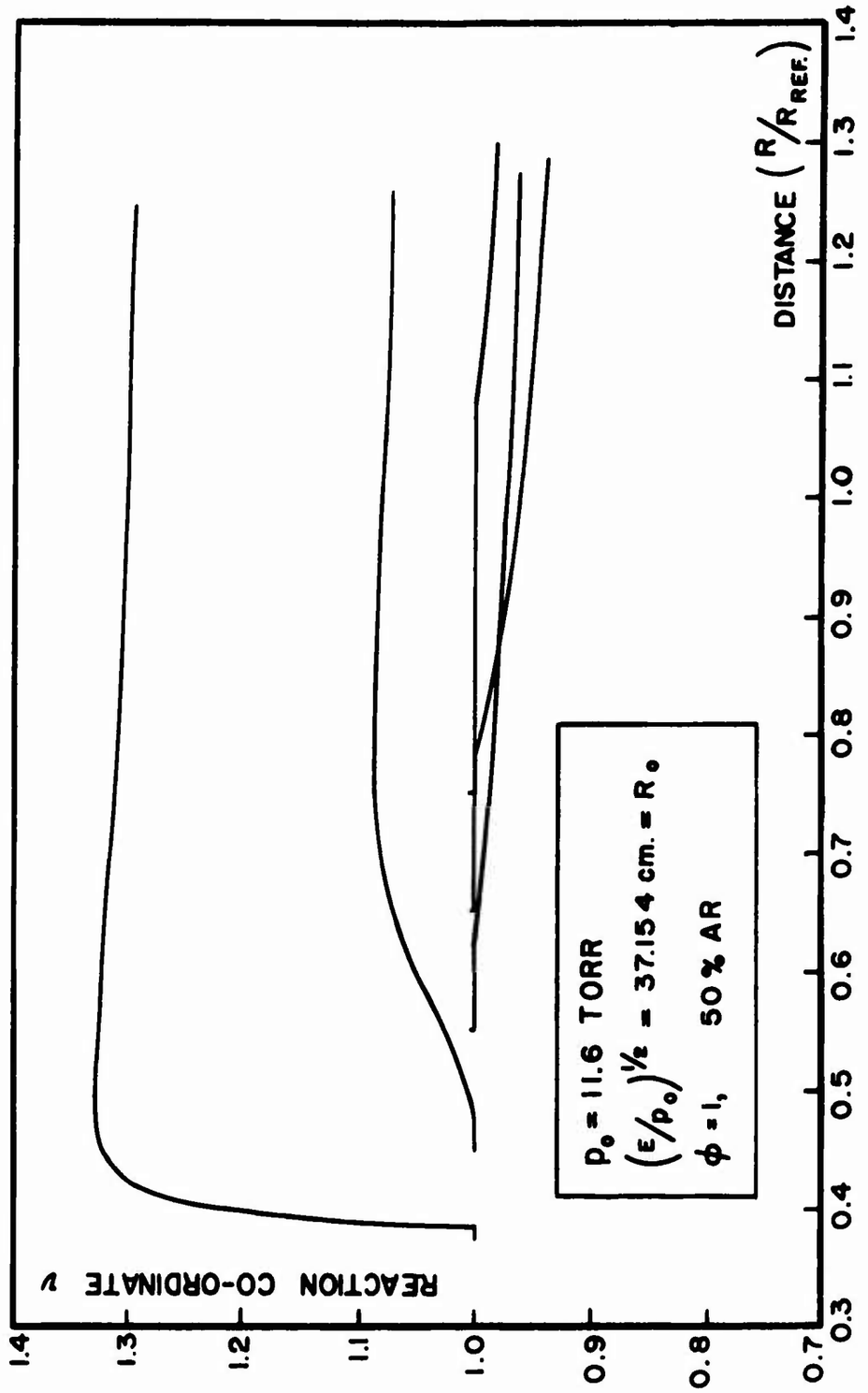
REACTION CO-ORDINATE ν
DISTANCE (R/R_REF.)
1.4
1.3
1.2
1.1
1.0
0.9
0.8
0.7
0.3
0.4
0.5
0.6
0.7
0.8
0.9
1.0
1.1
1.2
1.3
1.4
p_o = 11.6 TORR
(ε/p_o)^½ = 37.154 cm. = R_o
φ = 1, 50% AR

FIGURE 23

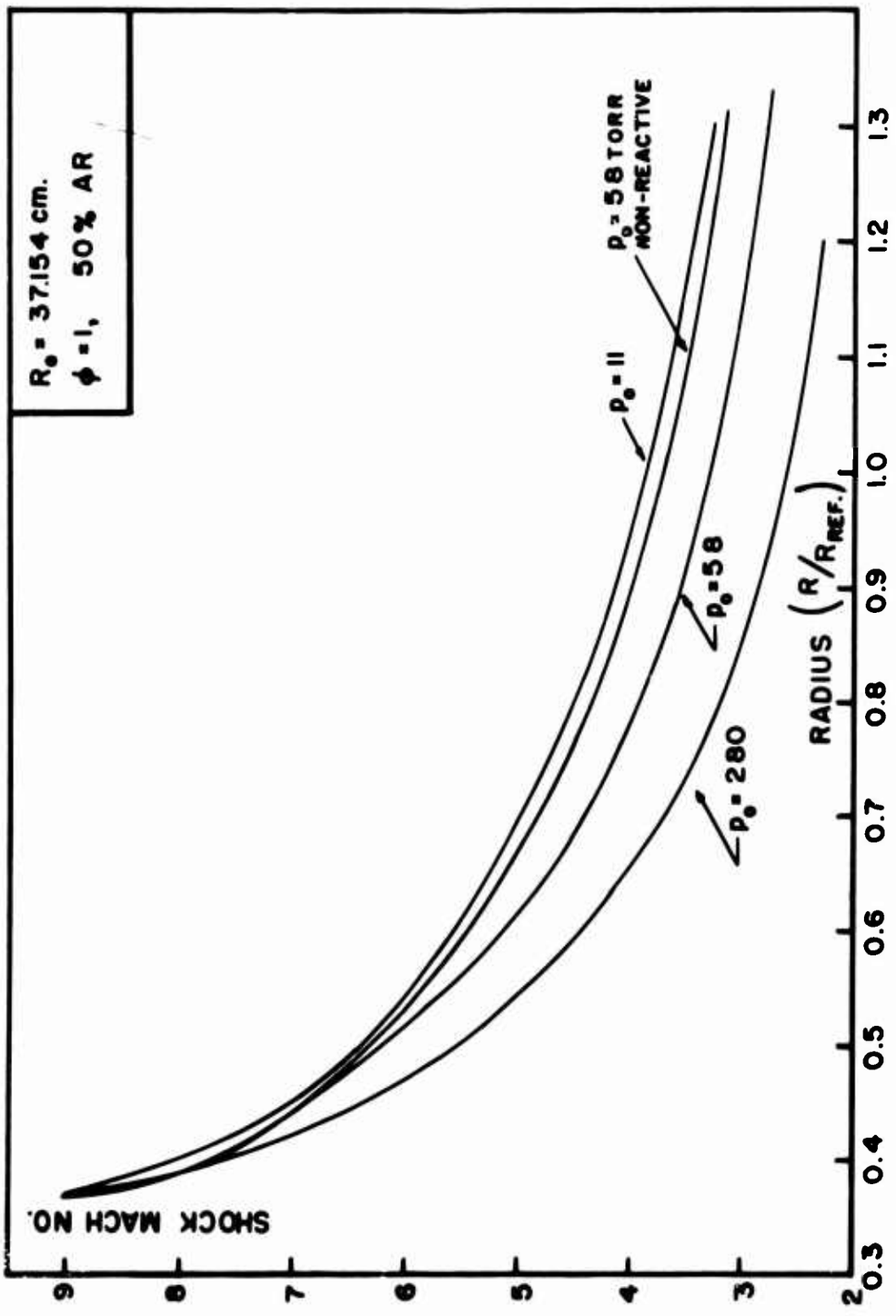
R_o = 37.154 cm.
ϕ = 1, 50% AR
p_o = 58 TORR NON-REACTIVE
p_o = 11
p_o = 58
p_o = 280
SHOCK MACH NO.
RADIUS $(R/R_{REF.})$
9
8
7
6
5
4
3
2
0.3
0.4
0.5
0.6
0.7
0.8
0.9
1.0
1.1
1.2
1.3

FIGURE 24

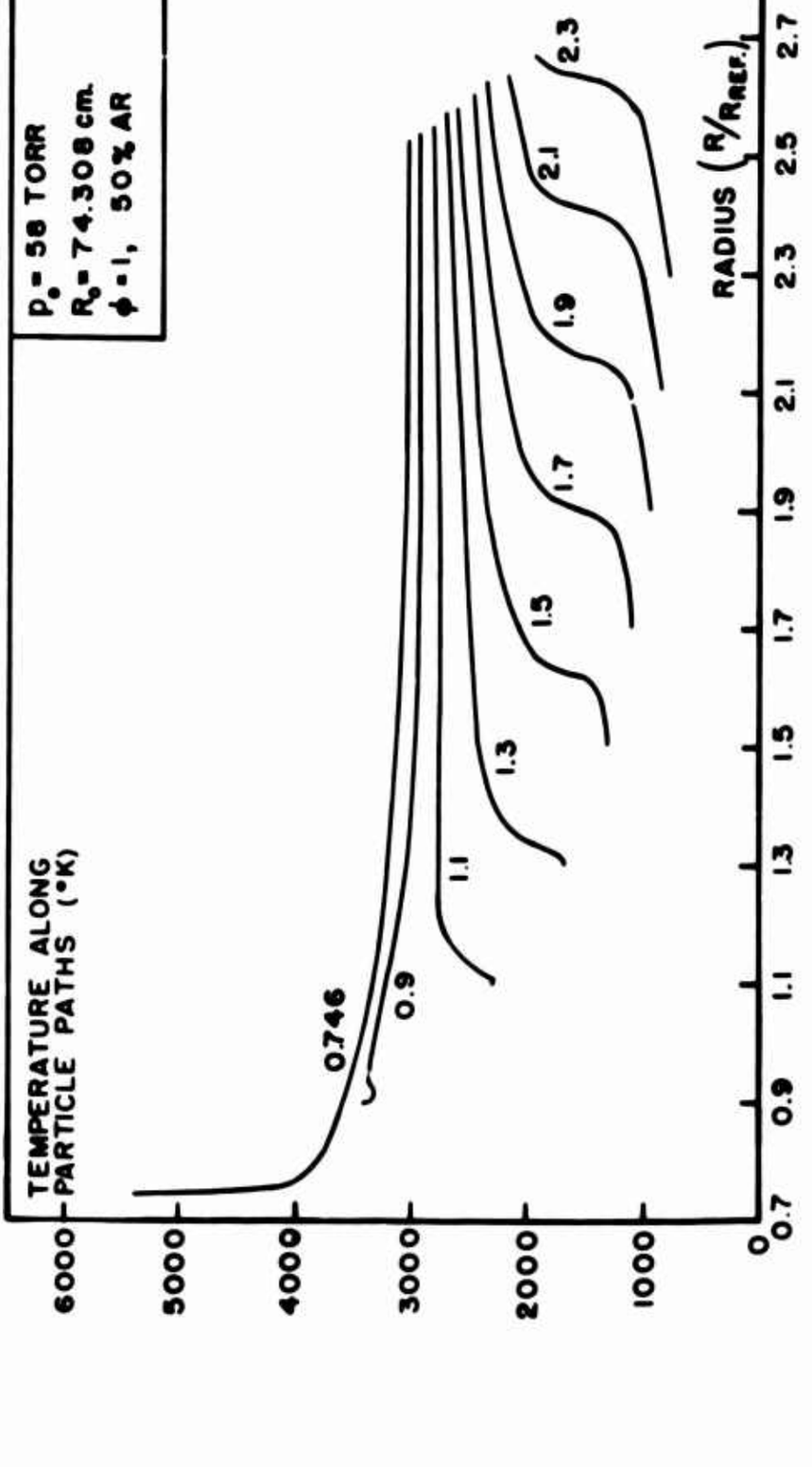
TEMPERATURE ALONG PARTICLE PATHS (°K)
P_0 = 58 TORR
R_0 = 74.308 cm.
ϕ = 1, 50% AR
RADIUS ($R/R_{REF.}$)
6000
5000
4000
3000
2000
1000
0
0.7
0.9
1.1
1.3
1.5
1.7
1.9
2.1
2.3
2.5
2.7
0.746
0.9
1.1
1.3
1.5
1.7
1.9
2.1
2.3

FIGURE 25

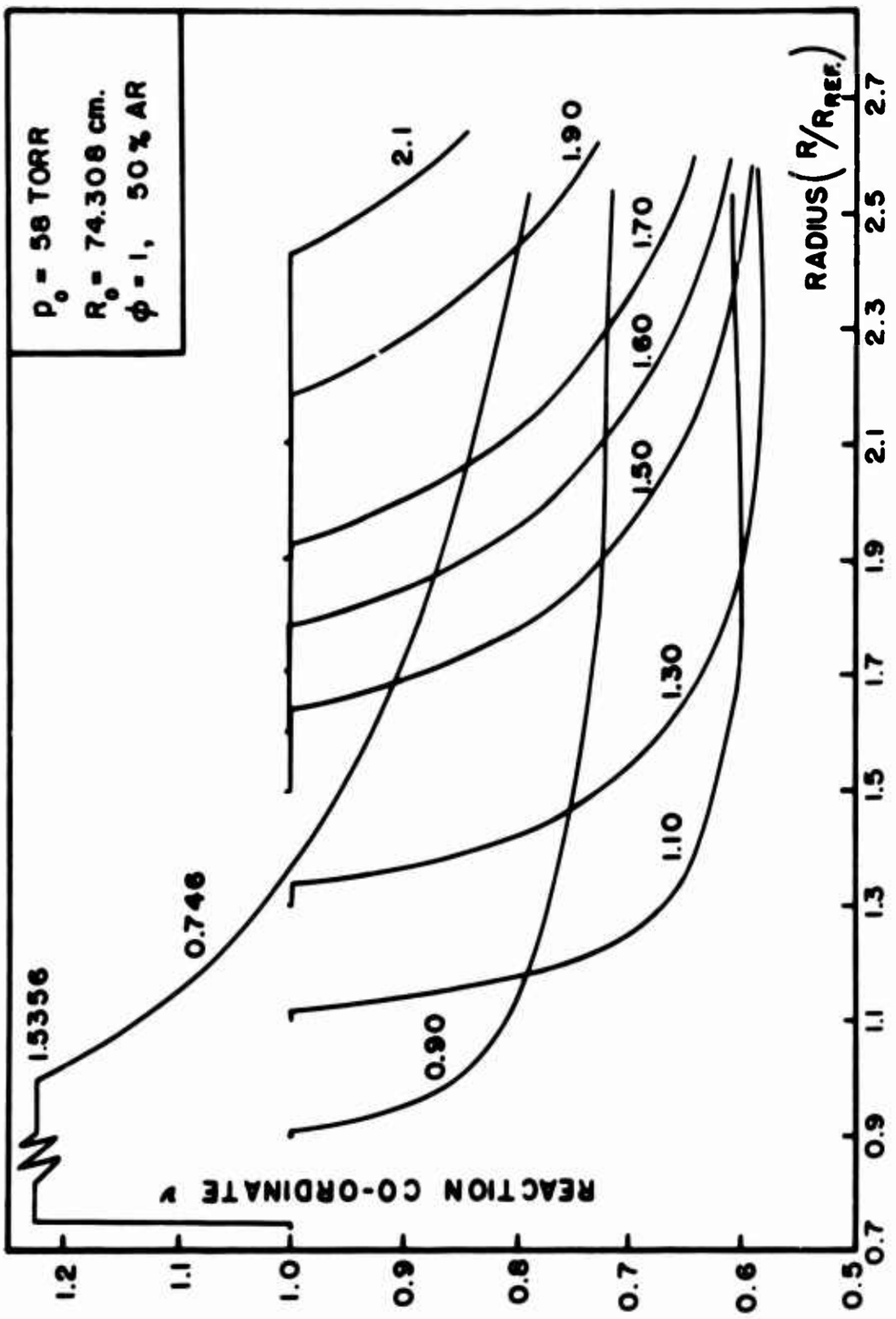
p_o = 58 TORR
R_o = 74.308 cm.
ϕ = 1, 50% AR
1.5356
0.746
0.90
1.10
1.30
1.50
1.60
1.70
1.90
2.1
REACTION CO-ORDINATE Y
RADIUS (R/R_REF.)
1.2
1.1
1.0
0.9
0.8
0.7
0.6
0.5
0.7
0.9
1.1
1.3
1.5
1.7
1.9
2.1
2.3
2.5
2.7

FIGURE 26

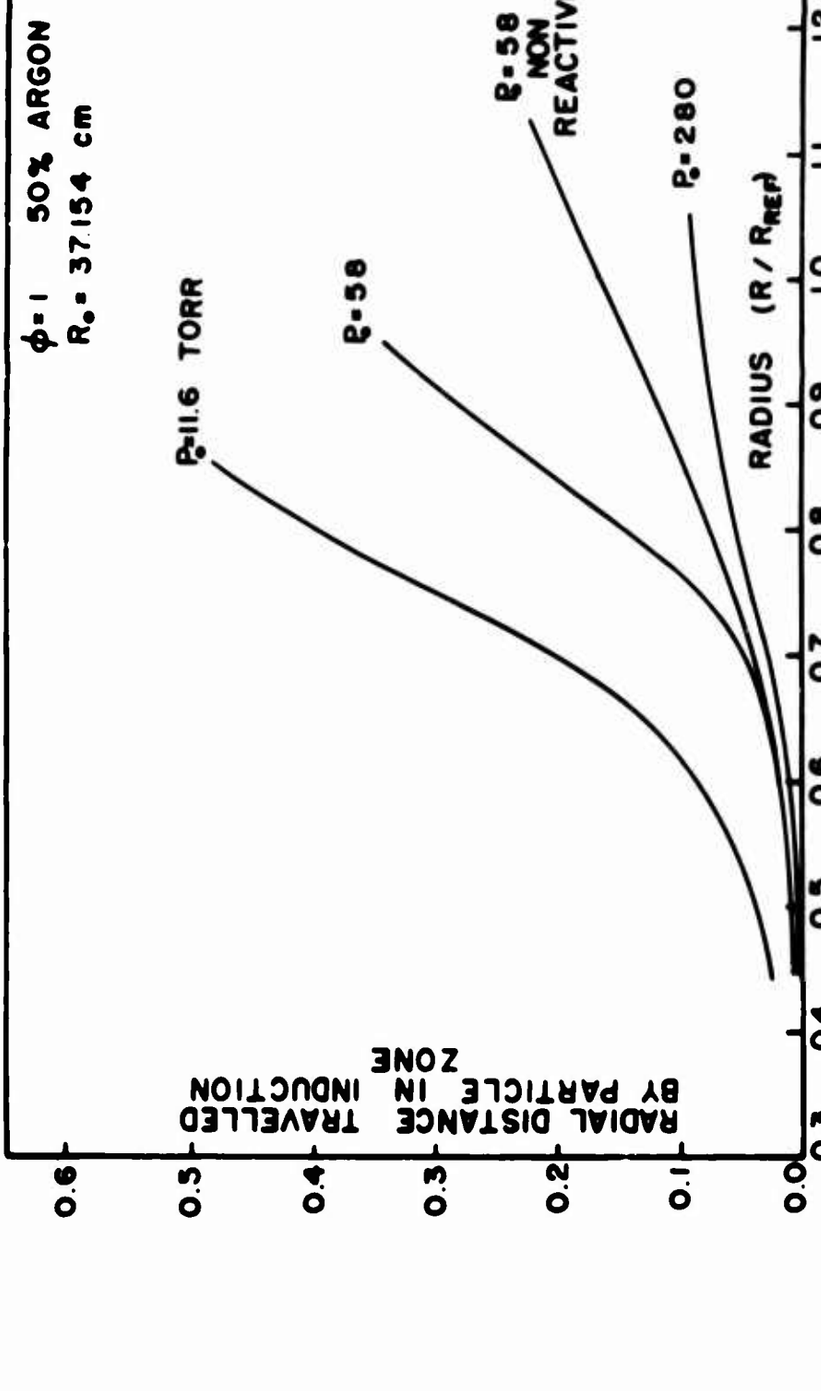
φ=1 50% ARGON
R₀=37.154 cm
P₀=11.6 TORR
P=58
P=58 NON REACTIVE
P₀=280
RADIUS (R/R_REF)
RADIAL DISTANCE TRAVELLED BY PARTICLE IN INDUCTION ZONE
0.0
0.1
0.2
0.3
0.4
0.5
0.6
0.3
0.4
0.5
0.6
0.7
0.8
0.9
1.0
1.1
1.2

FIGURE 27

(a) LEAN MIXTURE, ϕ=0.36, 60% ARGON, P_o=150 TORR

(b) RICH MIXTURE, ϕ=2.12, 60% ARGON, P_o=150 TORR

FIGURE 28. SMOKE TRACK RECORDS

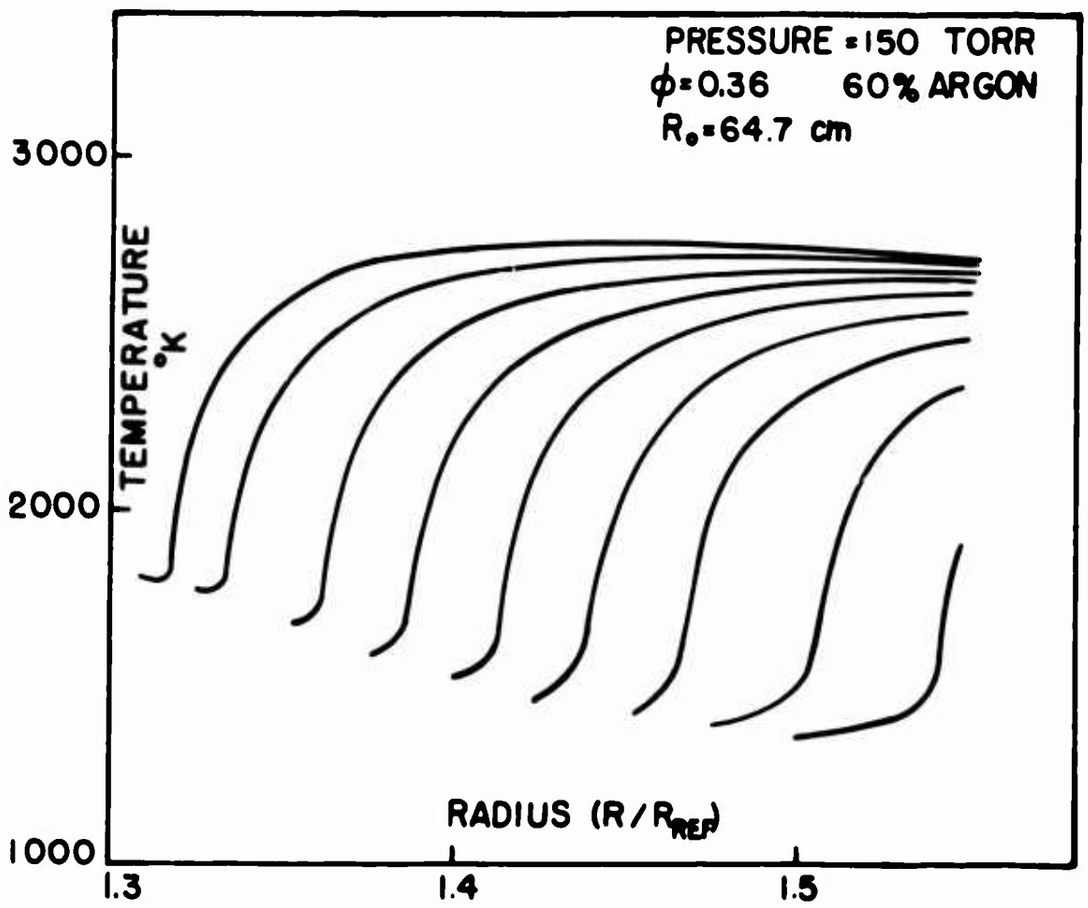
PRESSURE = 150 TORR
ϕ = 0.36 60% ARGON
R_o = 64.7 cm
3000
2000
1000
TEMPERATURE °K
RADIUS (R/R_{REF})
1.3
1.4
1.5

FIGURE 29

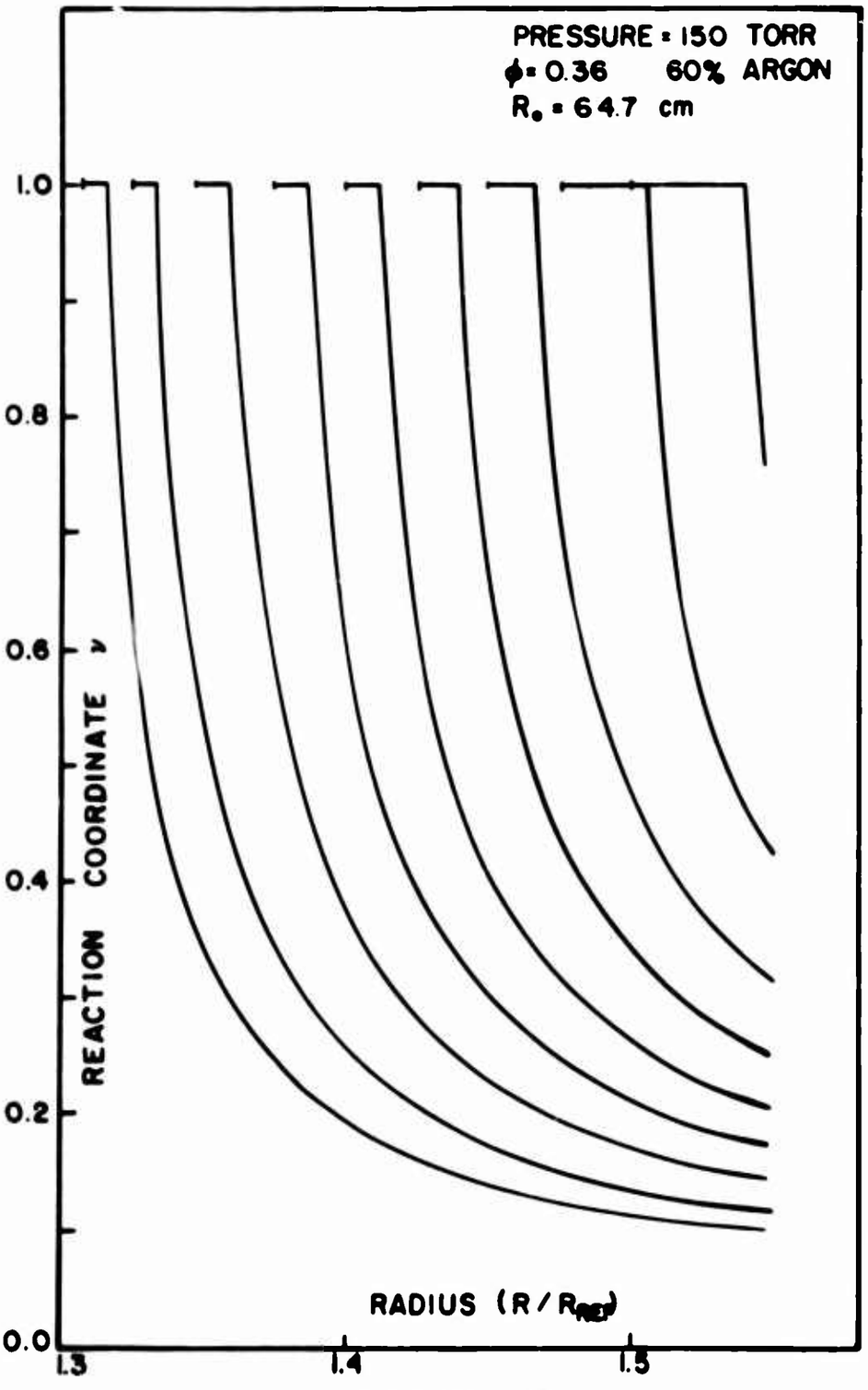
PRESSURE = 150 TORR
ϕ = 0.36 60% ARGON
R_o = 64.7 cm
1.0
0.8
0.6
0.4
0.2
0.0
REACTION COORDINATE ν
RADIUS (R/R_{REF})
1.3
1.4
1.5

FIGURE 30

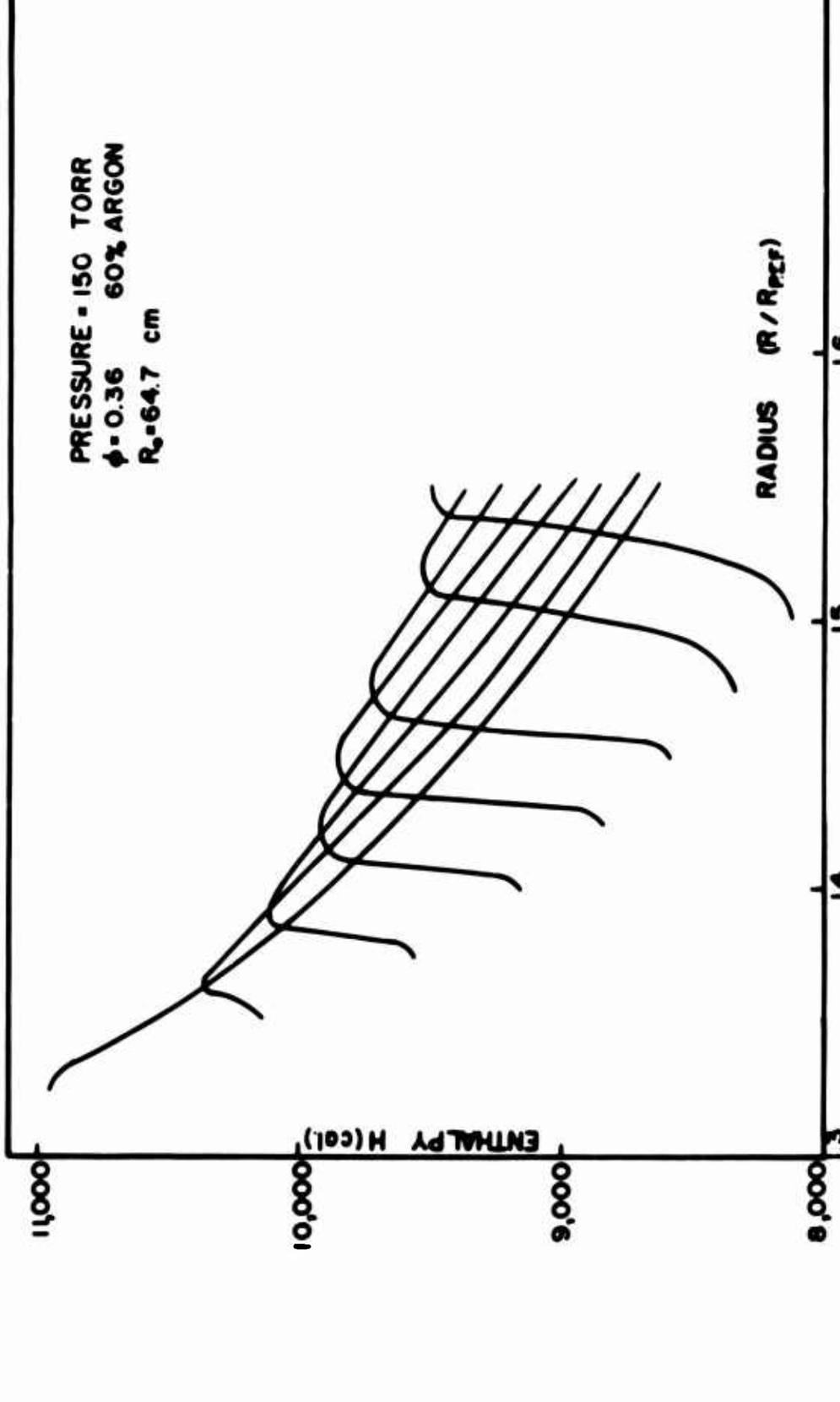
PRESSURE = 150 TORR
ϕ = 0.36 60% ARGON
R_o = 64.7 cm
ENTHALPY H (cal)
11,000
10,000
9,000
8,000
RADIUS (R / R_PCF)
1.3
1.4
1.5
1.6

FIGURE 31

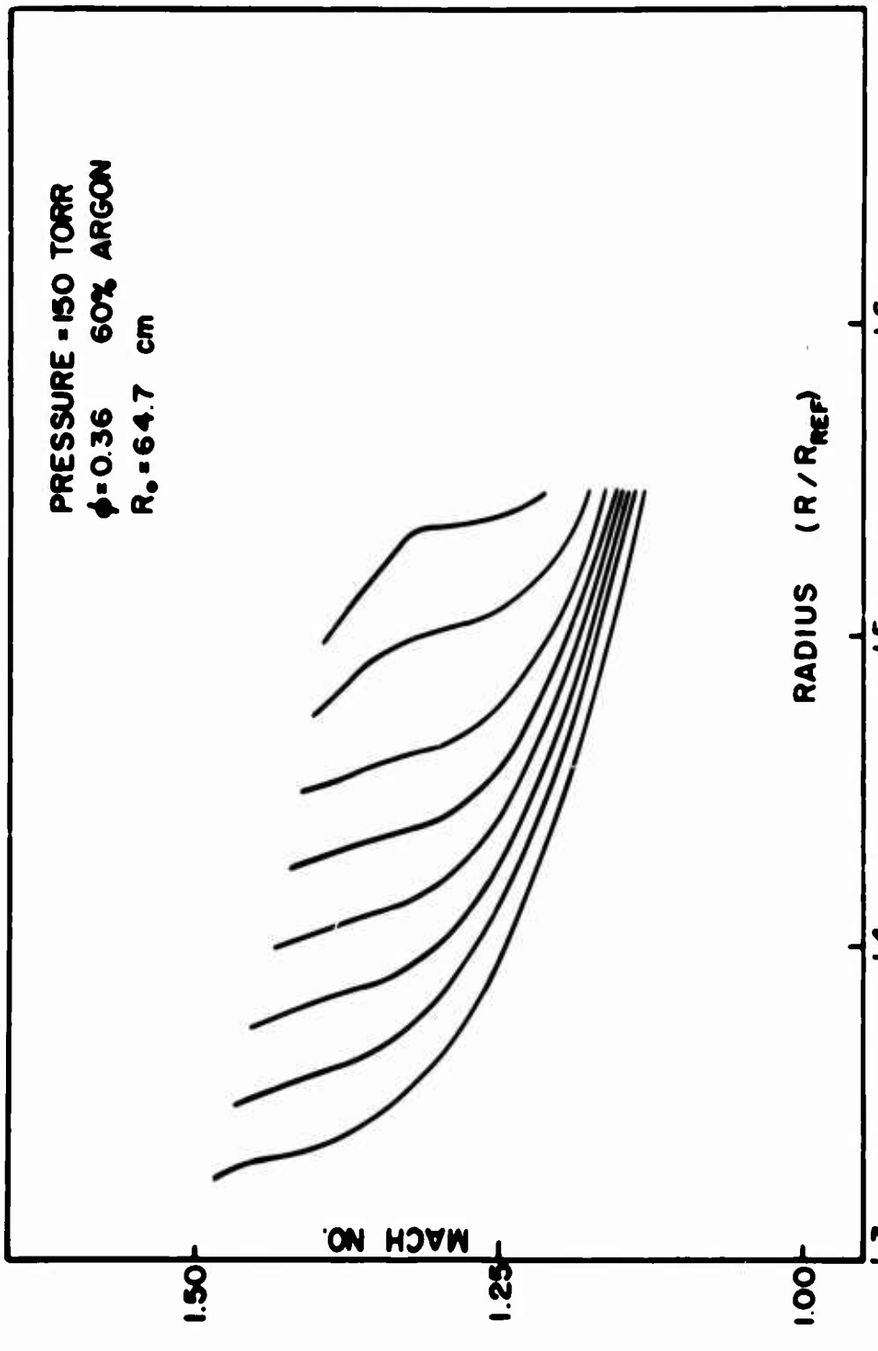
PRESSURE = 150 TORR
φ = 0.36 60% ARGON
R₀ = 64.7 cm
MACH NO.
1.50
1.25
1.00
RADIUS (R/R_REF)
1.3
1.4
1.5
1.6

FIGURE 32

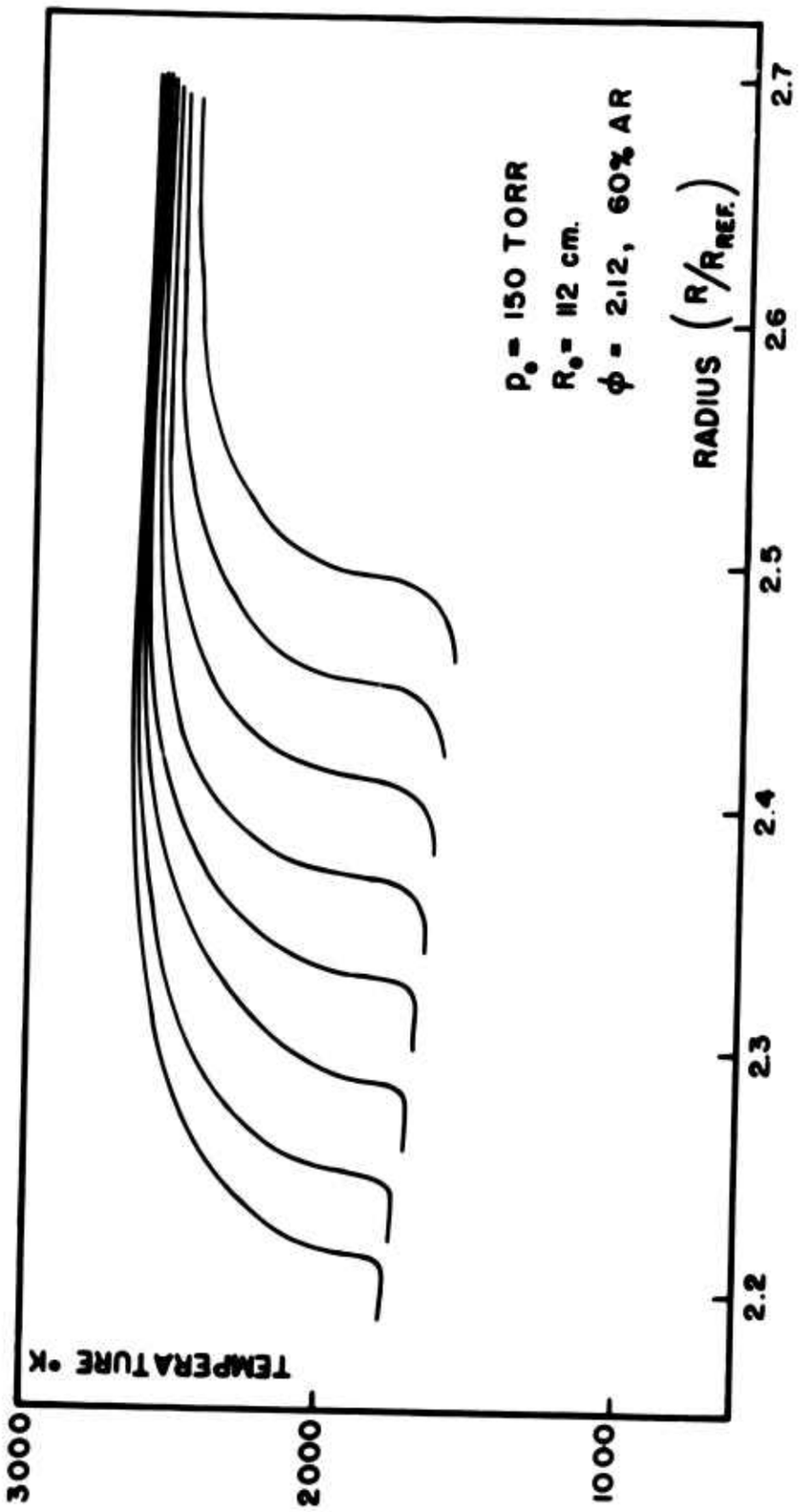
TEMPERATURE °K
3000
2000
1000
2.2
2.3
2.4
2.5
2.6
2.7
RADIUS (R/R_REF.)
P_o = 150 TORR
R_o = 112 cm.
φ = 2.12, 60% AR

FIGURE 33

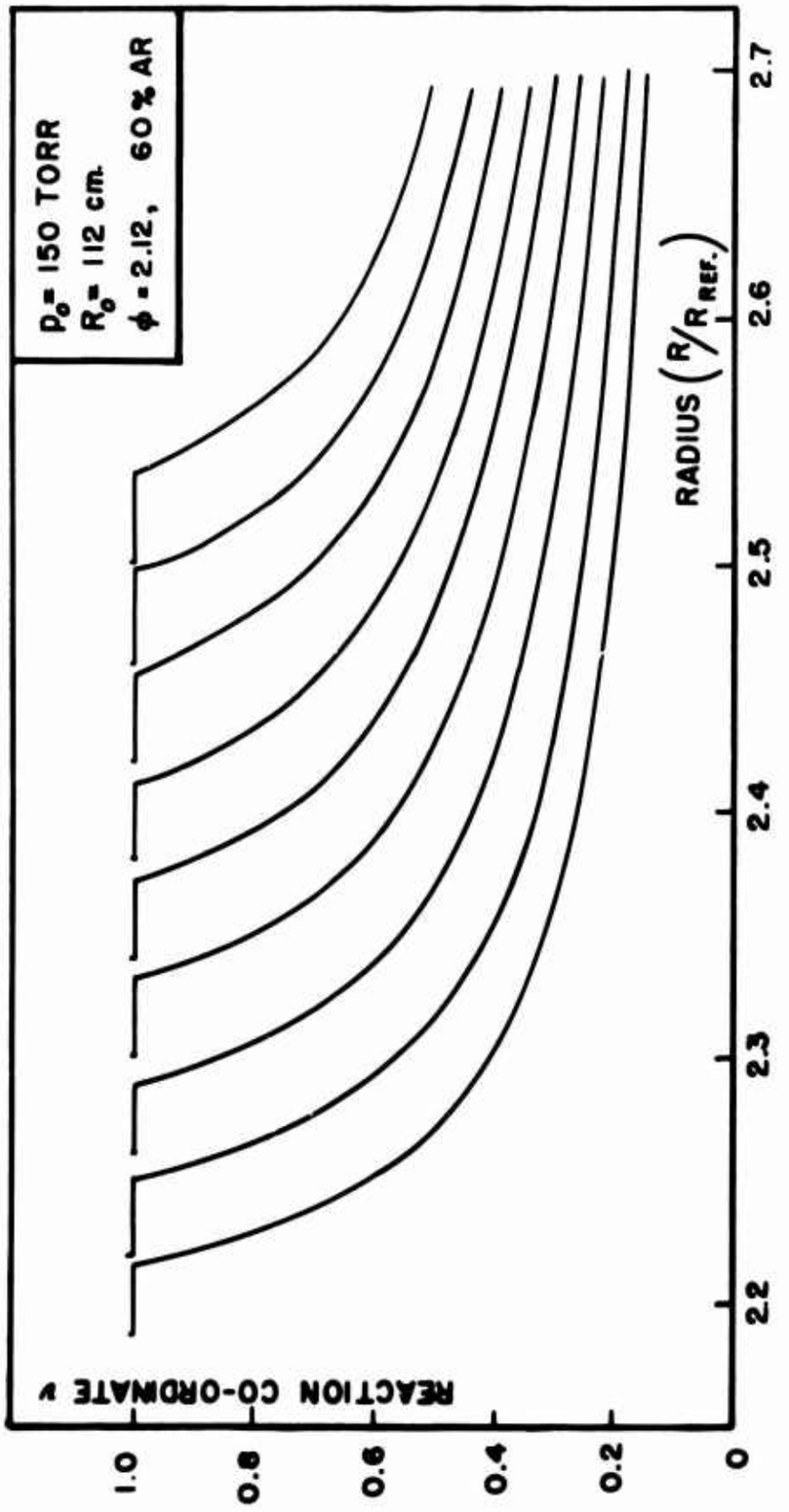
P_o= 150 TORR
R_o= 112 cm.
ϕ = 2.12, 60% AR
REACTION CO-ORDINATE y
RADIUS $(R/R_{REF.})$
0
0.2
0.4
0.6
0.8
1.0
2.2
2.3
2.4
2.5
2.6
2.7

FIGURE 34

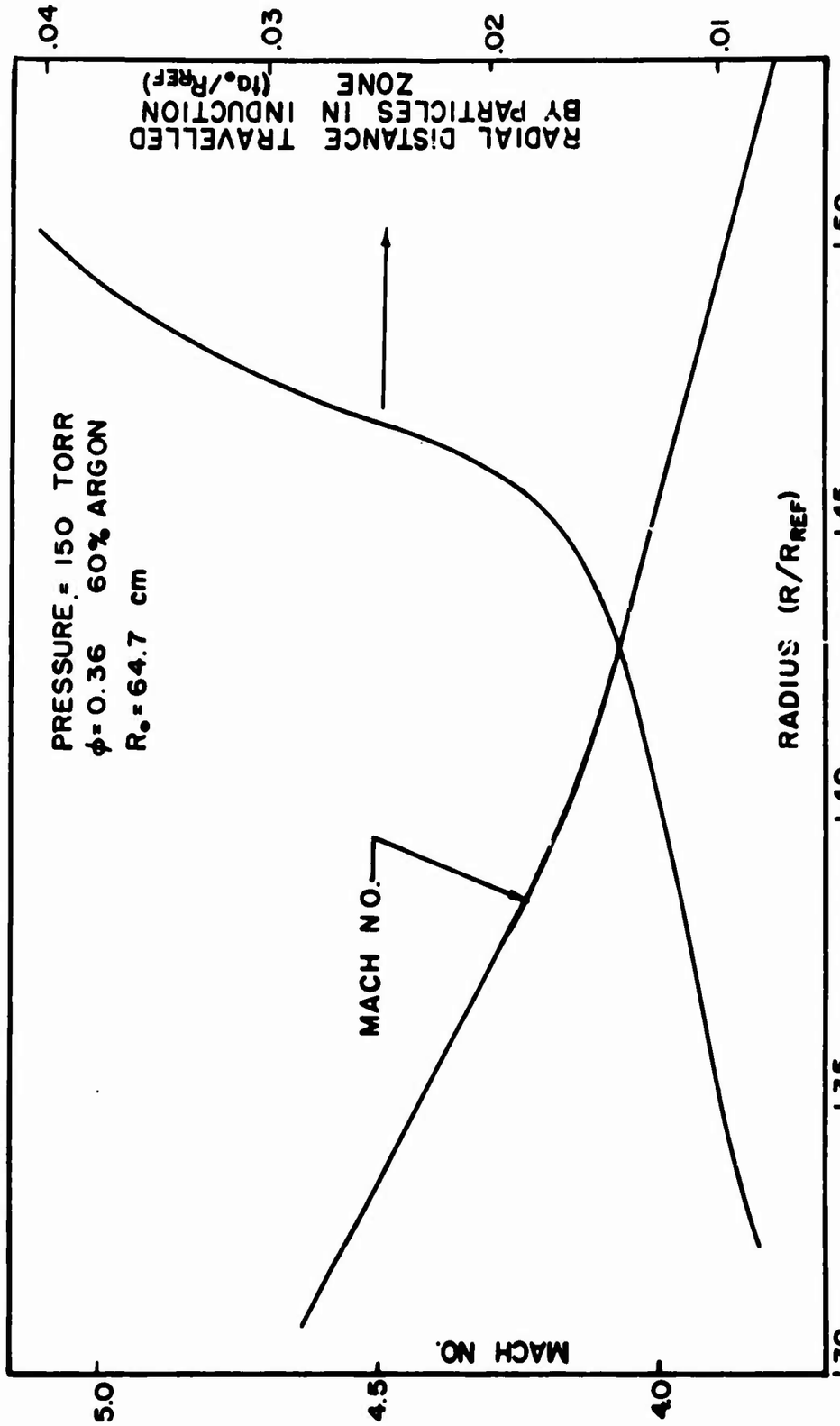
PRESSURE = 150 TORR
φ = 0.36 60% ARGON
R₀ = 64.7 cm
MACH NO.
RADIUS (R/R_REF)
RADIAL DISTANCE TRAVELLED BY PARTICLES IN INDUCTION ZONE (r₀/R_REF)
MACH NO.
5.0
4.5
4.0
1.30
1.35
1.40
1.45
1.50
.01
.02
.03
.04

FIGURE 35

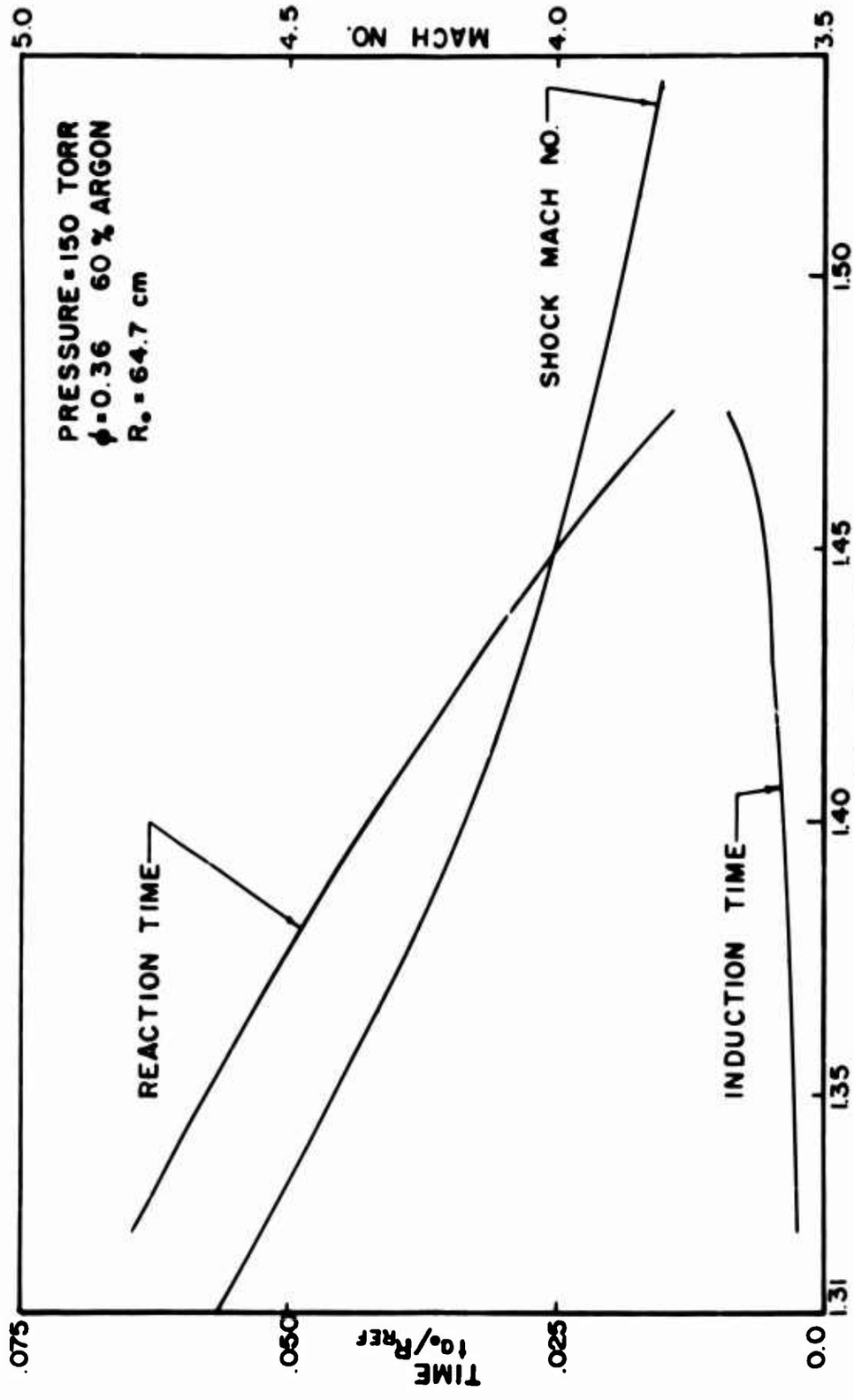
PRESSURE = 150 TORR
ϕ = 0.36 60 % ARGON
R_o = 64.7 cm
SHOCK MACH NO.
REACTION TIME
INDUCTION TIME
MACH NO.
TIME t_{0_o}/R_{REF}
RADIUS (R/R_{REF})
5.0
4.5
4.0
3.5
.075
.050
.025
0.0
1.31
1.35
1.40
1.45
1.50

FIGURE 36

VITA

Suryanarayaniah Rajan was born [redacted] He attended high school [redacted] He received his Bachelor of Engineering degree in Mechanical Engineering from the University of Mysore in 1961. The Indian Institute of Science, Bangalore, conferred on him the degree of Master of Engineering, with distinction, in 1963.

From 1963 to 1965 he was employed as a lecturer in the Department of Aeronautics and Applied Mechanics at the Indian Institute of Technology, Madras, India. He was employed as a Research Assistant in the Aeronautical and Astronautical Engineering Department from September 1965 to September 1969.

The author is a member of the Sigma Gamma Tau honor society and a member of the American Institute of Aeronautics and Astronautics.

He is one of the authors of the paper "Transverse Waves in Detonations. I. Spacing in the Hydrogen-Oxygen System", published in the AIAA Journal, Vol. 7, No. 2, 1969.

Unclassified
Security Classification

DOCUMENT CONTROL DATA - R & D

(Security classification of title, body of abstract and indexing annotation must be entered when the overall report is classified)

1 ORIGINATING ACTIVITY (Corporate author) University of Illinois Urbana, Illinois 61801	2a. REPORT SECURITY CLASSIFICATION Unclassified 2b GROUP

3 REPORT TITLE

ON THE INTERACTION BETWEEN CHEMICAL KINETICS AND GASDYNAMICS IN THE FLOW BEHIND A CYLINDRICAL DETONATION FRONT

4 DESCRIPTIVE NOTES (Type of report and inclusive dates)

5 AUTHOR(S) (First name, middle initial, last name)

Suryanarayaniah Rajan, Ph.D.

6 REPORT DATE March 1970	7a. TOTAL NO OF PAGES 112	7b NO OF REFS 66
8a CONTRACT OR GRANT NO DA-18-001-AMC-1016(X) b. PROJECT NO 1T061102A32B0100 c. d.	9a. ORIGINATOR'S REPORT NUMBER(S) BRL Contract Report No. 9 9b OTHER REPORT NO(S) (Any other numbers that may be assigned this report) N/A	

10 DISTRIBUTION STATEMENT

This document has been approved for public release and sale; its distribution is unlimited.

11 SUPPLEMENTARY NOTES	12 SPONSORING MILITARY ACTIVITY USA Aberdeen Research & Development Center Ballistic Research Laboratories Aberdeen Proving Ground, Maryland 21005

13 ABSTRACT

The interaction of chemical kinetics and heat release phenomena with the gasdynamics of the flow appreciably alters temperature, density, and flow velocity behind the incident shock wave. This in turn influences the strength and decay rate of the shock at later times. The detonation cell geometry and spacing are thus dependent upon the nonsteady kinetic rate processes in the shocked gas. Overall effects of the chemical processes for the H_2-O_2 system are strongly influenced by initial pressure and, to a lesser degree, gas composition.

DD FORM 1 NOV 68 1473 REPLACES DD FORM 1473, 1 JAN 64, WHICH IS OBSOLETE FOR ARMY USE.

Unclassified
Security Classification

14 KEY WORDS	LINK A		LINK B		LINK C	
	ROLE	WT	ROLE	WT	ROLE	WT
Gas Phase Detonation Transverse Wave Phenomena Shock Interactions in Reactive Flow Chemical and Gasdynamic Coupling						